DISCLAIMER:

This document does not meet the
current format guidelines of
the Graduate School at
The University of Texas at Austin.

It has been published for
informational use only.

The Dissertation Committee for Anjali Mary Fernandes Certifies that this is the approved version of the following dissertation:

QUANTIFYING THE SEDIMENTOLOGY, STRATIGRAPHY AND MORPHODYNAMICS OF SUBMARINE CHANNELS

Committee:

Ronald J. Steel, Supervisor

David Mohrig, Co-Supervisor

Craig Fulthorpe

Wonsuck Kim

Sverre Henriksen

QUANTIFYING THE SEDIMENTOLOGY, STRATIGRAPHY AND MORPHODYNAMICS OF SUBMARINE CHANNELS

by

Anjali Mary Fernandes, B.S.; M.S.

Dissertation

Presented to the Faculty of the Graduate School of

The University of Texas at Austin

in Partial Fulfillment

of the Requirements

for the Degree of

Doctor of Philosophy

The University of Texas at Austin

May 2012

Dedication

To my parents, Bernadette and Errol Fernandes

Acknowledgements

I thank my supervisors, David Mohrig and Ron Steel, who encouraged creativity and allowed me to work with plenty of freedom. I thank David for sharing his knowledge, love for teaching, infectious enthusiasm and also for his encouragement during my frequent moments of self-doubt. His example will always be an inspiration to me. I also owe special thanks to him and Chiu-Mi for the friendship that they and Todi offered at various times. I thank Ron for the valuable guidance he gave me every time I came to him with ideas, problems or questions. Committee members Sverre Henriksen, Wonsuck Kim and Craig Fulthorpe are sincerely thanked. The initial ideas for much of this study grew out of mapping the seismic data which was made available chiefly through Sverre's efforts at Statoil.

I owe a debt of gratitude to Jim Buttles, without whom the quantity and quality of the experimental data would not have been nearly as great. Jim's company through the long hours in the laboratory made this already exciting environment a fun and intellectually stimulating place to work. Early training in data analysis, imparted by Jim, gave me a jump-start into the world of quantitative data extraction and analysis. I also thank Joel Johnson for insightful suggestions which helped me sharpen the focus of Chapter Four of this dissertation, and for his help with instrumentation and data analysis at various times. Working in the Mophdynamics Lab. at the CRWR were made colorful

by the cheerful company of Michael Markowski, Lindsay Olinde, Alex Aronovitz, Bryant Kopriva, Katie Delbeqc and Aymeric-Peyret.

For thought-provoking discussions over beer, margaritas or coffee and for their cheerful camaraderie, I thank my colleagues and friends Virginia Smith, John Shaw, Yao You, Travis Swanson, Chris Armstrong, Aymeric-Pierre Peyret, Liz Rhinehart, Jeff Nittrouer, Manasij Santra, Joshua Dixon, Cornel Olariu, Julio Leva López, Rattanaporn Fongngern, Cristian Carvajal and Carlos Uroza. Excellent laboratory and field assistance provided by Michael Markowski, Liz Rhinehart, Elisabeth Steel and Julio Leva was very helpful in getting the different projects well on their way.

I owe special thanks to Andy Petter for the many discussions which helped refine the arguments I present here, for fun times in the field and for being a great source of support along the bumpy way to completing this degree. The success of the Brushy Canyon field project was largely because Andy helped me to focus the project goals early on, rather than to try and solve three different problems at the same time.

Funding for the field work in west Texas, provided by the RioMAR consortium of oil companies, the Jackson School of Geosciences and the Ike Crumbly AAPG Grant-in-Aid is gratefully acknowledged. I also acknowledge the funding for the experimental work, provided by RioMAR and the SEPM Weimer Research grant. I thank Statoil for covering expenses related to lodging and travel during my visits to Norway to work on the seismic data. I thank the West Texas Geological Society for the generous John Emery Adams financial award.

I must also thank the many people who work behind the scenes at the Jackson School, many of whom have done much to keep me on track and out of trouble at various times. Philip Guerrero, Candace Sandefur, Ty Lehman, Adrian Huh, Julie Lake, Michelle Damvar, Nicole Evans and Elsa Jimenez are just a few of these wonderful individuals. Philip's ability to swoop in and fix the worst situations often had me listening for the flapping of his cape. Of course, I must give special thanks to Ty, who often made time on the weekends to fix various computer-related emergencies and bought me a few more precious hours to complete those always-last-minute tasks.

I thank my dear friends, Marissa, Cheryl, Danae, Annabelle and Jessica, who were a great long-range cheering squad even though they never quite understood my fascination with rocks.

I thank my immediate and extended family for their encouragement and unquenchably quirky humor, even in the darkest of situations. I give special thanks to my brothers and sisters-in-law, Chetan & Shaamain and Ashish & Priya who have always supported my pursuit of higher studies. Finally, I owe an immeasurable debt of gratitude to my mother and late father, Bernadette and Errol Fernandes, who have been the strongest of models of faith, courage and resilience a young person could ask for.

QUANTIFYING THE SEDIMENTOLOGY, STRATIGRAPHY AND MORPHODYNAMICS OF SUBMARINE CHANNELS

Anjali Mary Fernandes, Ph. D.

The University of Texas at Austin, 2012

Supervisors: David Mohrig and Ronald Steel

This dissertation examines how turbidity currents interact with submarine channels. Turbidity currents display exaggerated super-elevation at the outer banks of channel bends, because they have low excess densities relative to the ambient sea-water. Low-velocity zones form where flows separate from the inner banks. In a high-resolution seismic volume, I mapped 226 inclined surfaces associated with bank-attached bars in 16 channel bends of 2 buried sinuous channels. Position and geometries of bars indicate construction from suspended sediment in flow separation zones. Concave-bank benches, first identified in rivers where they are built from fully-suspended sediment deposited within flow separation zones in channel bends, comprise approximately 19% of this data-set. Bars have high median slopes (10^{o}-11^{o}) and occupy less than 30% of channel width. Associated channels migrated a median distance of less than 70% of the channel width and incised 20-30% of the channel depth. These bars are therefore interpreted to have formed during sediment bypass or weak erosion.

I have analyzed the sedimentology and stratigraphy of a well-exposed channel complex, in the Permian Brushy Canyon Formation, west Texas. A steeply-inclined set of fine-grained sandstone beds (median dip=10^{o}) at the margin of the channel complex is interpreted as deposits of a bank-attached bar. Beds are characterized by sub- to super-

critically climbing ripple-lamination, planar stratification and trough cross-stratification. Paleo-transport directions are at high angles, 20-120^{o}, to the dip azimuths of interpreted bar surfaces. Geometries of bounding surfaces, sedimentation styles and grain-size data were used to construct a facies model for suspension-dominated, bank-attached bars, built within flow-separation zones in submarine channels.

I designed physical experiments to examine how erosional turbidity currents evolve channel- bend topography. Time-lapse bathymetry maps capture the evolution of raised benches tied to sedimentation within flow separation zones and erosion outside of separation zones. Erosional currents showed sensitivity to local conditions. The pattern of erosion was connected to roughness elements such as bend curvature and scours on the bed. Turbidity current run-up at the outside of bends produced a greater aerial extent of side-wall erosion than is commonly seen in incisional rivers.

Table of Contents

List of Tables

List of Figures

Chapter 1: Introduction

Modern acoustic imaging techniques have revealed ubiquitous canyons and channels on modern and ancient continental margins. These features are constructed by turbidity currents which are turbulent mixtures of sediment and water. Sediment suspended within turbidity currents imparts a marginally higher density to them, relative to the surrounding sea-water. These currents are drawn down the continental slope by the influence of gravity on this suspended sediment. Continental margin stratigraphy is constructed chiefly by deposition from turbidity currents and comprises the best preserved sedimentary record of past environmental states on Earth. Ancient channel deposits built by turbidity currents also house some of the largest hydrocarbon accumulations on Earth. Unfortunately, the scientific community possesses only a few direct measurements of turbidity currents in natural channels (Hay, 1987; Khripounoff et al., 2003; Xu and Noble, 2009; Xu et al., 2009) and no measurements of how turbidity currents evolve channels. This inhibits our progress towards understanding the local and non-local factors that influence the construction of continental margin stratigraphy by turbidity currents.

Scientists who study deep-water landscapes often use terrestrial analogs to understand the morphodynamics of submarine channels. The morphometrics of submarine and terrestrial channels has been shown to compare favorably (Pirmez and Imran, 2003). A crucial difference between these two environments is the ratio of densities of the transporting flows and the ambient fluid. In rivers, where water flows through air, this ratio is approximately 800; in submarine channels it is 1.01-1.10 (Straub et al., 2011). This ratio impacts the ways in which turbidity currents interact with topography. Channels which remain active for many thousands of years are often constructed by flows that are much thicker than the channel relief (Mohrig and

Buttles, 2007). Turbidity currents are also relatively insensitive to negative slopes and are capable of travelling up negative inclines for a considerable distance (Straub et al., 2011; Straub et al., 2008). These phenomena are never observed in terrestrial landscapes. Models that characterize the evolution of submarine channels therefore serve as useful complements to test the accuracy of models capturing the evolution of terrestrial channels. On channelized landscapes of other planets and moons (eg: Titan, Venus), the ratios of densities of transporting media to ambient fluid have been shown to fall between these ratios for sub-aerial and submarine environments on Earth (Straub et al., 2011). Models of landscape evolution for terrestrial and submarine environments therefore offer valuable insights into the evolution of extra-terrestrial landscapes.

The three papers presented in this dissertation contain three complementary data-sets. These data-sets are all targeted towards understanding how turbidity currents modify submarine channels through erosion and deposition. Because of their low excess densities, turbidity currents flowing through channel bends climb far up the outer channel banks (Straub et al., 2011). As a result, a low-velocity zone forms where flow separates from the inner banks. Straub and others (2011) document the formation of bars within flow separation zones in experimental channel bends. In this dissertation, I investigate the interactions of turbidity currents with channels under net erosional conditions, and at a range of spatial and temporal scales.

In Chapter 2, I use a data-set of 226 bar surfaces mapped in 16 channels bends of 2 buried submarine channels. These surfaces were mapped in a high-resolution seismic volume which images the Miocene and Oligocene continental slope of West Africa. I compare the quantitative shape of the final channel to the location and accretion geometry of bank-attached bar packages. Three basic bar shapes related to channel curvature are documented; shapes that

are convex or concave towards the final channel, and shapes that show low curvature. I systematically compare geometries of bars from submarine channels and rivers, including their surface slopes, cross-channel widths and their relationship to channel curvature. These comparisons are used to evaluate whether the mapped barforms were constructed dominantly by suspended load or by bedload. Presented data will show that the geometry and positions of mapped bars indicate that they were constructed predominantly from suspended sediment load. The methods used make a connection between morphology and process, which is useful when reconstructing environmental states from ancient landscapes. This study suggests that suspension-dominated bars built in zones of flow-separation in submarine channels have been under-recognized.

In Chapter 3, I present the mapped sedimentology and stratigraphy of an exposed submarine channel complex in the Brushy Canyon Formation of west Texas, USA. I systematically characterize a well-exposed bar situated within the deposits of a submarine channel complex in the Upper Brushy Formation. Current interpretations of bank-attached bars in submarine channels draw heavily on models for bedload-dominated, bank-attached bars in rivers (Abreu et al., 2003; Arnott, 2007; Dykstra and Kneller, 2009; Pyles et al., 2009). The mapped barform is interpreted to have developed in a low-velocity zone of flow separation at the channel margin. I contrast the bar deposits against deposits filling the thalweg of a submarine channel in the same complex, as well as deposits filling channels on the proximal basin floor. Granulometry, sedimentary structures and bed geometries are used to determine what material is being deposited in zones of high and low velocity in the upper slope setting, and to compare this against sedimentary structures and textures observed filling channels in a toe-of-slope setting. This comparison is used to define the particle sizes which are preferentially deposited on the

slope versus those which are transferred long distances onto basin floor. Sedimentary structures, bed geometries, and grain size data are used to: 1) estimate the paleo-hydraulic properties of the turbidity currents which constructed the slope channels stratigraphy; and 2) construct a facies model for thick, bank-attached bars built from sediment sourced from suspended load.

In Chapter 4, I use a targeted series of physical experiments to characterize how erosional turbidity currents modify subaqueous channel bends. Physical experiments have been effectively used to analyze the interactions between strongly depositional turbidity currents and channel bends (Straub and Mohrig, 2008; Straub et al., 2011; Straub et al., 2008). I use three experimental series to evaluate how patterns of erosion and deposition are affected by: 1) roughness elements such as bend curvature and scours on the bed and 2) the sediment transport capacity of currents. High resolution bathymetry maps and velocity measurements are used to define difference in the processes which modify incisional channels in the submarine and terrestrial environments. Turbidity currents running up at the outside of channel bends produced a larger aerial extent of side-wall erosion than is commonly seen in incising rivers. Bathymetry maps show the dynamic evolution of raised benches as a result of sedimentation within flow separation zones and erosion outside of separation zones. This data offers fresh insights into the origin and significance of similar benches which form in natural submarine channel bends.

Chapter 2: Geometries and Inferred Depositional Processes in Bank-attached Barforms in Sinuous Submarine Channels

INTRODUCTION

Recent technological advances in remotely-sensed data acquisition have provided the scientific community with high-resolution, three-dimensional, acoustic imaging of submarine channels on Earth's modern and ancient continental slopes (Jobe et al., 2011; Mayall et al., 2006; Normark et al., 1983). These channels often possess a sinuous planform, which has prompted frequent comparisons between geomorphic elements in submarine channels and those observed in meandering rivers (Kolla et al., 2007; Pirmez and Imran, 2003; Shepard, 1966; Shepard and Buffington.E.C., 1968; Shepard and Emery, 1973). One important element of both submarine channels and rivers are bank-attached bars associated with channel curvature. The processes governing the evolution of bank-attached bars in submarine channels have been a subject of enthusiastic study in the last decade (Abreu et al., 2003; Arnott, 2007; Dykstra and Kneller, 2009). These bars in turbidite-filled sinuous submarine channels can be important hydrocarbon reservoirs (Labourdette, 2007; Labourdette and Bez, 2010). Bar geometries preserve the migration history of the depositional bank of migrating sinuous channels. They are thus of interest to scientists studying the evolution of channelized landscapes in different environments. Due to the general infrequency of flow activity through sinuous channels on continental slopes and their highly energetic behavior, the in situ observation of turbidity current flow dynamics and sedimentation has been rare (Hay, 1987; Khripounoff et al., 2003; Xu and Noble, 2009; Xu et al., 2009; Xu et al., 2008). Thus, innovative techniques are required to relate morphology to processes of bar construction.

A variety of approaches and data-sets have been used to study flow fields in submarine channel bends and the processes associated with the deposition of bank-attached bars. These include the interpretation of three-dimensional seismic data (Abreu et al., 2003), outcrop characterization (Arnott, 2007; Dykstra and Kneller, 2009), numerical modeling (Das et al., 2004; Imran et al., 1999; Parker et al., 2001) and physical experimentation (Amos et al., 2010; Straub et al., 2011). The three-dimensional geometry of submarine channel barforms was first investigated using high-resolution seismic data (Abreu et al., 2003). The same authors presented core that penetrated submarine bars in the Girassol field, Block 17, offshore Angola. Channel 1, discussed in the present work, is part of the same channel complex. Bank-attached bars in outcrop have been interpreted at a range of scales displaying both bedload-dominated and suspension-dominated depositional styles (Abreu et al., 2003; Arnott, 2007; Dykstra and Kneller, 2009; Pyles et al., 2009). While details of barforms are well-preserved in outcrop, the shape of the associated channel and channel bends can seldom be directly observed. In addition to outcrop- and seismic-based studies, experimental observations have provided substantial insight into the formation of bars in submarine channels. Bars were reported by Straub and others (2011) to form in an experimental, sinuous, subaqueous channel modified by depositional turbidity currents. These bars developed just downstream of bend apices in zones of low-velocity connected to flow separation from inner-banks, as the current travelled around channel bends. The bar deposits were enriched in those particle sizes being transported in suspension and showed no evidence of being reworked once the sediment fell out of suspension; a testament to the relatively low current velocities in these separation zones.

Different transport processes build bank-attached bars in sinuous channels. Bars may be built predominantly from bedload by the down-channel movement of dunes which leave behind

some fraction of their mass (Dietrich and Smith, 1984) or built predominantly from suspended-load depositing in relatively protected zones along the channel bank (Smith et al., 2009). It is important to distinguish these processes, using subtle differences in shape and location, if we want to develop accurate environmental reconstructions of ancient landscapes.

The present work relates the quantitative shape of the final channel to the location and accretion geometry of multiple bank-attached bar packages. I document three basic bar shapes related to channel curvature; shapes that are convex or concave towards the final channel and shapes that show low curvature (Fig. 2.1, A). A quantitative comparison of bar geometries from submarine channels and rivers, including comparisons of surface slopes, cross-channel widths of bars and their relationship to channel curvature, is presented.

FLOW-FIELDS AND SEDIMENTATION IN RIVER BENDS

The most complete investigations of bank-attached bars are point bars built out of sediment deposited from bedload at the inner banks of channel bends (Bridge and Jarvis, 1982; Dietrich and Smith, 1984; Dietrich et al., 1979, 1984). These investigations show that point bars grow by accretion of sediment across the apex of bends. In planview, accretion patterns of these bars are expressed as distinct ridge and swale topography that is convex towards the associated channel. These bars grow until they achieve a stable lateral slope set by the balance of: (a) gravitational force which acts to move grains down the sloping bar surface towards the thalweg, and (b) the fluid drag associated with cross-channel helicoidal flow which acts to move the grains up the sloping bar surface towards the inner bank (Ikeda, 1989; Parker et al., 2003; Seminara et al., 2002). The lateral slope associated with the force balance connected with stable point bars usually ranges between 4 and 8 degrees. The width of a point bar may occupy up to

85% of the total channel width as documented in Muddy Creek, Wyoming, U. S. A (Dietrich et al., 1979). The slopes and cross channel widths of point bars from some well-studied rivers have been tabulated in Table 2.1.

Cohesion of the outer bank, which influences the rate of outer bank erosion, will also influence the channel asymmetry (Ikeda, 1989). Accretion along the inner bank of meanders may narrow the channel cross-section, reducing cross-sectional area and thereby increasing flow velocity and erosion at the outer bank (Nanson and Hickin, 1983). In addition, pronounced asymmetry concentrates accelerations of the high-velocity core of channelized flow against the outer bank of the sinuous bend, increasing rates of outer bank erosion and forcing lateral migration of the channel (Ikeda, 1989). Thus, channel asymmetry may be inferred to reflect as well as influence channel migration rates.

River bends associated with point bar development may migrate laterally over distances equal to several channel widths eg: River Endrick (Bluck, 1971). Many point bars transition downstream from bedload-dominated deposits near the bend apex to deposits built predominantly by suspended-load sedimentation (Hickin, 1979). These suspension-dominated deposits are connected to zones of low-velocity and flow separation along the channel bank (Fig. 2.2). The position of flow separation and re-attachment is connected to bank curvature and overall flow velocity. A mixing front develops along the interface between this zone of relatively static fluid and the high velocity portion of the main flow (Fig. 2.2). This front is characterized by turbulent eddies which bring parcels of fluid from the main current into this low-velocity zone. Bars in the separation zone are constructed from sediment advected into the low-velocity zone by these eddies. Bedload sediment does not cross the mixing front to enter the separation zone (Rubin, 1990; Rubin et al., 1998). Bars developing in these flow separation zones have

been called concave-bank benches (Hickin, 1979; Hickin, 1986; Page and Nanson, 1982; Taylor and Woodyer, 1978; Woodyer, 1975), counter point bars (Smith et al., 2009) and eddy accretions (Burge and Smith, 1999; Burge et al., 1996). Concave bank benches usually form just upstream of bend curvature at the outer bank of bends or across bend inflection points. They are concave towards the channel in planview. This concavity may be large or relatively small.

Widths of these bars are restricted by the width of separation zones, which is a small fraction of channel width (Hickin, 1979). The deposits of suspension-dominated bars drape pre-existing topography and are subject to only little reworking from eddy currents. Thus, they are able to maintain higher slopes than bedload-dominated bars, and may show a wider range of slopes. Burge and Smith (1999), measured eddy-accretion surface slopes of 25 degrees on the Kootenay River, Saskatchewan. Smith et al. (2009), measured counterpoint bar slopes that reached a maximum of 29 degrees on the Peace River, Canada. The slopes and cross channel widths of suspension-dominated bars from some rivers have been tabulated in Table 2.1.

Table 2.1: Geometric attributes of bedload-dominated and suspension-load-dominated bars in modern meandering rivers.

	River Names, Locations and Data Source	**Bar slopes**	**Widths of bars standardized by channel width**
Bedload dominated bars (point bars)	Muddy Creek, Wyoming, U. S. A. (Cross section constructed from bathymetry map) (Dietrich et al., 1984)	7.69	0.8
	Atchafalaya River (Cross section constructed from bathymetry map) Location : Meander near St. Martin Parish and St. Landry Parish (Atchafalaya River Hydrographic Survey, 2006)	4.36	0.82
	South Esk River, Scotland (Cross section constructed from bathymetry map) (Bridge and Jarvis, 1982)	7.59	0.69
	Trinity River, Texas, U. S. A. (Cross-sections from bathymetry surveys collected by Virginia Smith, Univ. Texas at Austin)	5.06	0.85
	Teshio River (Cross-sections through three point bars) (Ikeda, 1989a)	Bar 1: 11.5 Bar 2: 5.15 Bar 3: 8.21	0.70-0.80
	Klip River, South Africa (Published cross-sections) (Marren et al., 2006)	9.82	0.80
Suspended load dominated bars (concave bank benches, counter point bars, oblique accretions)	Squamish River, British Columbia, Canada (Measured from published cross-sections) (Hickin, 1979)	-	0.4
	Murrumbidgee River, Australia (Page et al., 2003)	5-29	-
	Peace River, Canada (Widths measured from published cross-sections) (Smith et al, 2009)	3-22	0.42
	Kootenay River, Canada (Burge & Smith,1999)	25	-
	Beaver River, Canada (Burge & Smith,1999)	25	-

COMPARISON BETWEEN FLOW IN BENDS OF SUBMARINE CHANNELS AND RIVERS

A key difference between currents traversing submarine channel versus river bends is the density of the current relative to the ambient fluid. Water, the transporting medium in rivers, is roughly 800 times denser that air. On the other hand, turbidity currents which are dense mixtures of sediment and water, are typically 1.01-1.1 times denser than the sea-water through which they travel (Straub et al., 2011). As a result of this difference, channelized turbidity currents can: (i) be considerably thicker than the channels they traverse (Mohrig and Buttles, 2007); (ii) show strong super-elevation at the outside of channel bends due to a combination of centrifugal effects and current run-up (Straub et al., 2008)(iii) easily separate from the inner bank of bends resulting in a well-developed zone of low velocity (Straub et al., 2011). Experimental data presented by Straub et al. (2011) showed that barforms developed in these zones and were characterized by the absence of bedload transport, consisting of the finer grain sizes in the system. The widths of these bars (Fig. 2.3) appear to be constrained by the width of the separate zones which is a small fraction of the channel width (Hickin, 1979; Straub et al., 2011)These bars built in zones of flow separation are markedly different from bars built from bedload as shown by Amos and others (2010) and Chapter 4. These bars have widths that scale with the entire channel width as with most point bars constructed by bedload in rivers (Table 2.1).

DATA-SETS AND METHODOLOGY

The two studied channels were mapped in a high-resolution seismic volume that has a horizontal grid spacing of 6.25m by 6.25m and a dominant frequency of approximately 65Hz. This seismic data is of sufficient quality to resolve individual bar surfaces defining the lateral

migration of channel bends. Continuous reflections within the seismic data have been shown to define lithologic boundaries (Abreu et al., 2003) and were used here to define bar surfaces and the final channel form. These surfaces were mapped as horizons on every inline and cross-line so that no interpolation or smoothing algorithms were necessary. The geometries of bar surfaces were then analyzed and compared to geometries of bank-attached bars from meandering rivers (Table 2.1).

THE SUBMARINE CHANNEL BANK-ATTACHED BARS

The two buried submarine channels described developed on the upper continental slope, roughly 200km from the shelf edge. Channel 1 evolved within confining levees and is the youngest channel in a long-lived channel fairway (Fig. 2.4). Bar packages associated with 11 channel bends were mapped in a continuous channel reach ~18km long (Fig. 2.5). The total number of mapped bar surfaces from this channel is 125. The channel shows an average depth of 44m, an average width of 435m and a sinuosity of 2.36 (Fig. 2.4; Fig. 2.5).

Channel 2 evolved within a canyon and has an average width of 550m, an average depth of 66m, and sinuosity equal to 1.81 (Fig. 2.6, A, B, E) . The planform of 101 bar surfaces in 5 bar packages associated with 3 channels bends and the final channel were mapped in a continuous segment that extends ~8km downstream (Fig. 2.2).

Table 2.2: Geometry of preserved bar forms in the two buried submarine channels (See Fig. 2.03 for the schematic showing how different parameters were measured).

		Median bar height standardized by average channel depth h/D_{avg} (See Figure 2.03)	**Median bar slope (degrees)**	**Median bar width standardized by average channel width w/W_{avg} (See Figure 2.03)**
Submarine Channel 1	Convex Bar Surfaces	0.3	8.58	0.22
	Low Curvature Bar Surfaces	0.4	10.7	0.23
	Concave Bar Surfaces	0.5	11.8	0.28
	All Bar Surfaces	0.4	10.5	0.23
Submarine Channel 2	Low curvature Bar Surfaces	0.22	11.14	0.15
	Concave Bar Surfaces	0.22	10.35	0.17
	All Bar Surfaces	0.22	10.9	0.16

GEOMETRIC ANALYSIS

The following geometric parameters were measured and used to characterize the properties bars and the two channels.

(i) Channel Curvature

Channel curvature was evaluated every one-half channel width along the centerline. Figure 2.7A shows the curvature values at each of these locations measured in degree/m. Curvature values associated with these high amplitude bends range from 0.15 to 0.35 degrees/m with a mean value of 0.25 degrees/m. Bars in bends with these high curvatures have been shown to be locked in position by the channel planform and can only evolve as the channel bend migrates (Whiting and Dietrich, 1993c)

(ii) Bar shape and relationship to channel curvature

Planform shapes of bar surfaces were used to define three categories (Fig. 2.1A):

1. Convex bar surfaces (Cvx): The bar surfaces are convex towards the final channel.

2. Concave bar surfaces (Ccv): These bar surfaces are concave towards the final channel.

3. Low curvature bar surfaces (LC): These bar surfaces have low curvature (tending to straight) in planform.

Consecutive bar surfaces record the deformation of the channel form through time. The oldest bar surfaces in each bend cannot be reliably connected to the shape of the preserved channel. Therefore, in order to evaluate the connection between bar surface shape and the shape of the local channel, only the youngest bar surfaces were used (Fig. 2.7A). Here I report the results for Channel 1, due to the greater number of bends mapped in this system.

This analysis shows that:

a) Convex bar surfaces either extend across or initiate at maximum channel curvature (Fig. 2.7A,B, eg: bars at points 21, 35), or initiate at maximum curvature and extend to minimum channel curvature. (Fig. 2.7A, B, eg: bar at point 12). Convex bar surfaces appear similar to point bars in terms of their location with respect to the bend apex.

b) Concave bar surfaces initiate near the point of minimum channel curvature and always terminate just upstream from the point of maximum channel curvature. (Fig. 2.7A. D, eg: bar at point 47)

c) Low curvature bar surfaces initiate at the highest channel curvature and extend to near the point of minimum curvature. (Fig. 2.7, A, C)

Low curvature and concave-shaped bars are morphologically similar to counterpoint bars and concave-bank benches in rivers (Hickin, 1979; Hickin, 1986; Smith et al., 2009)n (Fig. 2.2).

(iii) Preferred sites of bar growth

The relationships established in the above section has been applied to all the mapped bar surfaces in both channels. The percentages of these three bar shapes are summarized in Figures 2.1 B and C. Convex surfaces make up 18.4% of all mapped bar surfaces in Channel 1. Concave and low curvature surfaces make up 13.6% and 68.0% of mapped surfaces, respectively. Bar surfaces from Channel 2 are limited to low curvature (73.2%) and concave (26.7%) shapes only.

(iv) Bar Heights, Slopes and Widths

Figure 2.3 shows the schematic representation of the different geometric parameters measured. The heights (h) of bars were measured in those cases where the upper and lower terminations of bar surfaces were preserved and imaged (Fig. 2.3). Widths (w) of bar surfaces were the horizontal distances measured between the upper and basal terminations of fully preserved bar surfaces (Fig. 2.3). The reported bar surface slopes (h/w) always represent the steepest line of descent down a bar surface (Fig. 2.3). The widths of youngest bars surfaces were also measured from the inner side-walls of the final channel from four different channel bends in Channel 1.

Figures 2.8A and B present histograms of bar height standardized by average channel depth for the convex, low curvature and concave barforms in both submarine channels. Ninety-one data points were used from Channel 1 and 58 were used from channel 2. The three different

bar categories do not show much variation in standardized bar height, with the median height falling between 30-50% of channel depth for Channel 1 and 22% for Channel 2. Figures 2.9 A and B are histograms of bar surface slopes for both submarine channels. For the purpose of comparison, these figures also include range bars for the slopes of bedload- and suspension-dominated bars in rivers. Median slopes for convex, low curvature and concave bars in channel 1 are similar and range between 8.5 and 12 degrees. Low curvature and concave bars in Channel 2 show median slopes equal to 11 and 10 degrees respectively. Maximum bar slopes of 17-18 degrees were recorded. Median width measurements of bars in both submarine channels indicate that bars occupied approximately 22-28% of the channel cross-section in Channel 1 and 15-17% of the larger Channel 2 (Fig. 2.10 A and B). Bar widths measured from the four channel cross-sections through Channel 1 show that the youngest bars occupied roughly 40-50% of the cross-channel width (Fig. 2.11B). Measured bar heights, widths and slopes in the studied submarine channels are compiled in Table 2.2.

(v) Channel migration during bar formation

Measurements indicate that both Channel 1 and Channel 2 have migrated over relatively short distances relative to channel width. The initial channel planform of submarine Channel 1 was reconstructed using the average width of the final channel and the first definable accretion surface for each studied bend. Centerlines of the final channel and the reconstructed initial channel were used to define the distance migrated by each bend apex as the bend evolved (Fig. 2.12, A). Only Channel 1, due to the variety in bend shapes and the greater number of mapped bends, was analyzed in this way.

Bend apices have migrated farthest. Apices in Channel 1 display lateral migration over small distances equal to 0.4-2.4 times the channel width. Figure 1.12B is a histogram plot of the measured migration distances of individual channel bend apices, standardized by average channel width. Median apex migration distance for this data-set is equal to 70% of average channel width.

(vi) Weak channel incision during bar formation

Channel 1 was found to be weakly incisional during bar formation. To quantify the degree of downcutting, difference in elevation between individual bar toes and the deepest part of the local channel was measured (Z_b) and then scaled by local channel depth (D), given by the vertical distance from the outer levee-crest to the deepest part of the channel (Fig. 2.3). Where the computed distance between bar-toe and local channel base is positive, the channel has incised; where it is negative, the channel has aggraded. Figure 2.13 A show the distribution of all computed values for Channels 1 and 2 respectively. The majority of these values are positive, indicating general channel incision. The median of these values is roughly 19% channel depth or 18m, indicating that the channel incised roughly 19% of its final depth as it built laterally-accreting bars.

For Channel 2, the histogram plot Figure 2.13 B of bar-toe off-set from the local channel base shows a bi-modal distribution, with peaks at values of 0.1 and 0.4 for the ratio of bar-toe elevation above channel base to local channel depth. This is interpreted to represent two major phases of accelerated incision followed by weaker incision. Median values for bar-toe offset are inferred to represent median channel incision of roughly 28% of channel depth, i.e. 19m. Figure 2.14 investigates the occurrence of different phases of accelerated or weaker erosion. By plotting

the bar-toe offset from the local channel base through time within individual bar packages, I observe trends interpreted as accelerated or weaker incison rates with respect to channel migration rates (given by the slope of the black dotted line). Figures 2.14 A and B show a significant cluster of points near 40% of the channel depth, correlating with the flatter incision trajectory. This explains the peak on Figure 2.13B at 40% times channel depth. Figures 2.14A and C also show a cluster of points near 10% of the channel depth, contributing to the peak in the data at 10% of the channel depth.

COMPARING BAR GEOMETRIES IN SUBMARINE CHANNELS AND RIVERS

Bar geometries observed in the studied submarine channels were compared to both bedload-dominated and suspended-load dominated fluvial barforms from various meandering rivers around the world (Tables 2.1 and 2.2). In general, bedload- dominated river bars (point bars) have low slopes (4-11 degrees) and greater cross-channel widths (69%-85%) whereas suspended-load dominated bars (termed counter-point bars, eddy accretions and concave-bank benches by other workers) show a wide range of slopes, up to measured values of 25 degrees and cross-channel widths of 40-45%. Bedload-dominated point bars are therefore associated with greater cross-sectional asymmetry in rivers than suspension-dominated bars.

The preponderance of the studied submarine channel bars differ from fluvial bedload-dominated bars in that the former have steeper slopes and occupy less space in the associated channel (Fig. 2.9; Fig. 2.10; Fig. 2.11; Tables 2.1 and 2.2). Bank-attached bars in submarine channels and suspension-dominated bars in rivers show a greater geometric similarity; they occupy similar fractions of the associated channel and appear to form steeper slopes, sometimes approaching the submerged angle of repose (Fig. 2.9; Fig. 2.10; Fig. 2.11; Tables 2.1 and 2.2).

They also occur at similar locations when related to channel curvature i.e. in low curvature zones near the inflection points between bends and close to the concave outer bank of bends. Curvature relationships establish that submarine-channel bars which develop across maximum channel curvature are a minority in the submarine-channel data-set of bar surfaces.

DISCUSSION

Relating bar geometry and constructing process

Bar slopes in convex, concave and low curvature bar surfaces are similar, suggesting similar depositional processes for all three types (Fig. 2.9). The median slopes of 8.5-11.8 degrees are steeper than recorded slopes of river bars constructed from bedload deposition, and more similar to the higher range of values recorded for suspension-dominated bars in rivers (Fig. 2.9, Table 2.1). A maximum slope of 17 degrees was measured in this data-set. This value approaches the submerged angle of repose for cohesionless clastic sediment influenced by shear stress associated with turbidity currents (Kostic et al., 2002). These high slopes in submarine bank-attached bars suggest that they are constructed predominantly through suspended sediment deposition.

Low-curvature bar surfaces consistently initiate at the point of the highest curvature of the final channel and terminate near the inflection point between bends (Fig. 2.07, A and C). Concave bar shapes initiate close to or downstream of channel inflection points and terminate just upstream of maximum channel curvature (Fig. 2.07, A and C). Low curvature and concave bar surfaces are similar in form and location along channel curvature to the counter-point bars and concave-bank benches in rivers. Concave-bank benches and counterpoint bars form in flow

separation zones downstream of highly curving bends and are known to be locations dominated by suspended sediment deposition. Well-developed low-velocity, flow-separation zones have been documented in experimental sub-aqueous channels modified by turbidity currents and have been tied to the construction of bars (Straub et al., 2011). Figures 2.15, A and B, illustrate the interaction of a turbidity current with a sinuous channel. The formation of low-velocity zones where flow separates from inner banks is shown. The presented distribution of bar shapes shows that low curvature and concave bar surfaces are most common, whereas convex bars are less common (Fig. 2.01, B and C). The pre-dominance of these low-curvature and concave bar shapes suggests that submarine bank-attached bars commonly build in flow-separation zones associated with bend curvature. Convex bar surfaces are similar in planview to bedload-dominated point bars (Fig. 2.07, A and B). However, unlike point bars in rivers, they consistently show high slopes and small cross-channel widths in this data-set (Fig. 2.09; Fig. 2.10). Channel curvature strongly influences the upstream and downstream limits of the flow-separation zone (Straub et al., 2011, Chapter 4). Where a turbidity current encounters a high-amplitude bend (eg:, Bends 3 and 4 in Fig 2.05), it can be expected to separate from a large portion of the convex inner bank (Fig. 2.15). Convex-shaped bars with high slopes in this data-set are inferred to be the result of inner bank deposition within a flow-separation zone.

Cross sections through bars at submarine channel bends show a remarkable symmetry near maximum curvature (Fig 2.11, B). The surfaces of bars formed at the inner bank occupy only 40-50% of cross channel width (Fig. 2.10, A and B; Fig. 2.11, B). In contrast, cross sections through river channel bends with point bars show that the bar surface at the inner bank occupies between 60-80% of the channel cross section (Fig. 2.11, A). Pronounced asymmetry in cross-sections of rivers, induced due to rapid accretion of the inner bank, is widely believed to cause a

reduction of the channel cross-sectional area thereby increasing flow velocities (Parker et al., 2011). Erosion occurs at the outer bank of the river meander where the highest velocities are generally concentrated, thus forcing lateral migration of the fluvial channel. The symmetry of the submarine channel cross sections may suggest that inner bank accretion is the product rather than the driver of channel migration. The relatively small widths of these bar surfaces also suggest that their construction was restricted to the low-velocity flow-separation zones. Flow-separation zones usually occupy a small fraction of the channel width and are the only sites where suspended sediment can be deposited (Hickin, 1979). Bedload dominated bars would be expected to have widths which scale with the width of the channel.

Bar heights in the submarine channel dataset do not vary much between the three bar categories (Fig. 2.08). In Channel 1 median heights for the three categories all fall between 0.3 and 0.5 times the average channel depth (Fig. 2.08, A). In Channel 2, median bar height is 0.22 times the average channel depth for both low curvature and concave categories (Fig. 2.08, B). Similarity in bar heights in the two submarine channels suggests a similarity in the processes that construct these bar shapes. Interestingly, median bar height does not show much variation between submarine Channels 1 and 2. It is inferred that sediment accreting the bar faces was thus falling out from similar elevations within the flows, possibly indicating that the constructing flows did not vary too much in thickness.

Bedload-dominated river bars accrete rapidly and are usually associated with channels that migrate laterally over several channel widths (Bluck, 1971). Meandering rivers also exhibit frequent bend cut-offs. The two studied submarine channels have migrated over small distances and show no bend cut-offs (Fig. 2.05, A; Fig. 2. 06, E). The median apex migration in Channel 1 was 0.7 times the channel width (Fig. 2.12, B). This suggests that these bars did not accrete

rapidly and were associated with slow channel migration. Weak incision during channel migration and bar formation shows that these bars formed under conditions of sediment bypass and down-cutting.

Insights for outcrop studies of submarine channel barforms

Interpretations of submarine bank-attached bar outcrops have relied largely on models of bedload-dominated point bars in rivers (eg: Ross Formation, Ireland (Abreu et al., 2003); Rosario Formation, Baja California (Dykstra and Kneller, 2009); Tabernas Basin, Spain (Abreu et al., 2003); Windermere Supergroup, Canada (Arnott, 2007); Bruahy Canyon formation, west Texas (Pyles et al., 2009). These bars were interpreted to form from a combination of bedload and suspended load sedimentation.

These interpreted barform deposits are much thinner than the measured bar packages in the present work. The bulk of these examples also represent deposits on the margins of tectonically active basins. The relative proportions of bedload to suspended load travelling through these channels must be expected to be much higher than that in passive margin settings. I argue that the processes responsible for building these packages are likely to differ from the processes which build the steep, thick bar packages examined in this paper. It is always difficult, if not impossible, to constrain spatial information such as the channel depth and planform shape from outcrops. Channel shape exerts a first order control on the spatial patterns of flow and sediment transport. It is difficult to interpret the processes that construct these bars without this information. I suggest that suspension-dominated bank-attached bars have been under-recognized by scientists who study submarine channel outcrops. The insight provided by this study suggests that we should be looking for bars constructed from suspension in fine-grained

systems where most of the sediment travels in incipient or full suspension (eg: the Brushy Canyon Formation). Bars that are suspension-load dominated are can have a higher fraction of muddy sediment and will therefore weather poorly. The bars described in this chapter are also much larger than the scale of the average outcrop, and will thus be difficult to identify.

Concave-bank benches in sinuous submarine channels: Continuous or punctuated channel shifting?

Concave-bank benches, first identified in rivers, are known to form in low-velocity, flow-separation zones downstream of a high-curvature bend (Hickin, 1979; Woodyer, 1975). This is the first study to identify features similar to concave bank benches in submarine channels (Fig. 2.06, E). These features occur downstream of high curvature bends and/or at the concave outer-bank upstream of a high curvature bend, in probable low-velocity flow separation zones with possible flow recirculation.

Abreu et al., (2003), documented these features and interpreted them to be the result of punctuated channel shifting or "avulsion", but failed to record that these features consistently appear concave in planview and always show the same relationship with channel curvature. They note that some concave features are characterized by quasi-horizontal reflectors rather than the inclined reflectors usually associated with bars. They describe these geometries as "cut-and-fill" geometries and interpret that they are the result of channel avulsion. Other concave-shaped features in planview show closely spaced inclined reflections in cross-section and are described by Abreu et al., (2003) as characteristic of continuous lateral migration.

Our results indicate that the presence of concave-bank benches is entirely a result of channel curvature and are wholly unrelated to channel avulsion or punctuated shifting. The

cross-sectional shape of a concave bench is variable and should depend on the shape (width) of the flow separation zone: in a wide separation zone, the bar will aggrade vertically and develop predominantly horizontal stratigraphy; in a narrow low velocity zone, the bar deposits will drape the channel bank and create inclined strata. Recent experimental work (Straub et al, 2011; Chapter 4) illustrates how separation bar stratigraphy tends to drape existing topography.

CONCLUSIONS

The two studied submarine channels display sharp bend angles (30-70 degrees) associated with bar formation. Straight reaches between bends have lengths equal to 2-4 channel widths. High bend curvatures indicate that submarine bar evolution is connected to the evolution of channel bends, as in meandering rivers. Convex, concave and low curvature barforms have been identified in the studied submarine channels. I have established consistent relationships between the shapes of convex, concave and low curvature bar surfaces and the locations at which they occur along channel curvature (Fig. 2.07). Low curvature and concave bar surfaces are similar to counterpoint bars and concave bank benches from rivers and dominate the data-set of submarine bars. In rivers, these bars occur in low-velocity zones associated with flow separation and are constructed from suspended sediment load. This study is the first to document the presence of concave-bank benches in submarine channels (Fig. 2.06, E).

Most of the bars in this data-set form just downstream of high curvature bends and extend to just upstream of the next bend (Fig. 2.01). These are locations where flow separation normally occurs in rivers (Hickin, 1979; Hickin, 1986; Page and Nanson, 1982; Smith et al., 2009; Woodyer, 1975) and recently in experimental observations of channelized turbidity currents (Straub et al., 2011; Chapter 4). Figure 2.15 is a schematic which illustrates how

turbidity currents are inferred to interact with sinuous channels and how flow-separation zones form at the inner banks of bends. Internal shear between the faster moving fluid travelling with the high velocity core of the current and the slower moving or static fluid in protected zones down-stream of bend apices are inferred to generate eddies which advect sediment into these zones which are dominated by suspended-sediment fall-out.

Bars in the studied submarine channels were built during net bypass of sediment and some removal of sediment from the system, as indicated by observed weak incision seen in both channels (Fig. 2.13). The bases of some bar packages are shown to record phases of high and low incision rates relative to migration rates (Fig. 2.14).

The slopes of submarine channel bars are steeper and they fill less of the associated channel than bedload dominated bars in rivers (Fig. 2.09; Fig. 2.10, Fig. 2.11). In slope and cross-channel width, submarine channel bars resemble suspension dominated river bars. Heights of convex, concave and low curvature bars do not vary much (Fig. 2.08).

Symmetry of cross-section (Fig. 2.11) and very limited lateral migration (Fig. 2.12) observed in both the studied submarine channels suggest that these bars formed under conditions of sediment starvation, in low velocity zones away from the sediment-rich high velocity core of the current.

I conclude, therefore, that the geometries and patterns of evolution of submarine channel bank-attached bars and associated channel bends are consistent with a suspension-dominated sedimentation style rather than one characteristic of construction from bedload.

ACKNOWLEDGEMENTS

Financial support for this project was provided by the Jackson School of Geosciences, Statoil A.S.A. and the RioMAR consortium of oil companies. Many thanks to Sverre Henriksen for arranging access to the seismic data used for this work.

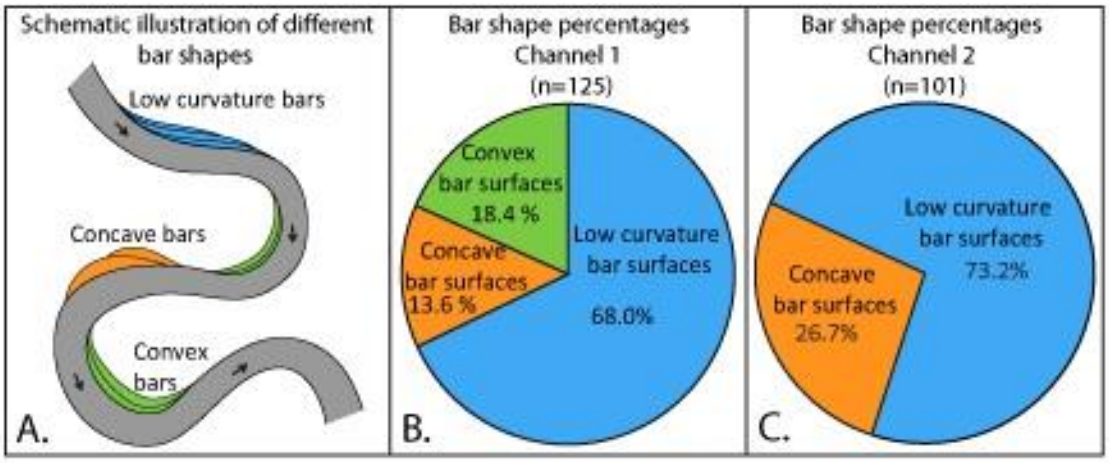

Figure 2.1: A) Schematic representation of bar shapes identified in the 2 studied submarine channels. In planview, convex bars are convex towards the channel, concave bars are concave towards the channel and low curvature bars are relatively straight. Percentages of convex, concave and low curvature bar surfaces mapped in Channel 1 (B) and in Channel 2 (C) are shown in pie-charts. Low curvature and concave bar surfaces, analogous to counter-point bars and concave-bank benches in rivers, dominate this data-set.

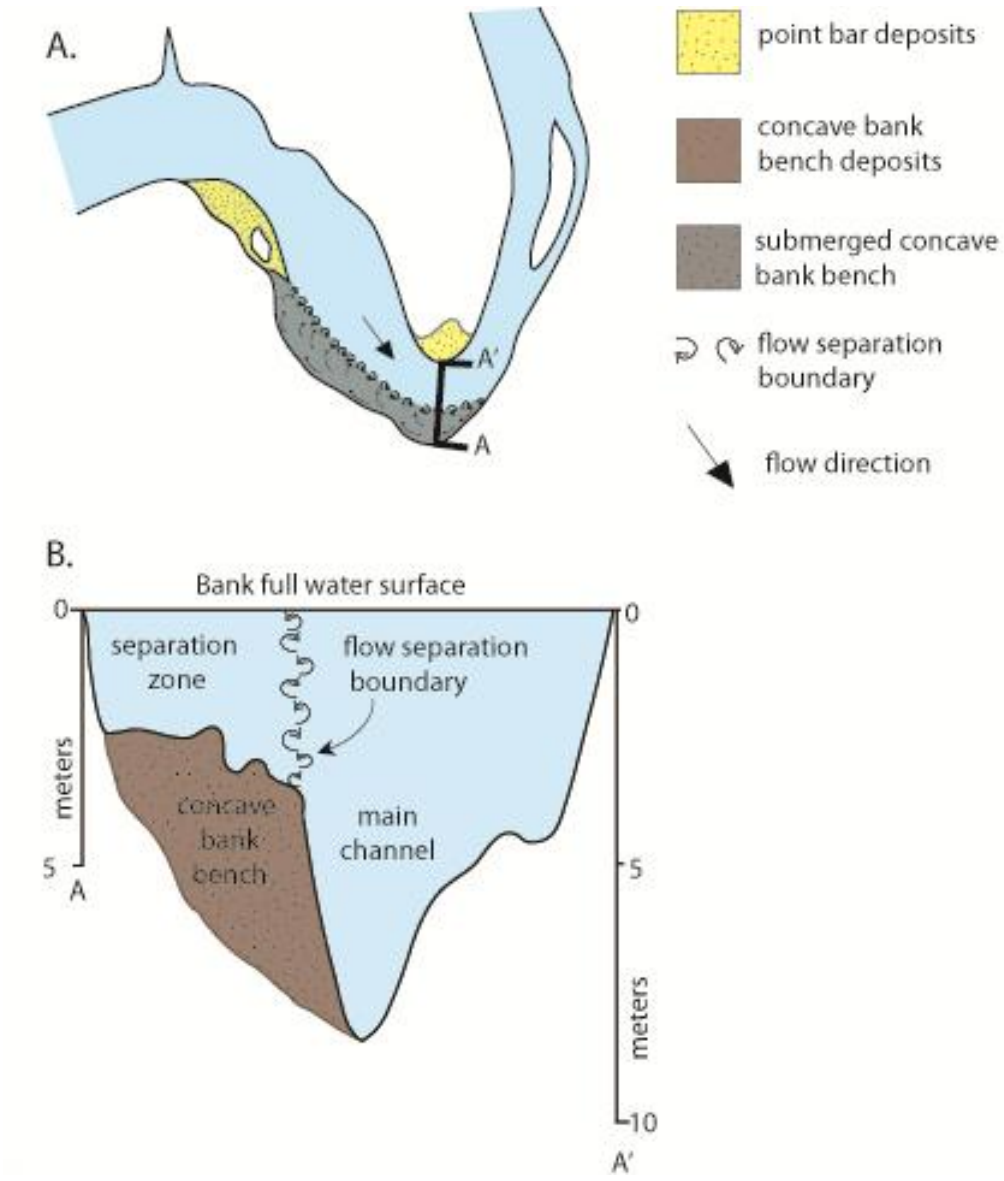

Figure 2.2: Sketch showing the planview and cross-section of a concave-bank bench on the Squamish River, in British Columbia (modified from Hickin, 1979).These suspension-dominated deposits are connected to zones of low-velocity and flow separation which develop along the channel bank, downstream of a protruding point bar.

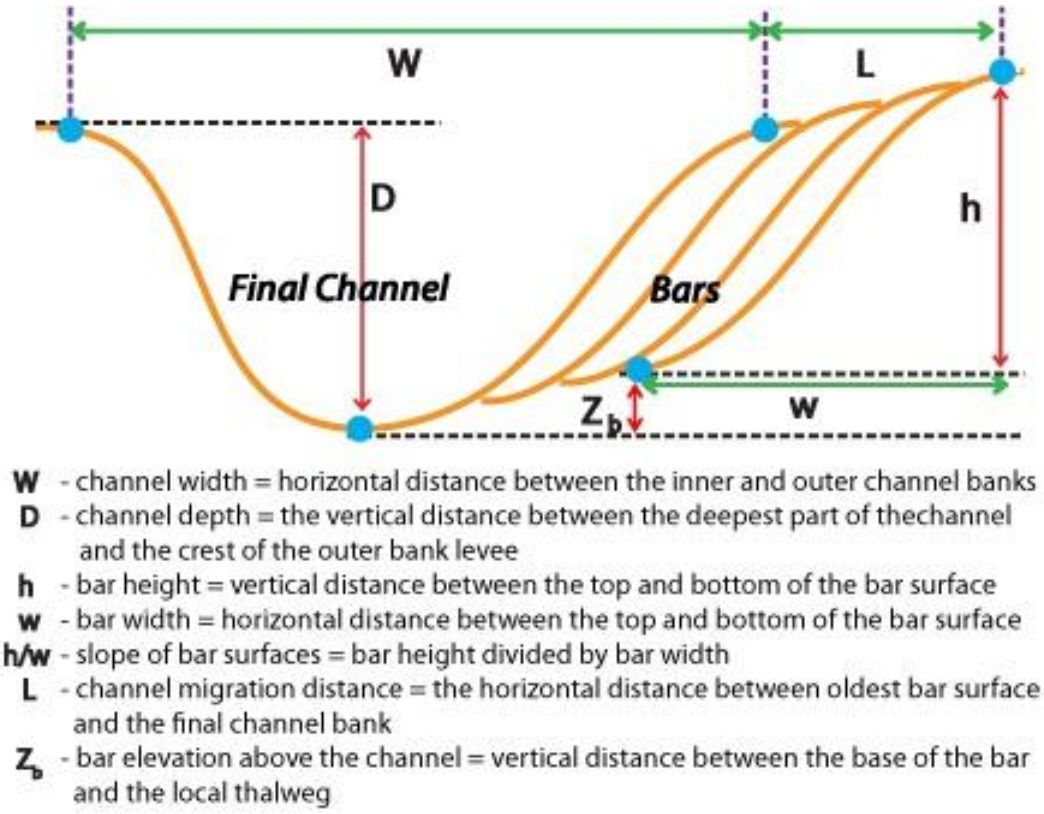

Figure 2.3: Schematic illustrating the different geometric parameters measured.

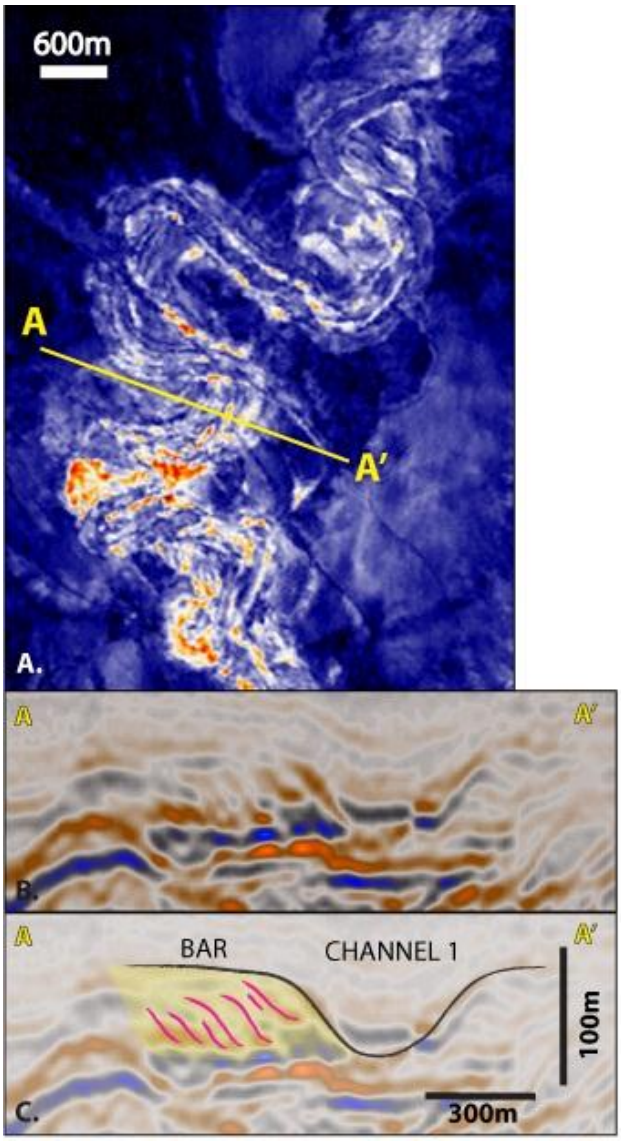

Figure 2.4: Seismic amplitude map (A) of the deposits associated with Channel 1. The seismic cross-section (B) and line-drawing (C) through A-A' shows the channel with the associated bar package. In the map and cross-section, hot colours indicate high reflection amplitudes (peaks) and cold colors indicate low amplitudes (troughs). Note the negative refections which are inclined towards the channel in (B) and (C). This package of reflectors is interpreted as the accreting bar package associated with the migrating bend.

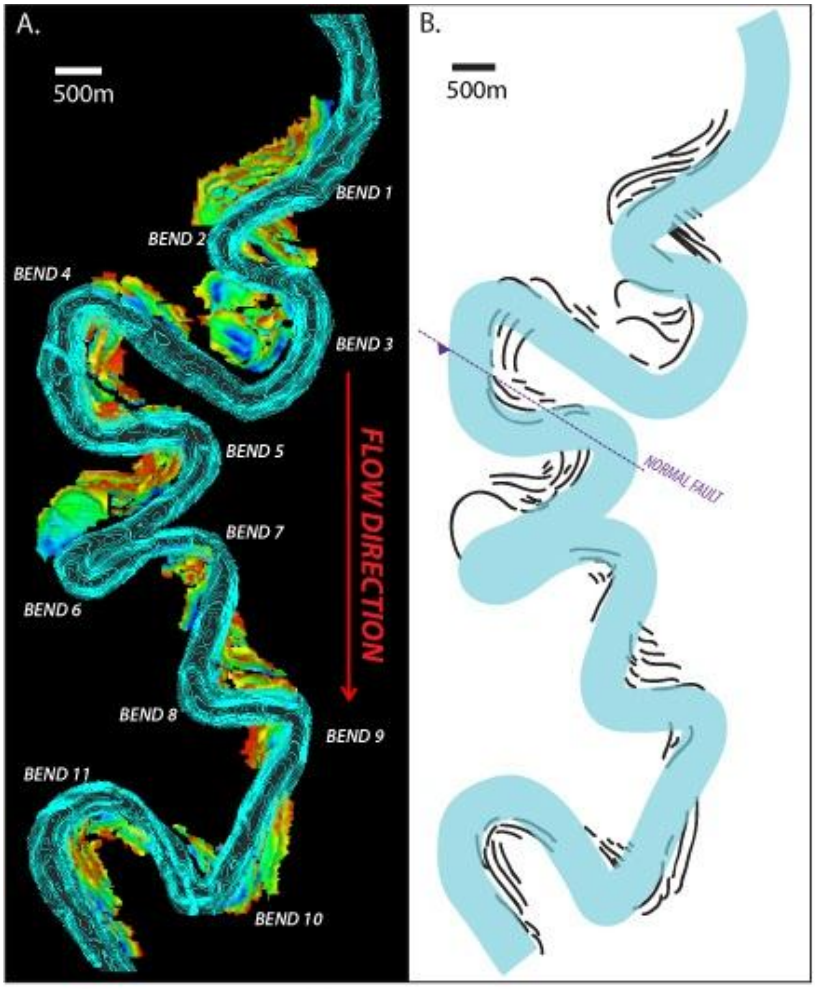

Figure 2.3: Map (A) and line drawing (B) of studied section of Channel 1 and its associated bar surfaces. These surfaces were generated by mapping the channel and each bar surface on every inline and cross-line in the seismic volume. The spacing between adjacent in-lines and cross-lines was12.5 m. The contour interval for the fine blue lines defining the channel is 3 m. Coloring on the bar surfaces represents relative elevation; red = topographic highs, blue = topographic lows. 125 bar surfaces were mapped in 11 bends of Channel 1. The associated channel was also mapped over a reach that was ~18km long.

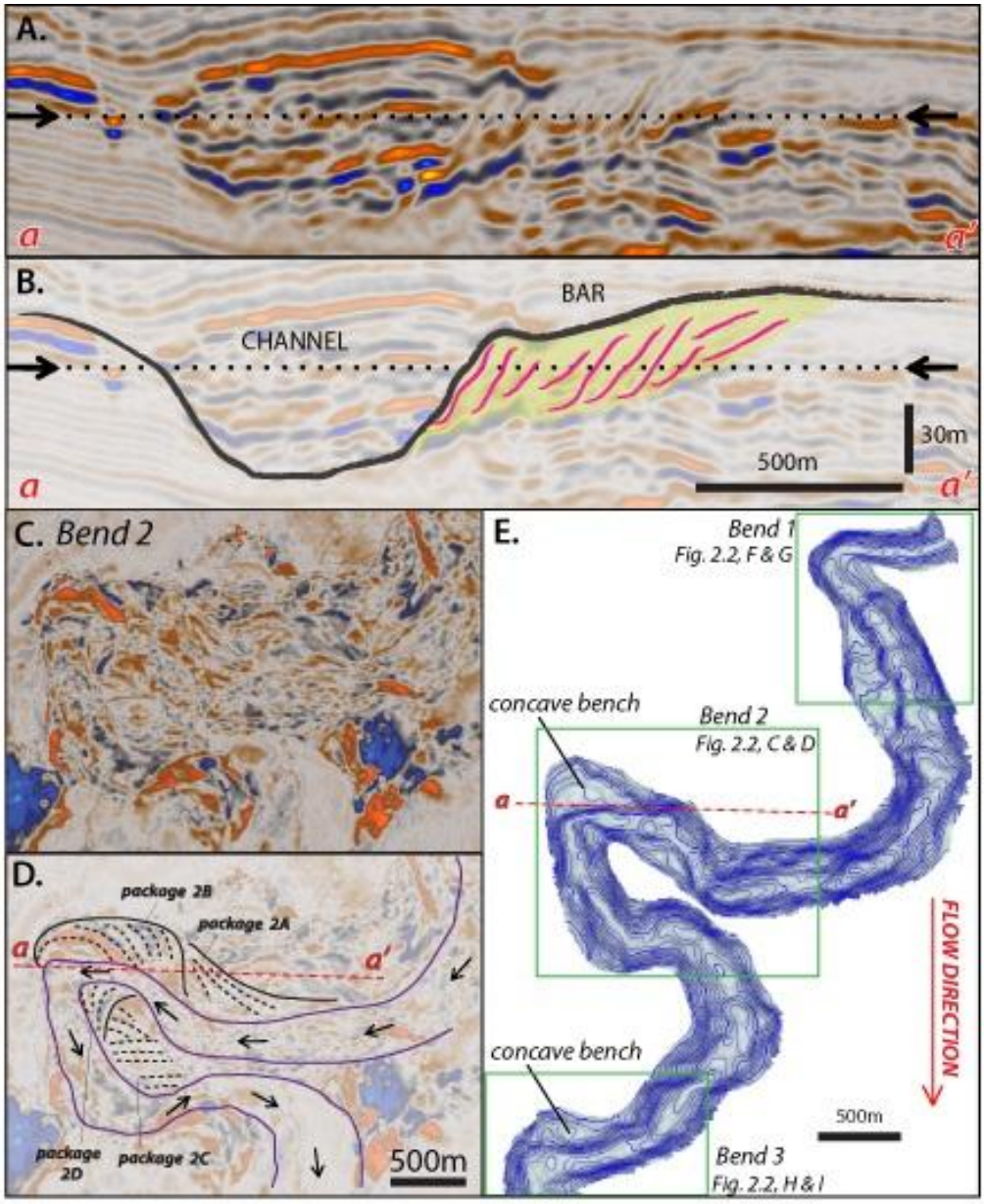

Figure 2.6: Seismic cross-section (A) and line-drawing (B) through a-a' shows Channel 2 with the associated bar package. Horizontal slice through the seismic volume (C) and line drawing (D) show bar packages associated with Bend 2. Arrows and dashed black lines on A and B indicate tthe location of the horizontal slice in C. Hot colours indicate high reflection amplitudes (peaks) and cold colors indicate low amplitudes (troughs). The mapped planform of Channel 2 is shown in (E). Blue contours in (E) are spaced at intervals of 5m.

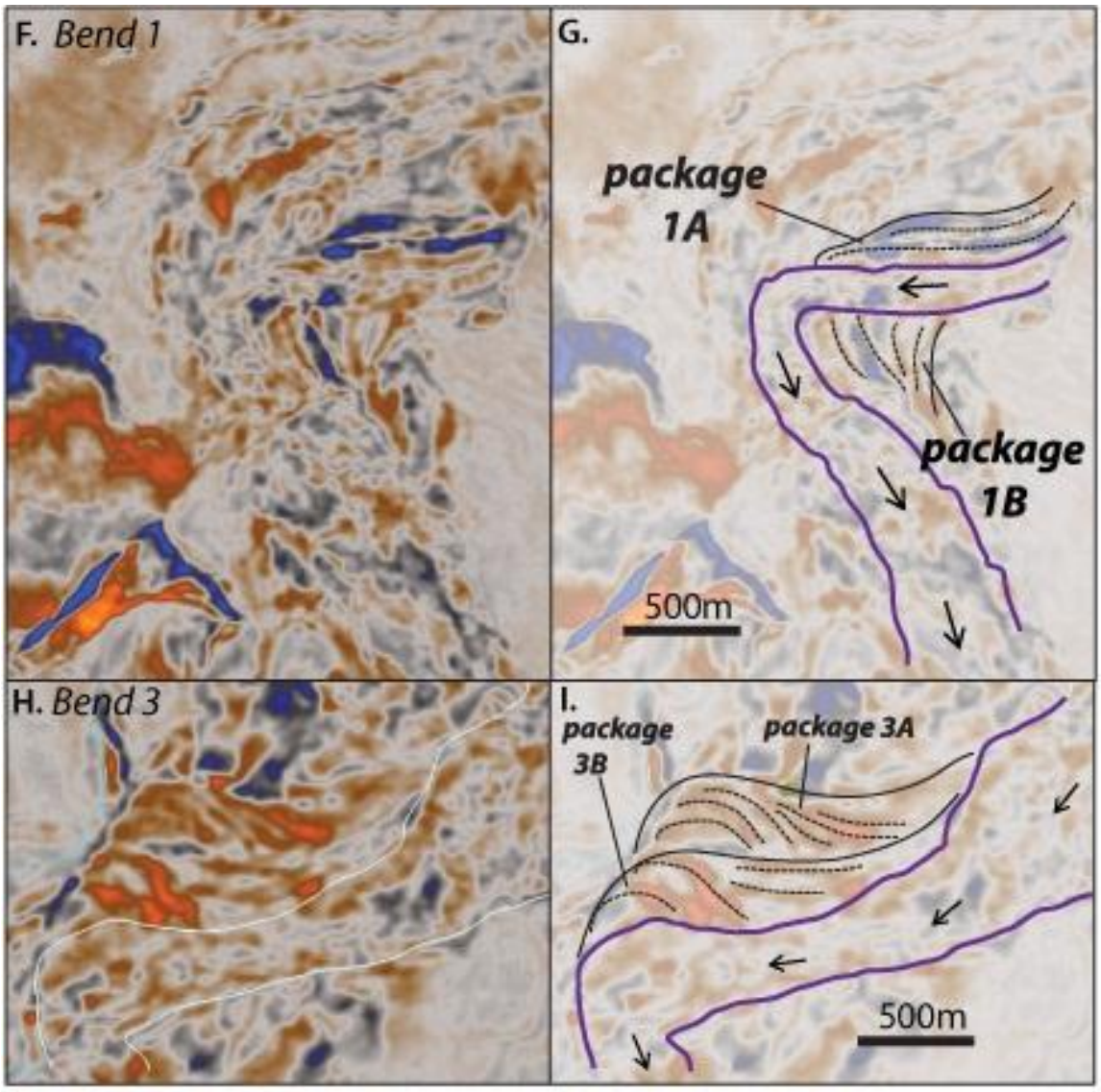

Figure 2.6 (continued): Bar packages at Bend 1 and Bend 3 are show in horizontal slices (F, H) and line drawing interpretations (G, I). 101 bar surfaces were mapped in Bends 1, 2, 3 (E) of through an ~8km-long segment of Channel 2. Channel 2 has an average width of 550m, an average depth of 66m, and sinuosity equal to 1.81.

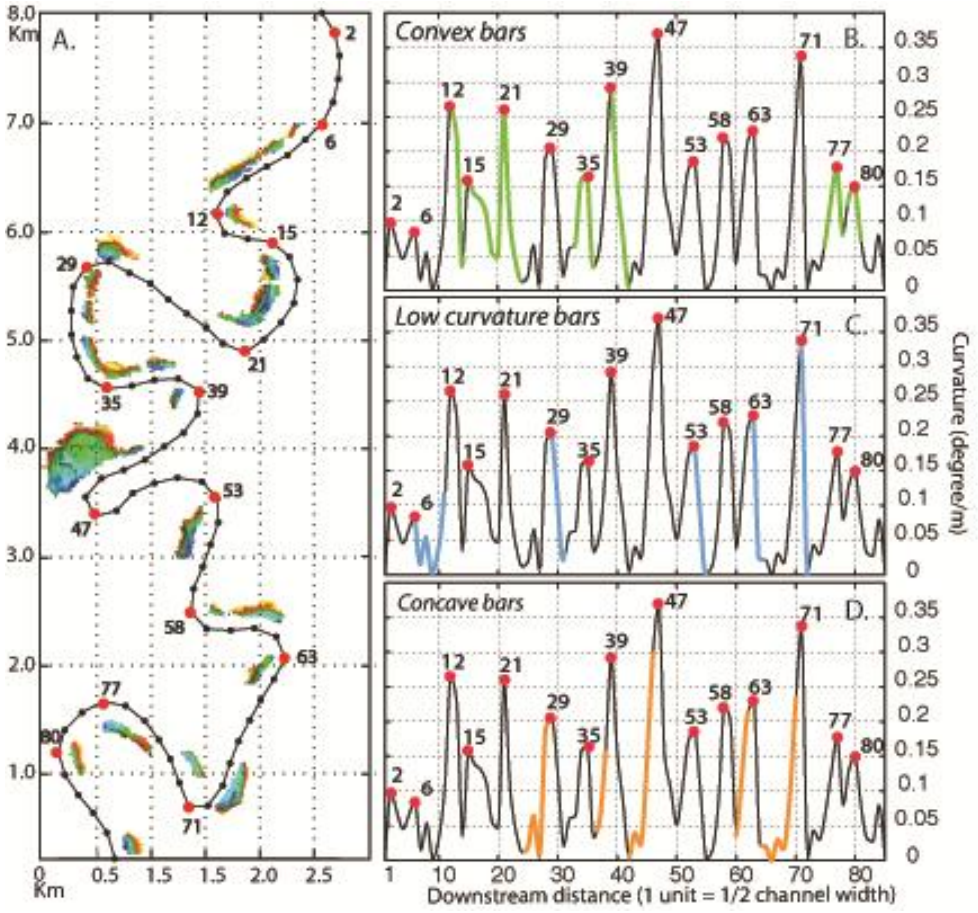

Figure 2.7: A) The youngest bar surfaces in Channel 1 are shown in relation to the channel centerline. Surfaces are color coded by elevation (blue = topographic lows, red = topographic highs). Black dots spaced every half channel width apart along the channel centerline are the locations at which channel curvature is analyzed. B, C and D show the relationships between channel curvature and bar shape. Curvature values are measured in degrees/m and show the change in channel centerline direction every half channel width. Curvature maxima are indicated by red dots on curvature plots as well as on the channel centerline in (A). Curvature values associated with these high amplitude bends range from 0.15 to 0.35 degrees/m with a mean value of 0.25 degrees/m. Locations of identified convex bars (B), low curvature bars (C) and concave bars (D) are marked in green, blue and yellow respectively. Convex bar surfaces extend across maximum curvature or initiate at maximum curvature and extend to minimum channel curvature. Low curvature bar surfaces initiate at the highest channel curvature and extend to just downstream of the minimum curvature. Concave bar surfaces terminate just upstream of the maximum channel curvature.

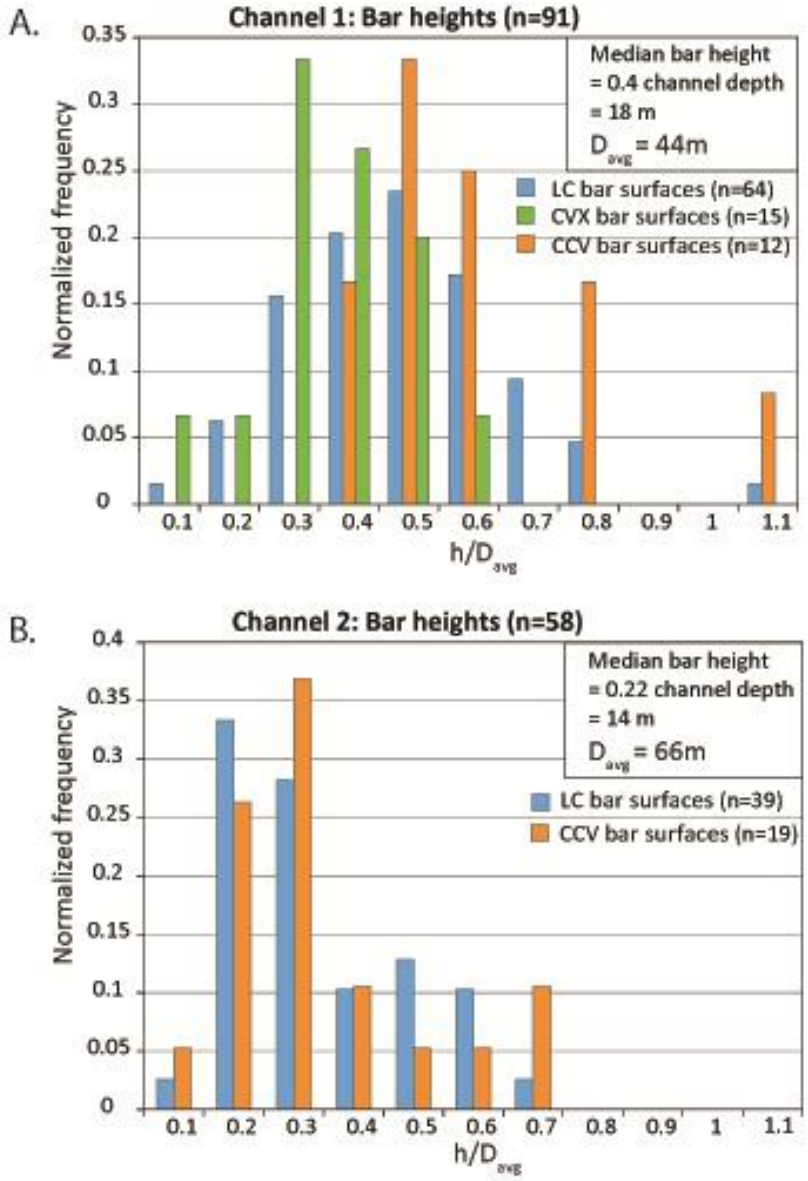

Figure 2.8: Histogram distributions of convex (CXV), concave (CCV) and low curvature (LC) bar heights in Channel 1 (A) and Channel 2 (B). Accretion heights were standarized by the average channel depth. Channel depth measurements represent the vertical distance between the deepest part of the channel at each bend and the crest of the levee at the outer channel bank. The three different bar categories show little variation in standardized bar height, with the median height falling between 30-50% of the average channel depth for Channel 1 and 22% for Channel 2.

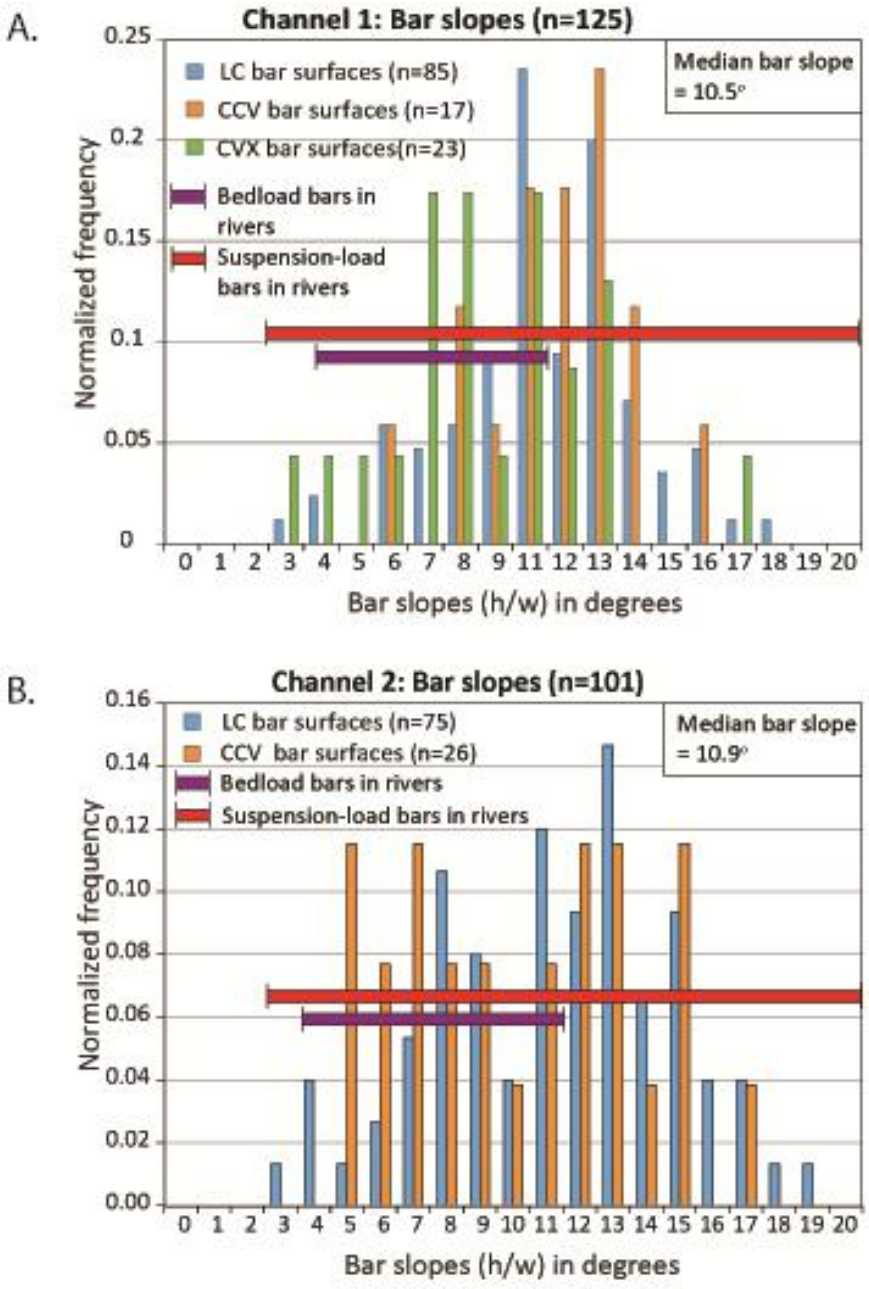

Figure 2.9: Histogram distributions of bar slopes in Channel 1 (A) and Channel 2 (B). . Median slopes for convex (CXV), concave (CCV) and low curvature (LC) bars in Channel 1 are similar and fall between 8.5o and 12o. Median slopes of low curvature and concave bars in Channel 2 are 11o and 10o respectively. Maximum bar slopes of 17-18o were recorded. A large number of submarine bar slope measurements exceed the range observed for bedload-dominated river bars.

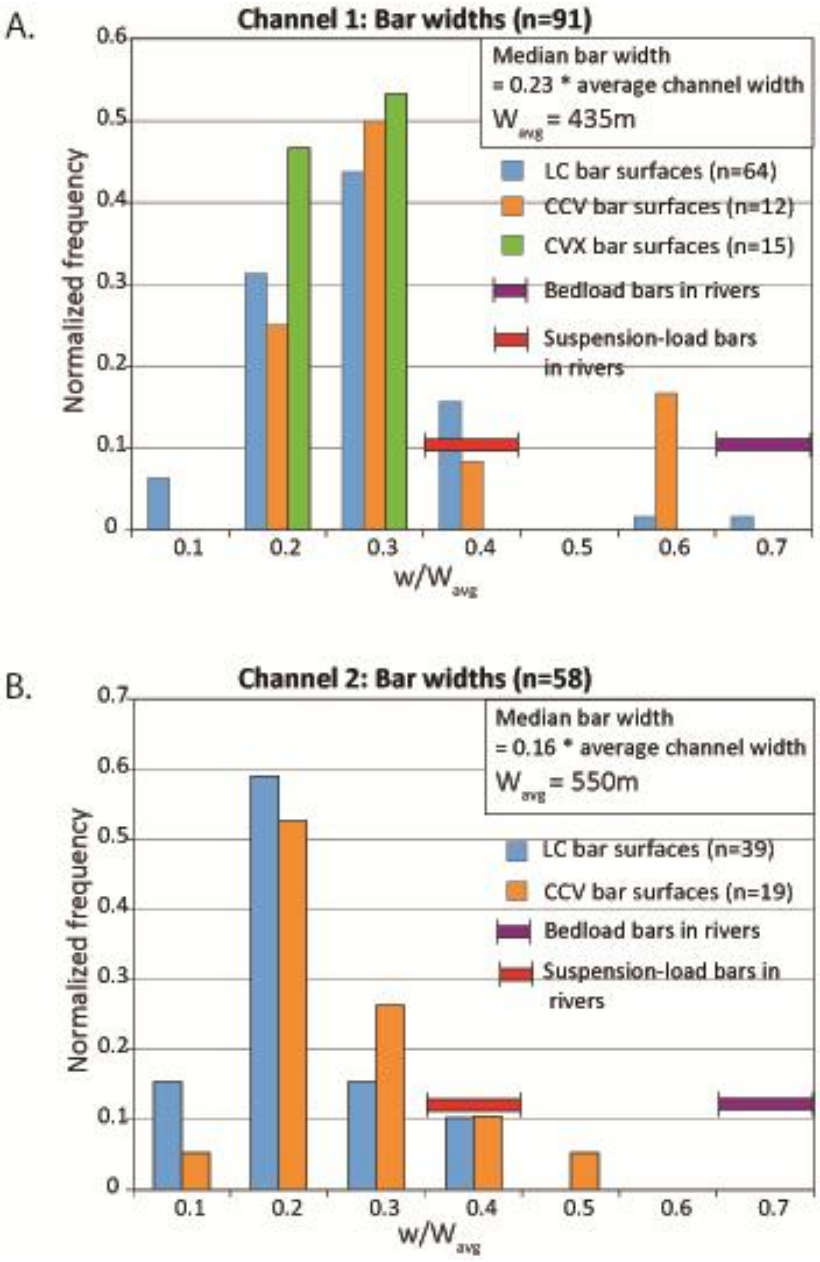

Figure 2.10: Histogram distributions of convex (CXV), concave (CCV) and low curvature (LC) bar widths in Channel 1 (A) and Channel 2 (B). Accretion widths were standarized by the average channel widths. Channel width measurements represent the horizontal distance between the inner channel bank and the outer chanel bank. Median bar-width measurements in both submarine channels indicate that bars occupied approximately 22-28% of the cross-section of Channel 1 and 15-17% of the cross section of Channel 2, a smaller width than that observed in point bars in rivers.

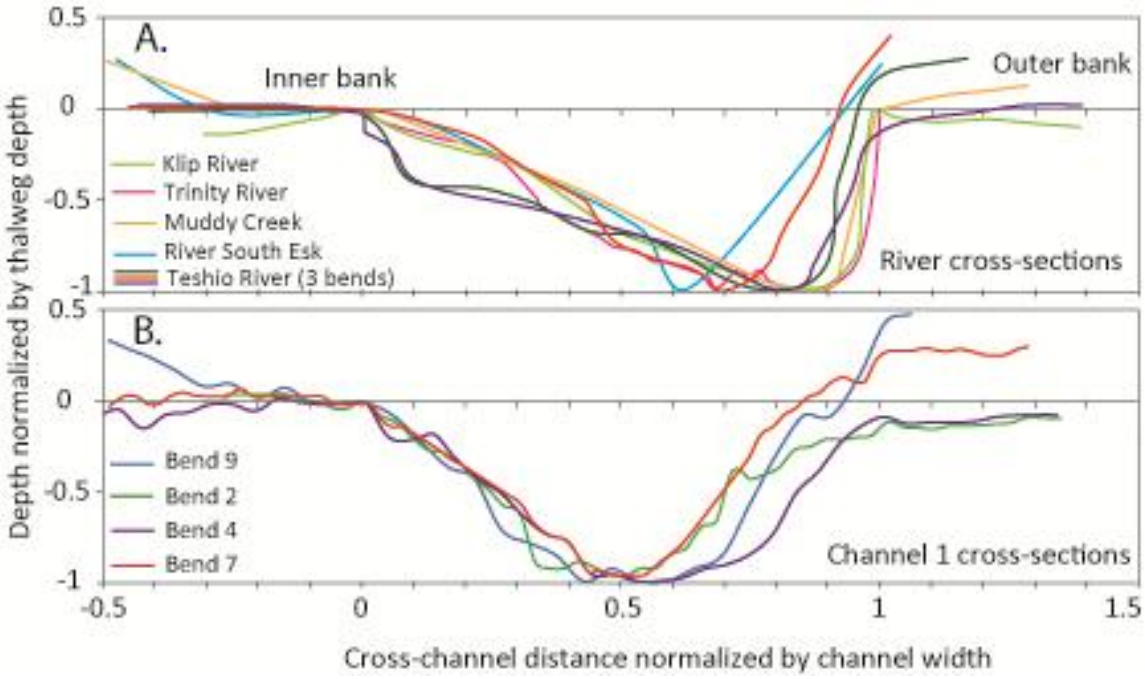

Figure 2.11: Channel cross sections at maximum curvature for (A) a few rivers and 4 bends from (B) Channel 1. Cross channel distance is standardized by channel width. Inner banks of channels are positioned at the origin (0,0). The sloping bar surface at inner bank occupies 50-85% of the channel cross-section in rivers and less than 50% of the channel cross section in the submarine channel. The plots show that the cross-channel asymmetry induced by accreting bars in rivers is greater than in Channel 1.

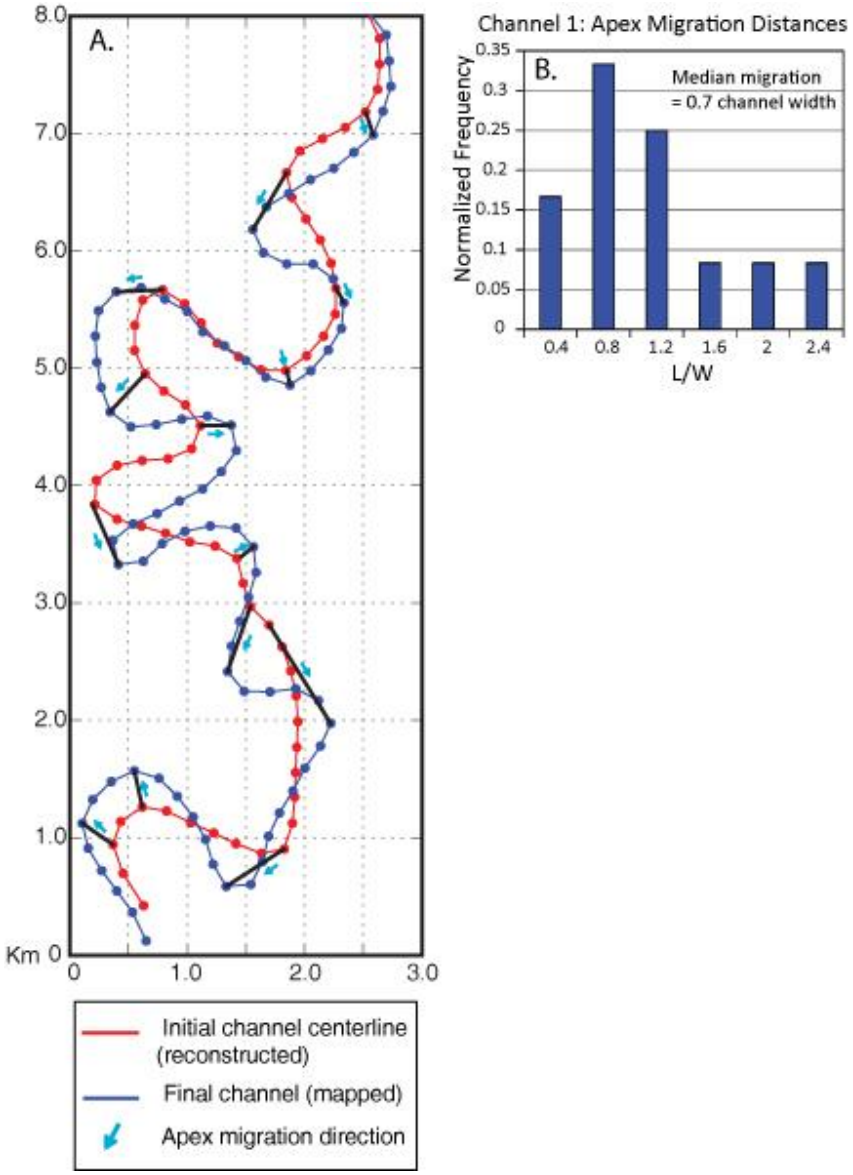

Figure 2.12: The initial and final centerlines in Channel 1 are compared in (A). The red line is the reconstructed plot of the initial channel centerline, obtained by fitting a channel of fixed width to the locations of the first bar surfaces at each bend. The blue line is the centerline of the final channel. Black arrows indicate measured distances that were used to construct plot (B). Plot (B) shows the histogram of the measured distances of apex migration standardized by the average channel width. The median of these values is 0.7 times the average channel width.

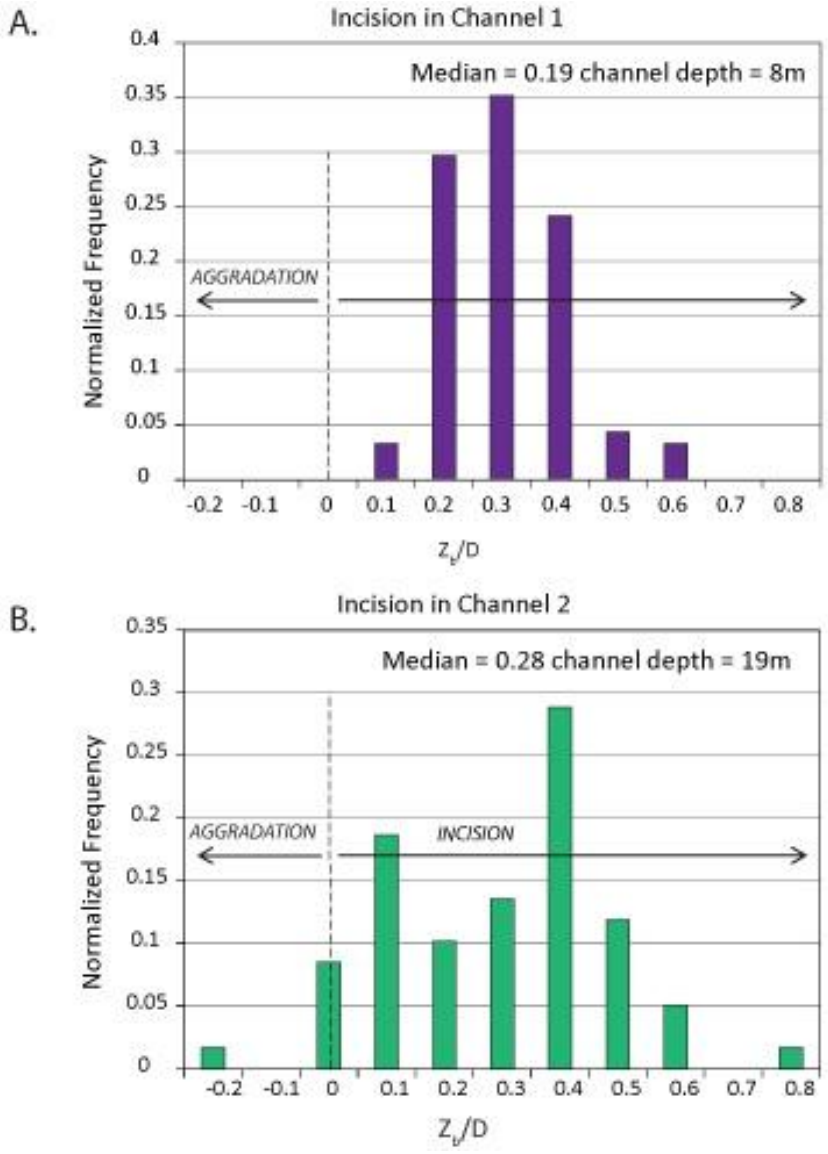

Figure 2.13: Histogram of bar elevations above the local channel base of Channel 1 (A) and Channel (B). Presented measurements are standardized by the local channel base. In Channel 1 (A), all bars are elevated above the local channel base indicating incision through time. Median of measured incision is 19% of the average channel depth. In Channel 2 (B), most of the bars are elevated above the final channel base, indicating net incision.. Bimodal distribution is interpreted to be due to variable rates of local incision relative to migration associated with the changing shape of the channel bend. Median of measured incision values is approximately 28% of the channel depth.

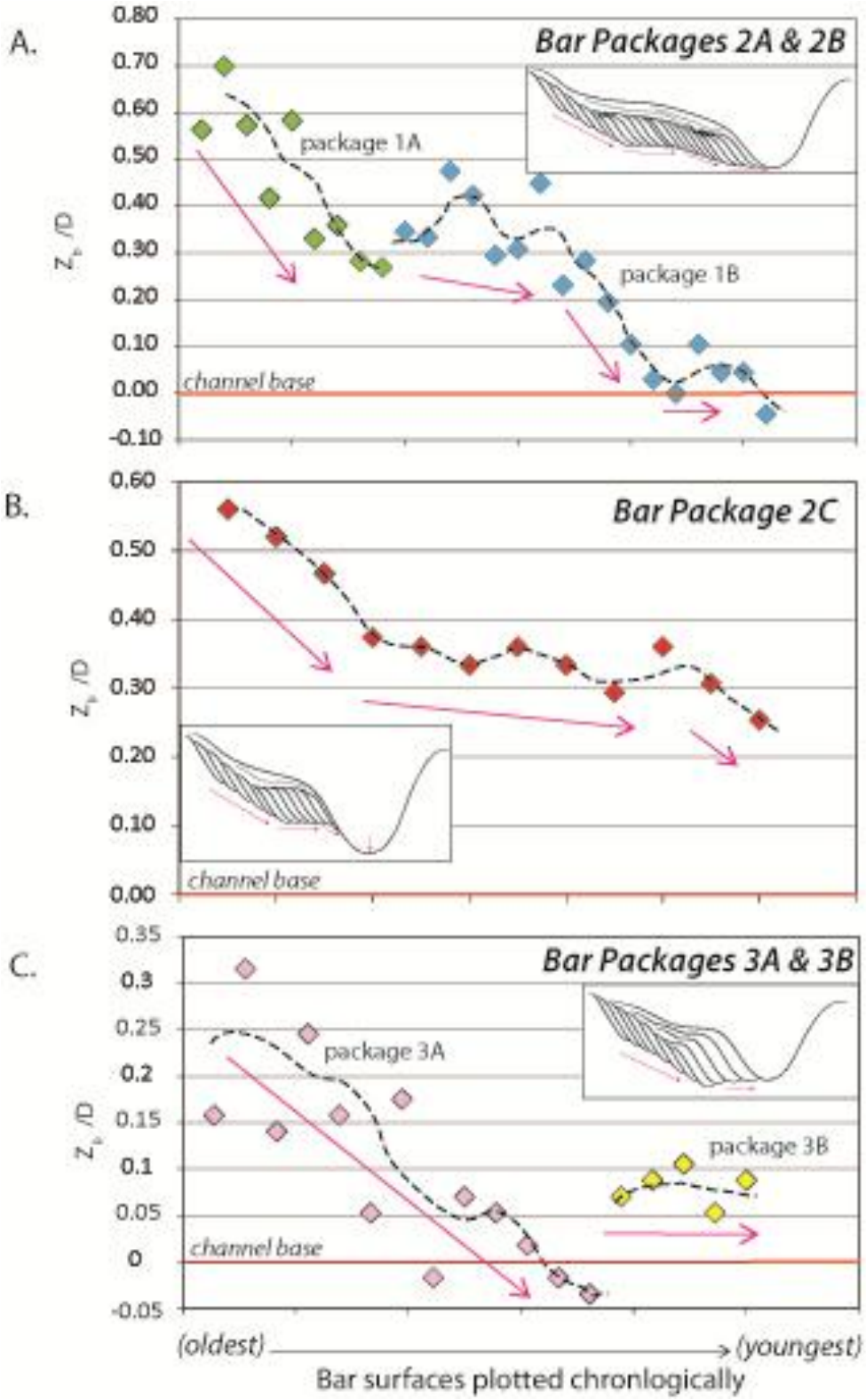
A.
Bar Packages 2A & 2B
package 1A
package 1B
channel base
B.
Bar Package 2C
channel base
C.
Bar Packages 3A & 3B
package 3A
package 3B
channel base
(oldest)
(youngest)
Bar surfaces plotted chronlogically

Figure 2.14: Elevations of bar-toes plotted in chronological order. Elevations are standardized by average channel depth. Changing elevations through time indicate variable rates of incision relative to bar accretion rates. Locations of bar packages 1A, 1B, 1C, 3A and 3B are shown in Figure 2.2 C and H. Black dotted lines are the moving averages of plotted bar elevations above the local channel base. Pink arrows indicate interpreted incision with lateral channel migration. Each plot shows the interpreted pattern of incision and migration in the inset sketch. Figure (A) shows two phases of accelerated incision associated with the development of bar package 1A and 1B. Bar package 1C (B) shows two phases of accelerated incision. Note that the toe of the final bar is perched at roughly 25% of the channel depth above the final channel base, indicating incision at this location without bar formation/local channel migration. Bar package 3A (C) show a relatively steady incision rate.

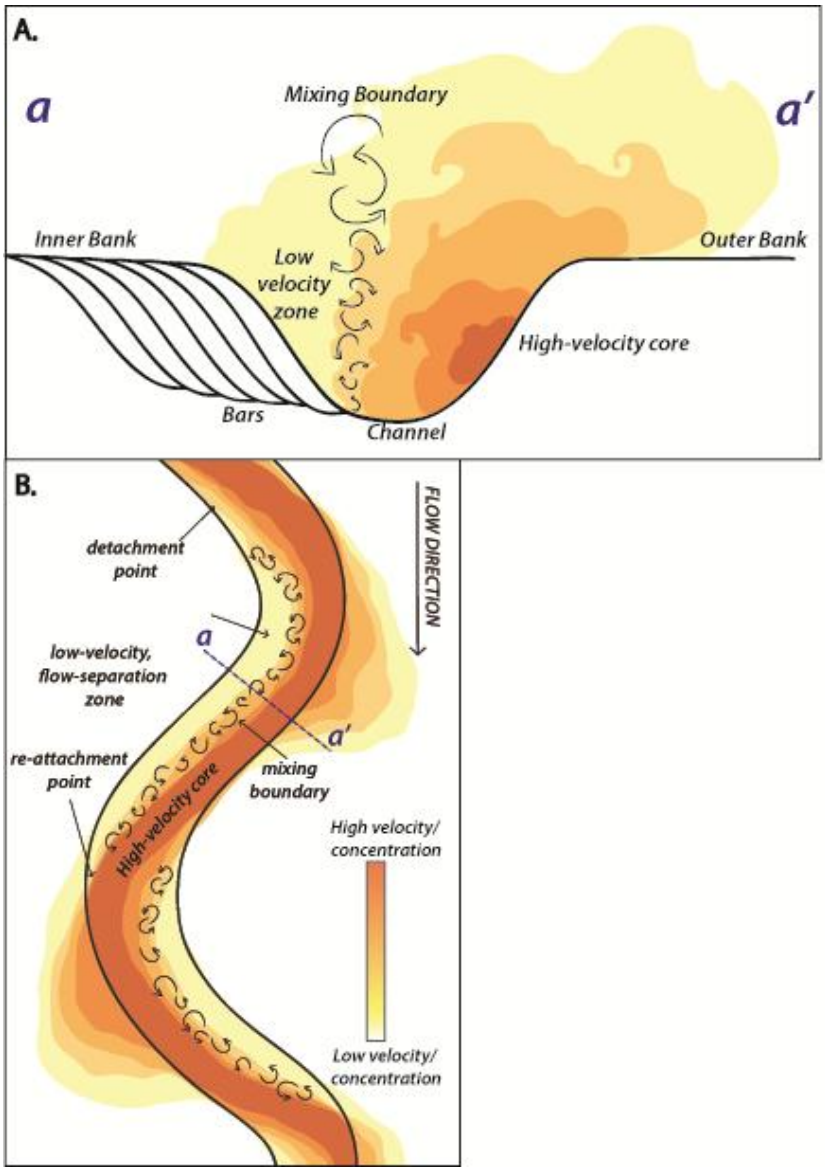

Figure 2.15: Schematics showing how a turbidity current interacts with a sinuous channel, shown in cross-section (A) and planview (B). The figure illustrates how the low velocity zone forms where flow separates from the inner banks of bends. Shear at the boundary between the slow-moving separated flow and the high-velocity, down-channel flow results in the formation of a "fence" of turbulent eddies, here called the mixing front. These eddies carry suspended sediment into the low velocity zone. Suspended sediment deposited in the low velocity zone constucts a bar at the inner bank. Sediment trasnported as bedload travels with the high-velocity core and does not enter the flow separation zone.

Chapter 3: Depositional Controls on the Stratigraphy of Submarine Channels in the Brushy Canyon Formation, west Texas

INTRODUCTION

The current work focuses on the sedimentology and stratigraphy of submarine channel deposits in the Brushy Canyon Formation of west Texas, USA. In particular, I analyze the origin and significance of large inclined bed-sets constructed from sediment deposited from suspension in low velocity zones along the margins of channels. Deposits of bank-attached bars in submarine channels have been interpreted in numerous outcrops around the world (Abreu et al., 2003; Arnott, 2007; Dykstra and Kneller, 2009; Pyles et al., 2009) (Abreu et al., 2003; Arnott, 2007; Dykstra and Kneller, 2009; Pyles et al., 2009). These interpretations and analyses have drawn heavily on models for bedload-dominated, bank-attached bars in rivers. Bank-attached bars in rivers can also be built out of sediment deposited from suspension (Hickin, 1979; Smith et al., 2009; Woodyer, 1975) and recent work indicates that suspension-dominated bars built in zones of flow-separation in submarine channels have been under-recognized by the community of scientists studying submarine systems (Chapter 2, Straub et al., 2011). This chapter presents a systematic characterization of a well-exposed bar situated within the deposits of a submarine channel complex in the Upper Brushy Formation. This bar is interpreted as having developed in a low-velocity zone of flow separation at the channel margin. The bar deposits are contrasted against deposits filling the thalweg of a submarine channel in the same complex, as well as deposits filling channels on the proximal basin floor. By combining granulometry with sedimentary structures and bed geometries I am able to

determine what material is being deposited in zones of high and low velocity in the upper slope setting and compare this against sedimentary structures and textures observed filling channels in a toe-of-slope setting. The comparison defines the particle sizes being trapped, preferentially deposited on the slope versus being transferred long distances onto basin floor. I also use sedimentary structures, bed geometries, and grain size data to: 1) estimate the paleo-hydraulic properties of the depositing turbidity currents; and 2) construct a facies model for thick, bank-attached bars built from sediment sourced from suspended load.

GEOLOGICAL BACKGROUND

The Late Permian Brushy Canyon Formation is part of a mixed siliciclastic-carbonate system, deposited on the margin of the Delaware basin, which was semi-restricted from the rest of the Permian Basin (Fig. 3.1, A, B and C). This basin had water depths estimated at 400-600m (King, 1942). The Brushy Canyon Formation overlies a steep carbonate slope (Beaubouef et al., 1999) associated with the development of a shallow water carbonate shelf (Fig. 3.1 A). It was deposited in the submarine environment during low stands in sea level that produced sub-aerial exposure and karstification of the carbonate shelf deposits (Kerans and Fitchen, 1995). The grain size of siliciclastic sediment composing most of the Brushy Canyon Formation is medium sand to silt-sized particles. This relatively narrow range of grain-sizes is interpreted as a reflection of sizes available in the upland source area (Kocurek and Kirkland, 1998). The

outcrops of the Brushy Canyon Formation form an oblique transect across the Delaware Basin, running from the shelf-slope break in the northwest to the distal basin floor in southeast. Sediment was introduced to the deep-water system through a number of point sources along the western margin of the basin (Beaubouef and Pirmez, 1999). The Brushy Canyon Formation has been subdivided into Lower, Middle and Upper members based on laterally persistent siltstone intervals (Beaubouef and Pirmez, 1999). I have studied channels from the Upper and Middle members.

STUDY SITES

This study presents data from: 1) an upper slope channel complex exposed on the western face of the southern Guadalupe Mountains (Fig. 3.1, A and D, Fig. 3.2 A and B), and 2) channel fills on the proximal basin floor (Fig. 3.1, A and D). The presented data on upper slope stratigraphy is from one continuous, 1.4km-long outcrop in three branches of Shumard Canyon (Fig. 3.2, A and B). The position of this outcrop is estimated to be roughly 2km from the shelf edge (Fig. 3.1 A). In the north branch of Shumard Canyon, these channel deposits unconformably overlie the Cutoff and Victorio Peak formations (Fig. 3.3, A and B). In the north-eastern and eastern branches of Shumard Canyon the channel base is incised into laminated silt-stones of the Brushy Canyon Formation. Data from the channel fills on the proximal basin floor were collected from exposures in Broken Rock Canyon and Popo Canyon. In the direction of paleo-transport, these two locations are 15km down-dip from the upper slope position (Fig. 3.1, A and D).

UPPER SLOPE CHANNEL COMPLEX

The total thickness of the Upper Brushy Canyon Formation in the upper slope position varies from approximately 135m in North Shumard Canyon to 170m in East Shumard Canyon. This stratigraphy contains four sharp-based sand-rich channel complexes (Fig. 3.2). My study focuses on the sedimentology and stratigraphy of the second complex (Fig. 3.2, A; Fig. 3.3, A and B), hereafter referred to as Channel Complex 1 (CC1). Thickness of the CC1 exposure is approximately 55m in North Shumard Canyon, 43m in North-east Shumard, and 25m in East Shumard. The uppermost 15m of CC1 is separated from the underlying beds by the thin organic-rich siltstone interval (Fig. 3.3, A and B), and is not included in this study. CC1 fills in erosional topography which truncates roughly 19m of siltstones and also cuts into 7m of the underlying carbonate slope. The greatest relief on the basal erosional surface is 26m (Fig. 3.3, A and B).

The studied stratigraphy of CC1 is composed of two distinct phases (Fig. 3.3, A and B)

1. Thickly-bedded sandstones confined within the erosional container.
2. Steeply inclined beds situated above the erosionally confined beds.

FACIES ASSOCIATIONS ON THE UPPER SLOPE

Three facies associations were differentiated within slope channel stratigraphy to broadly reflect their depositional environment. The facies and stratigraphy of this channel complex was originally described in (Rossen, 1985)

Facies Association 1

This facies association is only observed in the lower, erosionally confined stratigraphy of CC1 (Fig. 3, A and B). This facies association includes three subcategories.

1. **Facies 1A (80-90% of the lower confined fill):** Sharply-based, medium- to very thickly-bedded, planar stratified, trough cross-stratified, or structureless upper-fine sandstones (Fig. 3.3, A and B ; Fig. 3.6, A and B; Fig. 3.7, A and B). Bases of these beds often have meter-scale erosional topography (Fig. 3.6, A and B). Trough-cross stratified or planar stratified sandstones have flat tops and onlap erosional topography (Fig. 3.8, A-B). Structureless beds sometimes have concave-up tops tangentially onlap erosional topography (Fig. 3.6, A and B). Rip-ups clasts and tests of fusulinids are sometimes present in these beds.

2. **Facies 1B (5-10% of the lower confined fill):** Very thin to thin beds with thin plane-laminations, climbing ripples and mud drapes (Fig. 3.8, C). These thin beds are inter-bedded with thicker beds of Facies 1A (Fig. 3.8, A and B). Erosional bases of Facies 1A often cut into these beds of Facies 1B (Fig. 3.8, A and B). . They are also

found onlapping the margins of the erosional container, where thick beds of Facies 1A transition laterally into these thinly-bedded, finer-grained deposits (upper very-fine sands) (Fig. 3.9, A and B).

3. **Facies 1C (5-10% of the lower confined fill):** Medium to very thick , cross stratified gravel-rich beds, with a matrix content of lower-medium sand, sand-sized shell fragments and fusulinids (Fig. 3.10 A, B). Gravels contain carbonate clasts, fragments of bivalve shells, ammonoids and sandstone clasts. These gravel-rich beds often transition upwards into Facies 1A.

Facies Association 2

This facies association characterizes 15-20m of the stratigraphy above the erosionally confined deposits of facies association 1 (Fig. 3.3, A and B; Fig. 3.4, A and B; Fig. 3.5, A, B, C and D).

1. **Facies 2A (~40% of beds above the confined fill, see Fig. 3.4 and 3.5, B):** These beds are dominantly thinly-bedded, ripple-laminated sandstones with sub- to super-critical climb angles, occasionally alternating with thin beds of planar stratified sandstones (Fig. 3.11, C, D and E). These beds are steeply dipping where they over lie or drape basal scours (Fig.3.12, A). Ripple transport directions are oriented at 20-120 to bedding dip azimuths (Fig. 3.12, B; Fig. 3.13, B and C).

2. **Facies 2B (~20% of beds above the confined fill, see Fig. 3.4 and 3.5, B):** Medium to thickly bedded, trough cross-stratified sandstones (Fig. 3.11, F). Dune transport is oriented between 10 and 180 degrees to bedding dips (Fig. 3.13, B and D).

3. **Facies 2C (~40% of beds above the confined fill, see Fig. 3.4 and 3.5, B):** These beds are dominantly thinly- to thickly-bedded, planar-stratified sandtones (Fig. 3.11, A). They are sometimes composed of inter-layered upper fine sand and lower fine sand (Fig. 3.11, B). They often have rippled tops.

Facies 2A-C are arranged into a large set of inclined beds (Fig. 3.4 A) with a median dip angle of 10^{o} (Fig. 3.14). Local dips of individual beds are highest towards the top of the set, and are lowest towards the set base, where bed slopes approach horizontal (Fig. 3.4, A and B; Fig. 3.5, A and B). Rippled- and trough-cross-stratified beds often transition laterally down the bedding dip into thickly bedded planar stratified sandstones (Fig.3.4, A and B). Scours commonly separate depositional units within the 12-15m bed-set (Fig. 3.4, A and B; Fig. 3.5, A and B). Due to scouring, individual beds thin towards their updip and down-dip terminations (Fig. 3.4, A and B; Fig. 3.5. A and B). A decimeter-thick interval of organic-rich silt-stone is present at the top of this set of inclined beds, and defines the top of the studied interval (Fig. 3.3, B).

Facies association 3

This facies association occurs outside of the confined channel (Fig. 3.3, B), and is the background sedimentation separating the four larger channel units of the Upper Brushy Canyon Formation.

1. **Facies 3A:** Plane-laminated siltstones (Fig. 3.15, A and B),

2. **Facies 3B:** Thinly bedded, sharply based, plane-laminated very fine grained sands, rich in mud and silt. These beds can form relatively prominent ledges within the siltstones of Facies 3A (Fig. 3.15, B).

CHANNEL FILLING FACIES ON THE PROXIMAL BASIN FLOOR

Facies 4: Facies four comprises sandy channel fills which range in thickness from 10 to 50m. (Fig. 3.16, A). These channel fills contain an abundance of thick and very thick beds of fine-grained sandstones containing stratification associated with sub- to super-critically climbing three dimensional dunes (Fig. 3.16, B and C; Fig. 3.17, A-D).

PALEOCURRENT DATA FROM THE UPPER SLOPE

Multiple paleocurrent indicators of were collected to establish sediment transport-directions within CC1. I collected 103 measurements of fusulinid long axes orientations in Facies 1 A and 1C of the basal confined deposits. These measurements are shown in Figures 3.13A and have a south-easterly trend. Dip azimuths of inclined beds (n=47) in

Facies 2 A-C are shown in Figure 3.13B, and have a northeasterly mode. Measured orientations of dune troughs (n=31) and ripple crests (n=196) in facies association 2 in North, Northeast and East Shumard canyon are shown in Figures 3.13, C and D . Ripple orientations from Rossen (1985), are incorporated into the data-sets from East (n=3) and North (n=12) Shumard Canyon (west wall) (Fig. 3.13, C).

GRANULOMETRY

Methods: Rock samples were ultrasonically disaggregated using a Misonix ultrasonic processor (S-4000). This device broke down rock samples into their constituent grains. Some of these samples were examined optically using a petrographic microscope to confirm that the process of disaggregation was complete. Disaggregated samples were wet sieved at 32 microns to divide the medium silt and finer mud from the coarse silt and sand. The particle sizes of the coarse silt and sand fraction of each sample were measured using a Retsch Technology Camsizer (a digital, image-processing particle size analyzer). The Camsizer uses digital photographic images to accurately measure particle diatmeters between 0.03-30mm.

Grain size distributions of sands show distinct relationships with the facies defined above. These relationships are summarized in Table 3.1, and Figure 3.18. There is very little internal variation in grain size between samples from Facies Association 2 (Fig. 3.18, F, H, J). There is a significant difference between sizes present in Facies Association 2 and Facies Association 4, and those in Facies 1 A & C (Fig. 3.18, A, D, K).

Grain sizes coarser than 250µm, while present in the thickly-bedded units of Facies 1A and the sandy matrix of Facies 1C are generally poorly represented in facies association 2. Grain size distributions tied to samples from Facies Association 2 can be bimodal. The primary mode systematically occurs at 120 microns and the secondary mode occurs at 210 microns (Fig. 3.18 G, I, K). The potential significance of this bimodality will be addressed in the interpretation section.

Gravel occurring in Facies 1 C was measured in the field using techniques described in Kellerhals et al. (1975). 187 measurements of the long axes of gravels were measured on scaled photographs, in order to generate the size distribution for gravel in Facies 1C shown in Figure 3.18, B.

Table 3.1: Facies associations and grain-size statistics

Facies	**n**	**D25 (>32 µm)**	**D50 (>32 µm)**	**D75 (>32 µm)**	**D95 (>32 µm)**	**Weight fraction of fines (wt. of <32µm fraction / total wt. of sample)**
Facies 1A	4	103-146	162-205	232-290	356-469	0.23 - 0.28
Facies 1B	5	96-110	118-136	146-179	220-270	0.20 - 0.28
Facies 1C	2	110 - 127	118-167	220-252	381-438	0.25 - 0.28
Facies 2A	13	90 – 118	118 - 270	136 – 179	192- 290	0.18 – 0.37
Facies 2B	5	96- 118	118-156	146-220	205-310	0.19-0.39
Facies 2C	12	96 -118	110 -156	136 -220	220-310	0.11-0.33

Facies 3A	2	78-84	103-110	136	205-220	0.40-0.44
Facies 3B	2	90	118	156-167	252-270	0.44-0.54
Facies 4	5	78-103	103-127	136-156	192-236	0.13-0.15

INTERPRETATIONS AND DISCUSSION

(i) The stratigraphic organization within CC1

Stratigraphic relationships between facies associations 1, 2, and 3 in CC1 suggest two different stages of channel development: An earlier phase (Stage 1) associated with sedimentation resulting in a considerable reduction in the relief of the erosionally based channel (Fig.3.19, A-C), and a later phase (Stage 2) associated with construction of a large bank-attached barform in the submarine channel (Fig. 3.19, C).

Stage 1

This early phase is characterized by deposition within a steep-walled, erosional channel cut into the carbonate margin. (Fig. 3.19, A-C; Fig. 3.3, A-B). Paleocurrent data indicate a south-easterly trend for the channel axis (Fig. 3.13, A). Stage 1deposits are dominated by medium to very thick beds of Facies 1A and 1C (Fig. 3.6, A-B; Fig. 3.7, A-B, Fig 3.10, A-B). This phase of deposition aggraded the channel bed and reduced the erosional relief of the channel. Conglomerates and gravelly sandstones are interpreted as the product of deposition from pure bedload.

Stage 2

The second stage is dominated by 15-20m of stratigraphy built from steeply-dipping (median dips=10^{o}, (Fig. 3.12, A; Fig. 3.14), fine-grained sand stones, with repetitive internal scouring (Facies Association 2) (Fig 3,.19, D, Fig. 3.3, A-B, Fig. 3.4, A-B, Fig. 3.5, A-D).. These beds are interpreted as the deposits of a thick bank-attached

barform. The two cross-channel outcrops in north and north-east Shumard Canyon show that these bar deposits extend for approximately 400m laterally, while they extend for roughly 600m in the downdip direction. This barform is inferred to have formed in a relatively low velocity zone associated with either bend curvature in a sinuous channel or with local planform irregularity (eg: a slumped side-wall). Silt-rich deposits of facies association 3 are laterally adjacent to stage 1 and stage 2 of CC1and are interpreted as overbank deposits which aggraded outside the initial erosional confinement (Fig 3.19, B-D, Fig. 3.3, A-B).

(ii) Suspension-dominated bars in channels

Flow separations associated with planform roughness have been documented to occur in channels in two ways: 1) downstream of high-curvature bends which cause the formation of a low velocity zone downstream of the bend apex (Bagnold, 1960b; Hickin, 1979; Straub and Mohrig, 2008), and 2) where an obstruction to the flow causes a low velocity zone to form just downstream of the obstruction (Rubin, 1990). The re-attachment bar documented by Rubin et al., (1990) on the Colorado River represent a good example of the associations of sedimentary facies in a bar built in a separation zone. Measurements made by (Rubin, 1990; Rubin et al., 1998) document that a bank-attached bar can be constructed from suspended sediment that rains out of the flow within the low-velocity separation zone. Once the suspended sediment is deposited it is weakly reworked as bedload. The resulting stratigraphy of this bar is dominated by beds containing dune

cross-strata and climbing ripples. The points at which flow separates and reattaches from the channel bank are both sensitive to flow discharge and velocity. The degree of reworking and planform shape, orientation and angle of climb of the bedforms in these deposits are heavily influenced by flow reversals associated with the dynamics of the detachment and reattachment points.

Similar grain size distributions (Fig. 3.18, E-J) and close association of thick stacks of ripple-laminated beds containing abundant climbing ripples, trough-cross stratified beds and planar-stratified beds of Facies Association 2 (Fig. 3.11, A-F; Fig. 3.4, A; Fig. 3.5) suggest that these strata were built by sediment deposited from suspension and reworked to varying degrees on the bed. We interpret that these strata are deposits associated with a bar built in a low-velocity zone of separated flow along the channel margin (Fig. 3.20). Internal scouring is interpreted to be associated with reworking along the surface of the bar as its shape evolves. Scouring of the bar can be expected to be more common on the parts of the bar that are closer to the dynamically shifting detachment or reattachment points bounding the separation zone (Rubin, 1990). Lateral transitions down the bar packages reflect little change in grain size but commonly show a higher degree of reworking (Fig. 3.18, E-J, 3.4, B), indicating a greater proximity to the high-velocity core of the transporting current (Fig. 3.20). Changing bedding dips in North Shumard (from south to north) reflect complex curvatures associated with the evolving surface of the bar (Fig. 3.13, B).

Bar deposits generally show a narrow, unimodal distribution of grain-sizes with median grain-sizes close to 150 μm (Fig. 3.18, E-J). A few grain-size distributions show

a bi-modal or weakly bimodal grain–size distribution in which a second peak appears at approximately 250μm (Fig. 3.18, F, G, H). These distributions correspond to deposits which show very thin or thin beds of structureless, upper fine-grained sandstone overlain by planar-stratified lower fine sandstone (Fig. 3.11, B). These deposits are interpreted to be associated with pulses of currents carrying transiently suspended sediment load. This is may have occurred in parts of the bar that were more proximal to the high-velocity core carrying higher concentrations of sediment in transient suspension (Fig. 3.20).

(iii) Slope to basin floor paleo-transport

A comparison of grain size distributions from the upper slope and basin floor channels (Fig. 3.18, L) reveals a remarkable overlap between the particle sizes of sediment preserved in the upper slope bar (Stage 2) and the distributions of sediment filling channels on the basin floor. Thickly-bedded, climbing dune stratified deposits filling in the basin floor channels (Fig. 3.17, A-D) indicate that these deposits accumulated from sustained sedimentation from suspended load. Thus, we interpret that the upper slope channels were sites of bypass of large volumes of fully suspended sediment. Some of this fully suspended sand was trapped and deposited in the low velocity zone associated with flow separation, where it constructed the thick bar. The rest of this fine and very fine sand bypassed the slope and filled channels on the proximal basin floor.

Grain sizes coarser than 250micron are common in the channel filling deposits of the upper slope (Stage 1) but absent in the bar deposits (Stage 2), overbank deposits and basin floor channel fills (Fig. 3.18,A, C, D, E, G, I, L). These particle sizes are interpreted to have been travelling near the channel bed as either transiently suspended material or as bedload. This slower moving fraction of sediment load is not found in the channel axes on the basin floor (Fig. 3.18, L) and is interpreted to have been trapped on the slope via deposition.

(iv) Sediment transport and paleo-hydraulics for deep-water systems

Bed architecture, sedimentary structures and grain-size information can be used quantitatively reconstruct flow properties associated with the depositing turbidity. Critical parameters and relationships that are used to carry out a reconstructive analysis are reviewed here. Reconstructions commonly relate the characteristic transport properties for a particle, the critical shear stress required for initial motion (τ_{cr}) and settling velocity (w_s), to a characteristic property of the transporting fluid, its boundary shear stress (τ) or shear velocity (u_*). The boundary shear stress is the shear stress applied to the bed by a viscous fluid flowing over it. The boundary shear stress *(τ)* is related to the shear velocity *(u*)* by:

$$\tau = \rho_c u_*^2 \qquad (1)$$

where ρ_c is the density of the fluid. Well-established, empirical relationships can be used to estimate values for τ_{cr} (Wiberg and Smith, 1987) and w_s (Dietrich, 1982) for particles with a given size, shape and density, and for given density and viscosity of the transporting fluid. The critical shear stress for any particular particle can be written as

$$\tau_{cr} = \frac{(\tau*)_{cr}}{(\rho_s - \rho_c)gD} \qquad (2)$$

where ρ_s is the density of the grain, g is acceleration due to, D is the nominal grain diameter, and $(\tau^*)_{cr}$ is the dimensionless critical shear stress (Bagnold, 1941). I use the relationship established by Wiberg and Smith (1987) to estimate the dimensionless critical shear stress as a function of particle diameter relative to the bed roughness scale k_s (taken as the median grain diameter on the bed). Estimates for grain settling velocity were calculated using the method of Dietrich (1982).

Particles will begin to move along the bed once their critical shear stresses are exceeded. Grains travel very near the bed and frequently interact with it. This mode of transport, referred to as bedload transport, as maintained as long as the boundary shear stress and particle critical shear stress are comparable. As values for the boundary shear stress or shear velocity increase, upward-directed fluid velocities become great enough to advect moving particles into the flow interior. Particles travelling high up in the flow travel at the same velocity as the transporting current and are advected over large distances. This mode of grain transport is referred to as suspended load transport. As

long as the shear velocity of the flow, which scales with the magnitude of upwardly directed turbulent, instantaneous velocity, is greater than the settling velocity of particles, these particles are traveling in suspension (Bagnold, 1966; Jerolmack et al., 2006; Nino et al., 2003; van Rijn, 1984b). The ratio w_s/u^* can therefore be used to characterize when grain are traveling very near the bed versus well up into the interior of a flow. When w_s /u^* is small, particles travel well up in the interior of the flow at the same velocity as the current and have long excursion lengths (Jerolmack et al., 2006; Smith and Hopkins, 1972).When w_s /u^* is large, particles will move as bedload, saltating, sliding or rolling along the bed. Particles moving as bedload will move at a lower velocity than the particles suspended within the interior of the current.

Empirical relationships between the ratio w_s /u^* and transport style have been established based on observations of sediment motion in air and water (Bagnold, 1941, 1966; Chepil, 1945; Laursen, 1958; Nino et al., 2003; Nishimura and Hunt, 2000; Sagan and Bagnold, 1975; Shao and Yan, 2000; Smith and Hopkins, 1972; van Rijn, 1984a, b). In this study I adopt the following relationships:

1) for pure bedload: $\tau > \tau_{cr}$ and $w_s /u^* > 3$

2) transient suspended load: $1/3 < w_s /u^* < 3$,

3) full suspension: $w_s /u^* \leq 1/3$.

Estimating turbidity current velocity

The depth-averaged current velocity (u) can be related to shear velocity through a momentum balance that employs a friction coefficient (C_D):

$$(u*)^2 = C_{\mathrm{D}}(u)^2 \qquad (3)$$

For this study I use a value of 0.002 for the turbidity-current coefficient of friction (Parker et al. 1987).

Estimating suspended-sediment concentration in turbidity currents

Estimating the depth-averaged concentration of suspended sediment within a turbidity current can be carried out of using the densimetric Froude number (Fr_d):

$$Fr_{\mathrm{d}} = \sqrt{\frac{u^2}{\left(\frac{\rho_{\mathrm{c}}-\rho_{\mathrm{a}}}{\rho_{\mathrm{a}}}\right)gh}} \qquad (4)$$

where ρ_a is the density of the ambient fluid and h is the mean flow depth. The depth-averaged concentration (C) of suspended sediment in the current is then equal to:

$$\rho_{\mathrm{c}} = \mathrm{C}\ \rho_{\mathrm{s}} + (1\text{-C})\ \rho_{\mathrm{a}} \qquad (5)$$

Estimates for C are determined using the appropriate range for densimetric Froude numbers, 1.0 – 1.2, associated with turbidity currents flowing down slopes from 0-10 degrees (Britter and Linden, 1980).

Estimating shear velocity from bedload deposits

The 50^{th} percentile (median grain size or d_{50}) of sediment transported as bedload has been used to estimate basal shear stresses in coarse grained braided rivers (Paola and Mohrig, 1996). We used 185 measurements of gravel clast long axes after Kellerhals et al. (1975) and Paola and Mohrig (1996) to estimate the median clast size of the gravels and the critical shear stresses required to initiate transport of these gravels. The critical shear stress required to initiate motion is generally higher than that required to continue to transport sediment (Nino et al., 2003). Thus, this estimate sets a lower limit for the boundary shear stress applied by the transporting currents. Isolated gravel beds suggest that these clasts were transported by shear velocities close to the critical threshold for motion, and were trapped in topographic lows where their motion was halted. Gravels contain carbonate clasts which overlie an erosional channel base incised into siltstones, indicating that this material was advected into this zone from farther upstream, rather than being associated with a locally deflating surface resulting in the surficial concentration of clasts.

Estimating shear velocity from suspended load deposits

Settling velocities of the 95th percentiles (coarse fraction) of climbing rippled deposits, which estimate the shear velocities that would be needed to transport these grain sizes in full suspension.

Brushy Canyon reconstructions

Estimates of flow hydraulics and paleo-transport for Stage 1 stratigraphy are summarized in Table 3.2. I estimate the shear velocity for depositional currents using the critical shear velocity for gravel transport. In order to do this, I first calculated the dimensionless critical shear velocity for observed gravel using the method of Wiberg and Smith (1987), shown in Equation (2), and Equation (1). Grain-sizes travelling as fully-suspended load were estimated using the relationship $w_s / u^* \leq 1/3$ (Laursen, 1958; Smith and Hopkins, 1972) where u* is associated with initial motion for observed gravels. Depth averaged flow velocity was estimated from shear velocity using the drag coefficient of Parker et al. (1987) and Equation (3). Suspended sediment concentrations were estimated using Equation (4) and appropriate estimates for current thickness. The relief associated with sandstone beds draping concave–up topography was used to set the lower limit of current thickness (2.5m, Fig, 3.6). My estimates indicate that these currents had depth-averaged velocities of 1.34-1.88m/s and were dilute flows with concentrations lower than or equal to 5%. For flows with a 5% sediment concentration, our predictions show that particle sizes 241 microns and finer were transported as fully suspended load

while fractions coarser than 241 microns were transported as bedload or transiently suspended load (Fig. 3.21, A). For flows with a 1% sediment concentration, particle sizes 227 microns and finer were transported as fully suspended load while fractions coarser than 227 microns were transported as bedload or transiently suspended load (Fig. 3.21, A). These constraints show that the upper-fine or medium sands deposited in medium to thick beds associated with Stage 1 were sourced from bedload or transiently suspended load (Fig. 3.21, A)

Reconstructed flow hydraulics and paleo-transport for the stratigraphy of Stage 2 are summarized in Table 3.3. I used the settling velocity of the coarse fraction of climbing ripple-laminated deposits only (d_{95}=192-236 microns) to estimate shear velocity of the transporting fluid. Height of the barform was used to constrain the lower limit of current thickness to 12-15m. Results show that currents associated with constructing bar stratigraphy had depth-averaged velocities of 0.96-1.56m/s and were dilute flows with concentrations equal to or lower than 1%. These flows transported particle sizes coarser than 236 microns as incipiently suspended load and particle sizes coarser than 1-2.5mm as pure bedload (See Fig. 3.21, B).

Table 3.2: Estimates of paleo-flow hydraulics and paleo-transport from Stage 1 deposits

	Using critical shear stress of gravels with median clast size =0.005m (after Wiberg and Smith, 1987)	**Constraints imposed by bed geometry**
Shear velocity (m/s)	0.059-0.067	minimum relief associated with concave-up sandstone beds = approximately 2.5m
Depth averaged velocity (m/s)	1.34-1.50	
Current thickness (m)	>2.5	
Volumetric sediment concentration	0.01-0.05	
Fully suspended particle sizes (concentration = 1%)	213 micron and finer	
Fully suspended particle sizes (concentration = 6%)	228 micron and finer	

Table 3.3: Estimates of flow hydraulics and paleo-transport from stage 2 deposits

	Using settling velocity of d95 of climbing ripple lamination (192-236 microns, after Smith (1967)	**Constraints imposed by bed geometry**
Shear velocity (m/s)	0.043-0.07	Relief of inclined beds = 12-15m = lower limit of current
Depth averaged velocity (m/s)	0.96-1.56	
Volumetric sediment concentration	0.01 or less	

(v) A facies model for suspension-dominated submarine bars

I interpret the set of inclined beds making up facies association 2 as a suspension-dominated bar built from sedimentation in a low velocity zone of flow separation near the channel bank. This type of barform differs from the classic point bar where the sediment building the bar is primarily sourced from bedload transported into the reach and migrating downstream along the surface of the bar. Dunes which build point bars are transported by coherent flow that extend across the channel from the thalweg and up across the bar surface (Dietrich and Smith, 1984). The sediment that builds a separation-bar is advected into a localized low velocity zone along the channel bank and trapped there (Hickin, 1979; Rubin, 1990; Rubin et al., 1998). Sediment settling out of suspension in this low velocity zone can be re-worked on the bed to varying degrees by eddies to form a variety of sedimentary structures and orientations as documented by Rubin (1990) and Rubin et al. (1998). Point bars built by dunes migrating across a transverse slope commonly have low surface slopes of 4-8 degrees. The median value of all the measured dips in the inclined beds of the interpreted bar deposits of facies association 2 (Stage 2) is 10^{o}, with maximum measured values of 22 ^{o}. These dip values show similar ranges and median values to the bar slope values presented in Chapter 2, where planform geometries suggest sedimentation from suspended load in low-velocity zones. I suggest that large barforms on the scale of those often imaged in acoustic datasets (Chapter 2, Abreu et al., 2003) may be under-recognized or poorly exposed in outcrop because of their large size and the likelihood that they are relatively mud-rich.

A review of the geometries and depositional processes associated with bank-attached bars in meandering rivers has been discussed extensively in Chapter 2, drawing on the results of past work (Bagnold, 1960a, b; Hickin, 1979; Leeder and Bridges, 1975; Leopold et al., 1960; Page and Nanson, 1982; Page et al., 2003; Smith et al., 2009; Woodyer, 1975). Chapter 2 presents measurements of bank-attached bars in sinuous submarine channels imaged in a high- resolution seismic volume. These bars are interpreted to have been constructed in flow-separation zones associated with channel curvature. Thicknesses of these bars scale with channel depth (Abreu et al., 2003; Chapter 2) and measured dips along bar surfaces showed a median value of ~11 degrees, with measured maximum dips of 18 degrees.

Some grain-size distributions in Facies Association 2 show a bi-modal grain–size distribution in which a second peak appears at approximately 210µm (Fig. 3.18, F, G,H, J). The coarser grain sizes making up this second mode are interpreted to be tied to the fluctuations in the locations of the detachment and reattachment points. These fluctuations occasionally allowed for pulses of transiently suspended sediment to be carried into the separation zone.

CONCLUSIONS

In the studied channel complex two stages are identified:

1) An initial stage where preserved stratigraphy is composed of thickly-bedded units of trough cross-stratified, planar-stratified or structureless sands, interspersed with a few

gravel-rich beds. These deposits are interpreted to be associated with aggradation of the channel bed and reduction in channel relief.

2) A later stage where stratigraphy is dominated by a steeply dipping set of beds made up of fine grained sandstones. These deposits are interpreted to represent the development of a thick barform built from suspended load deposits in a low velocity zone of flow separation at the margin of a channel.

Grain size data, sedimentary structures and paleohydraulic constraints indicate that this bar was built predominantly by fully suspended sediment, with minor contributions from incipiently suspended sediment. The occasional incorporation of incipiently suspended material into the bar is interpreted to have occurred at locations more proximal to the mixing boundary along the edge of the flow separation zone (Fig. 3.2). Variable bed shear stress along the bar surface resulted in varying degrees of reworking and in the preservation of a wide variety of sedimentary structures including planar stratification, trough cross-stratification, and climbing-ripple lamination commonly displaying mud drapes. The internal stratigraphy of the bar displays repeated scouring, interpreted to be the result of reworking of the bar surface as bar shape changed. I interpret that the high median slopes of beds indicate the bar could not have been constructed through deposition connected with bedload transport, but rather that it had to have been built from suspended sediment deposition. I suggest that this facies model is applicable to all submarine channel bars built from suspended sediment load.

Channel fills on the proximal basin floor are composed of thickly-bedded units of climbing-dune stratified sandstones, displaying sub- to super-critical angles of climb.

These deposits are interpreted to be sourced from suspended sediment load. Similarity between the grain size distributions of sand filling these basin floor channels and the sands building the bar in the channel on the upper slope suggest:

1. Some well-suspended sediment travelling through upper slope channels were trapped in low velocity zones associated with flow separation from the channel bank, but is otherwise bypassed in large volumes to the basin floor where they fill in basin floor channels.

2. Sediment sizes coarser than 250 microns travel as pure bedload or transiently suspended load on the upper slope but were removed from transport via deposition on the slope before the currents arrived at the basin floor.

Paleo-hydraulic reconstructions from the slope-channel fills show that deposits were constructed by dilute (less than 5%) turbidity currents with depth-averaged velocities between 0.96-1.88m/s.

ACKNOWLEDGEMENTS

I thank the Guadalupe Mountains National Park service for assistance and support in carrying out this work. Charlie Kerans, Charlie Harmen and Joseph El-Azi are thanked for their assistance with the air-borne LiDAR data-set. Christine Rossen is thanked for offering insights and field notes on the upper slope study area. Elisabeth Steel, Julio Leva Lopez, Carlos Pirmez and Christine Rossen are thanked for field assistance rendered to A.M.F. and D. M. Financial support for this project was provided by the Jackson School

of Geosciences, the RioMAR consortium of oil companies, the Ike Crumbly AAPG Grant-in-Aid, the West Texas Geological Society John Emery Adams Scholarship and the SEPM Weimer Research Grant.

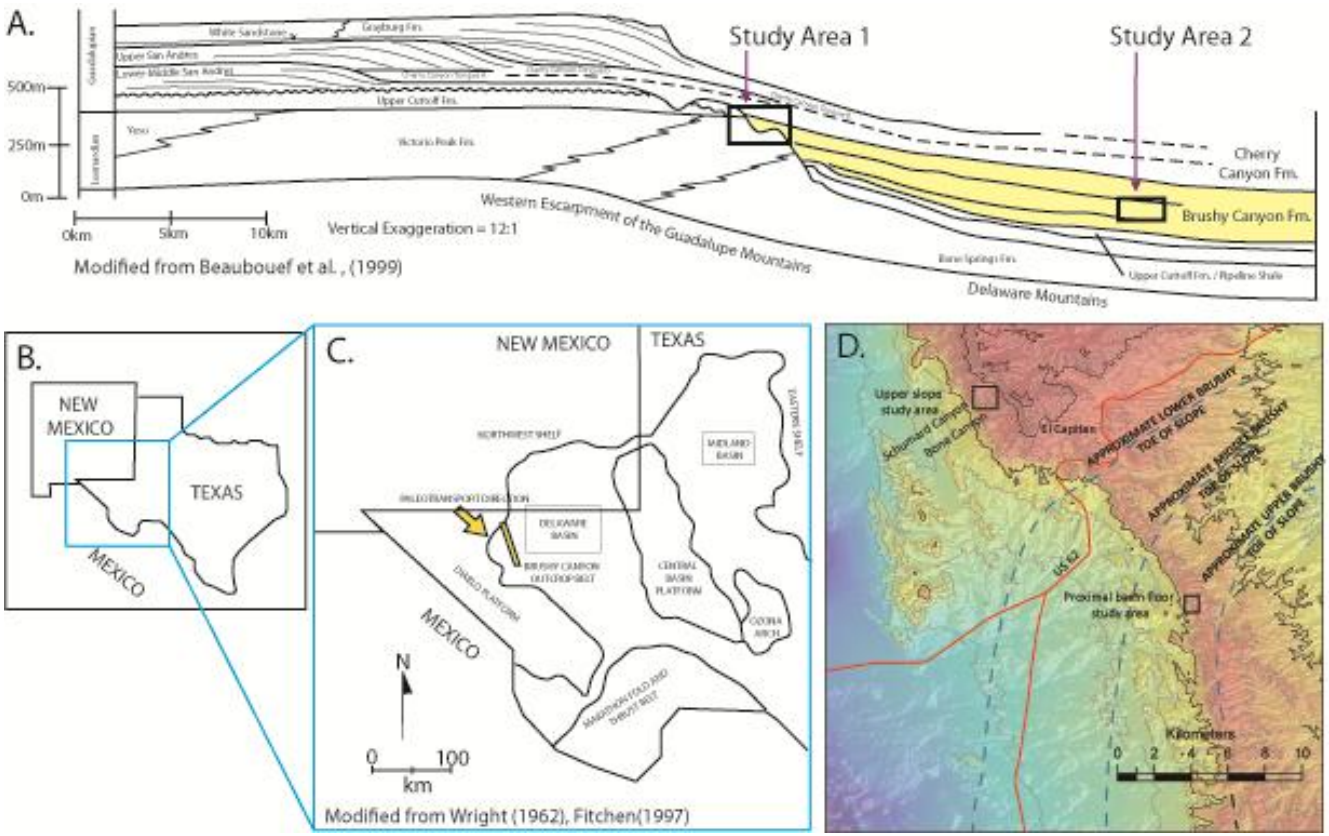

Figure 3.1: A) A cross-section showing pertinent stratigraphic relationships associated with the Brushy Canyon Formation and surrounding formations (modified from Beaubouef et al., 1999). B) Geographic location of the Delware Mountain group. C) Paleogeography of the Permian Delaware Basin, showing the Brushy Canyon formation outcrop belt. D) Elevation map draped by slope and contour maps showing the locations of the two study areas (cold colours are low relief, warm colors are high relief) on the upper slope of the Upper Brushy Canyon Formation and the proximal basin floor of the Middle Brushy Canyon Formation.

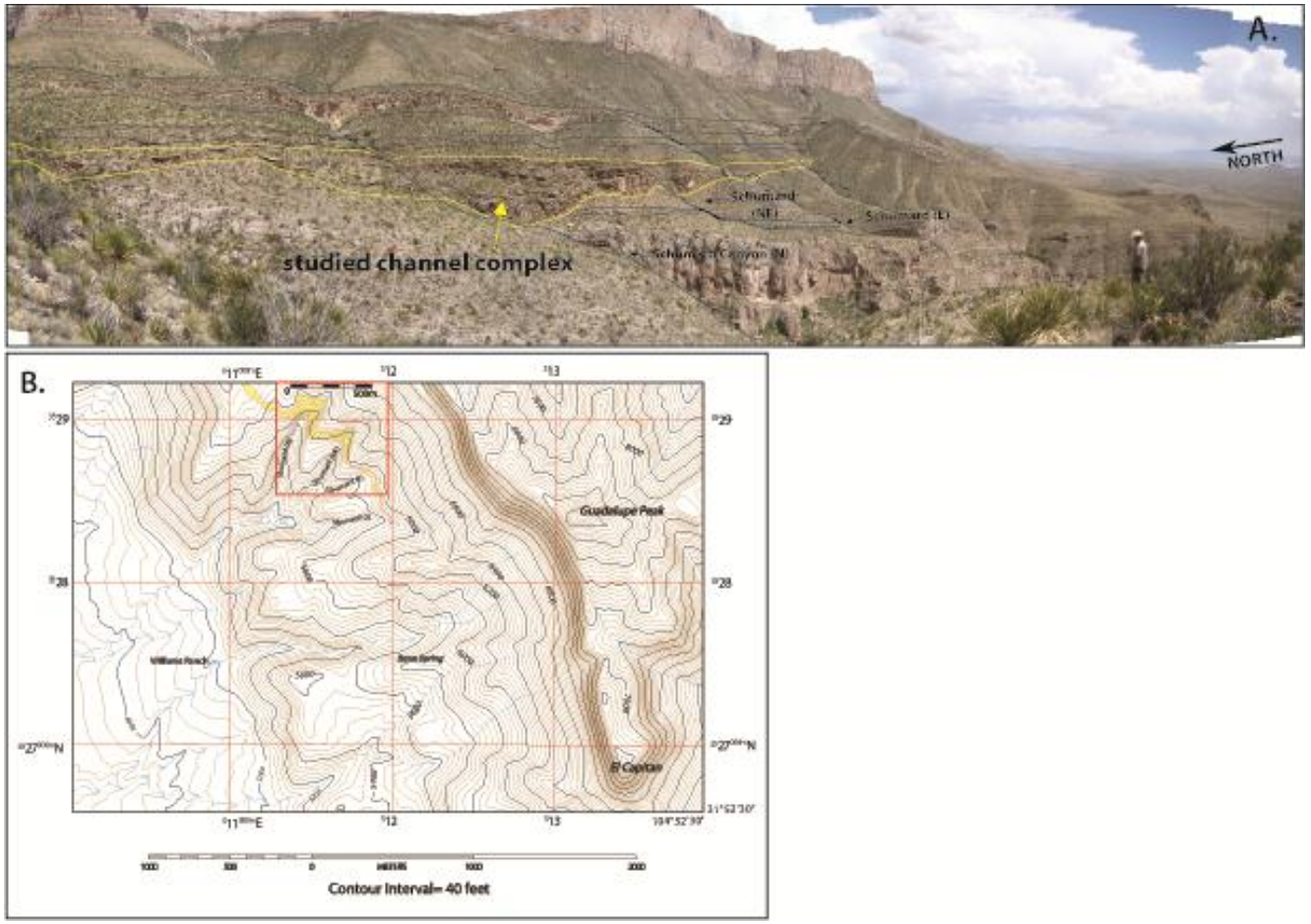

Figure 3.2: A) A dip-oblique overview photograph of the Brushy Canyon upper slope channels exhumed on the western face of the Guadalupe Mountains. Photograph taken from the west wall of the north branch of Shumard Canyon, looking south. B) A contour map showing the location of upper slope Channel Complex 1 in Shumard Canyon.

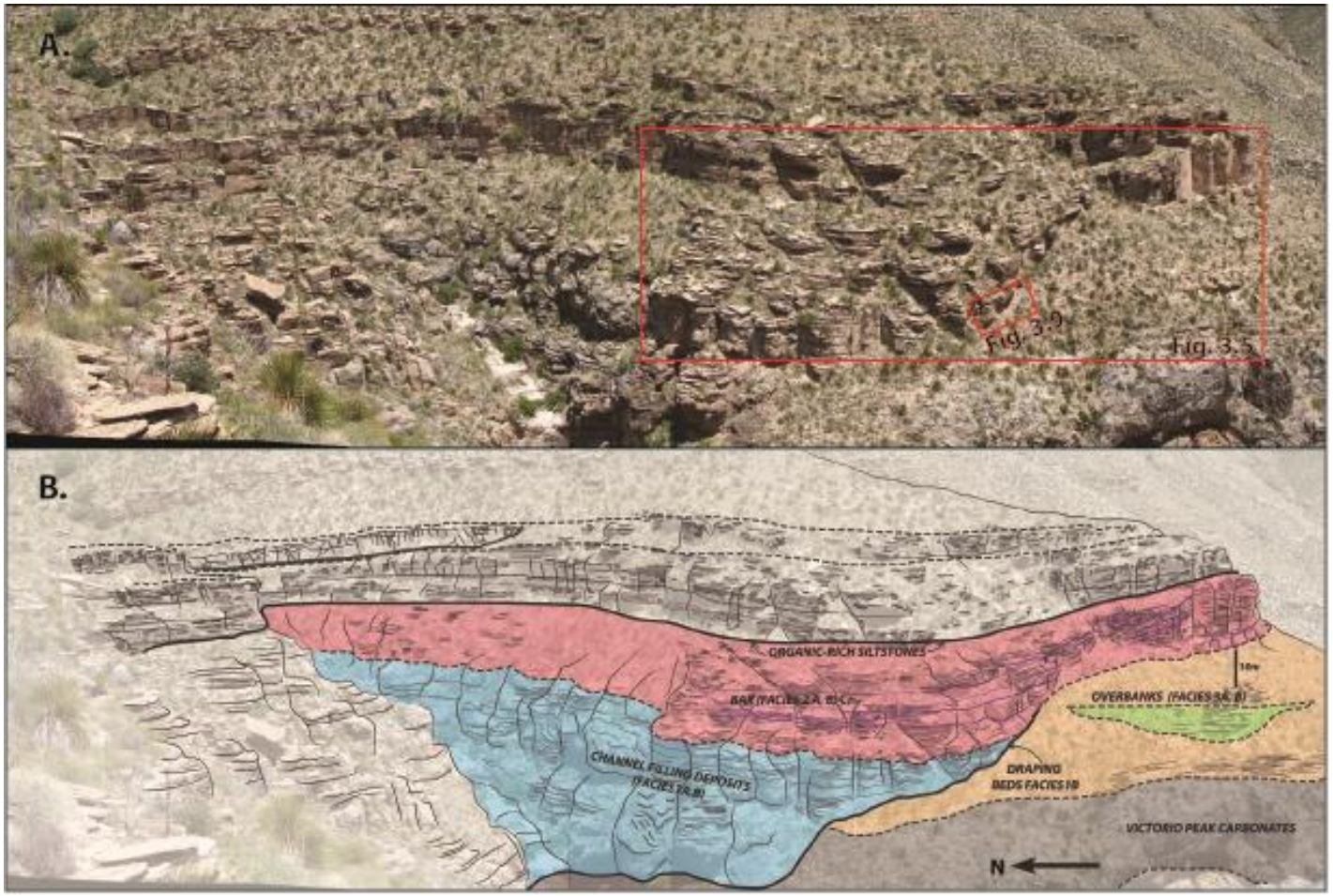

Figure 3.3. A) Exposure of Channel Complex 1 on the East wall of North Shumard Canyon, with red boxes indicating locations of Figures 5, 6, 7. B) A line drawing highlighting the broad stratigraphic relationships between Facies Associations 1, 2 & 3 and the underlying carbonates.

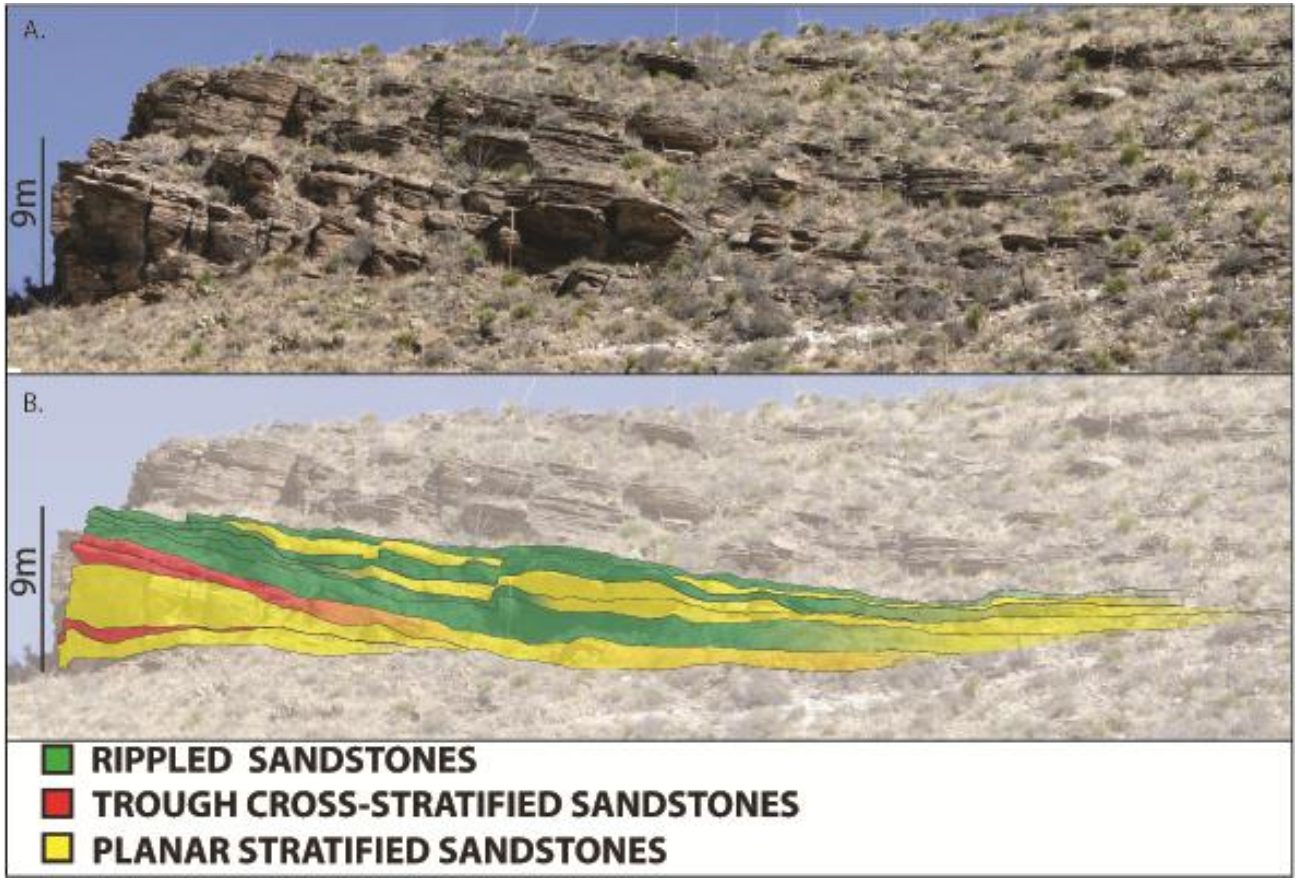

Figure 3.4: Photograph (A) and mapped facies (B) of the interpreted bar deposits of Facies Association 2, on the north wall of NE Shumard. Deposits composed of steeply-dipping bed-sets displaying repetitive internal scours and lateral transitions between thick stacks of climbing ripple-laminated deposits, trough cross-stratified beds and planar-stratified beds are interpreted as sediment deposited from suspension and reworked to variable degrees on the bed.

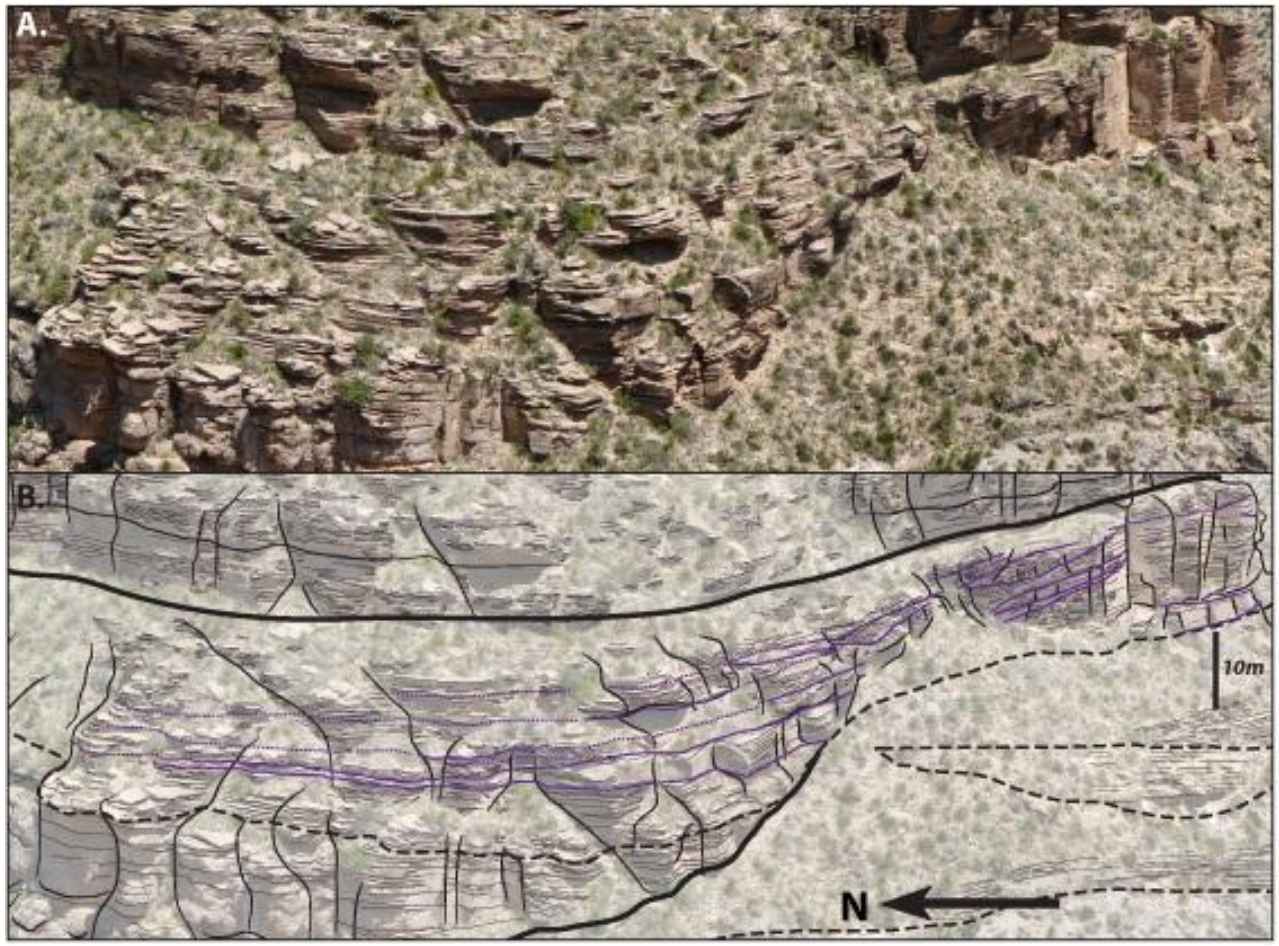

Figure 3.5: A) Steeply dipping beds of the interpreted bar package of facies association 2 in Stage 2 of Channel Complex 1. B) A line drawing showing the mapped internal scours (solid purple lines) and interpreted correlations (dashed purple lines) within facies association 2 in North Shumard.

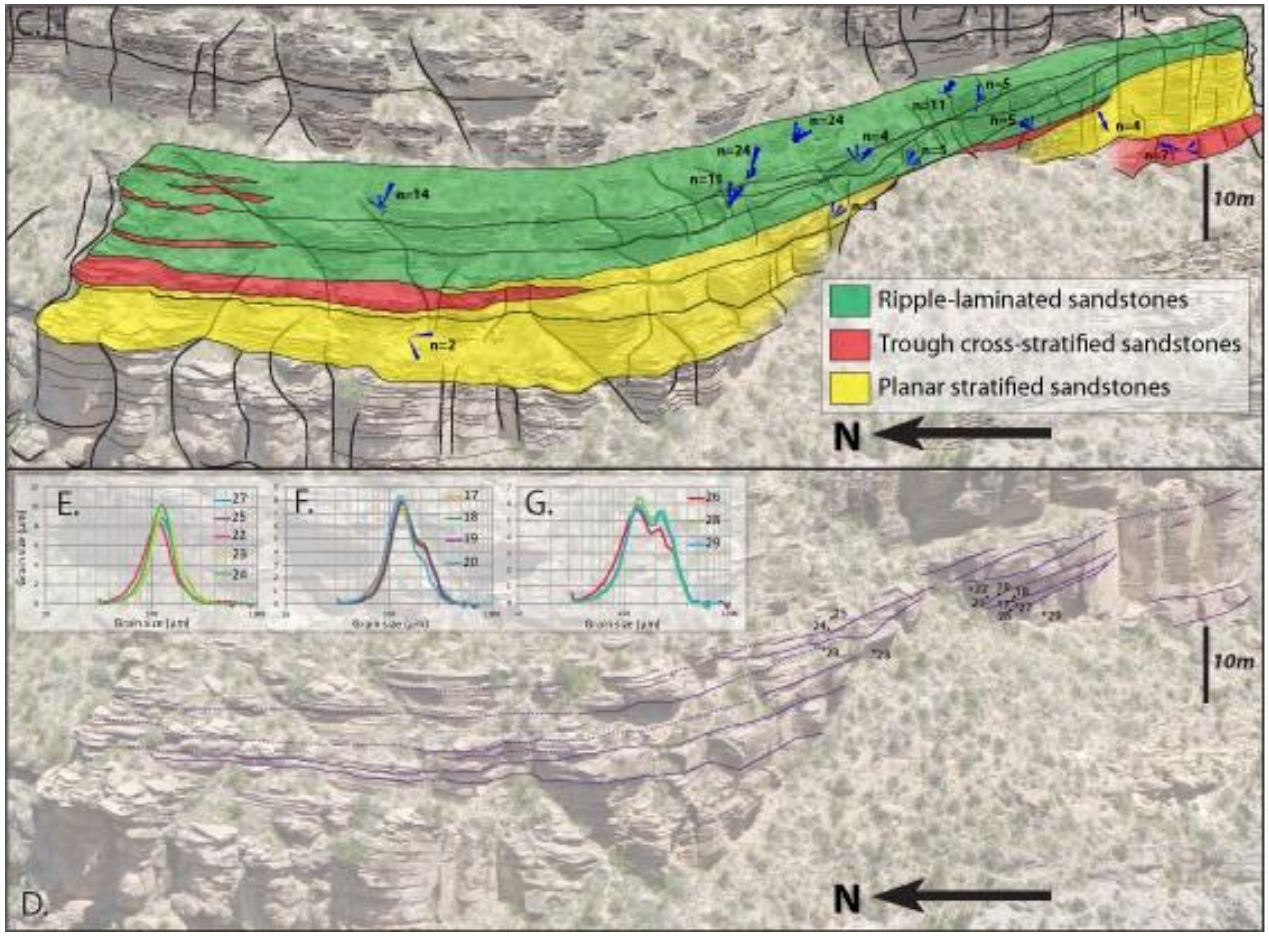

Figure 3.5: C) Ripple directions and facies mapped within Facies Association 2 in North Shumard. Ripple transport is generally at high angles to the visible dip of the beds. D) Histograms and sample locations from Facies Association 2 in North Shumard. Deposits are generally well-sorted (E), but sometimes show weak bimodality (F, G) interpreted as a dual source from suspended load ad bedload.

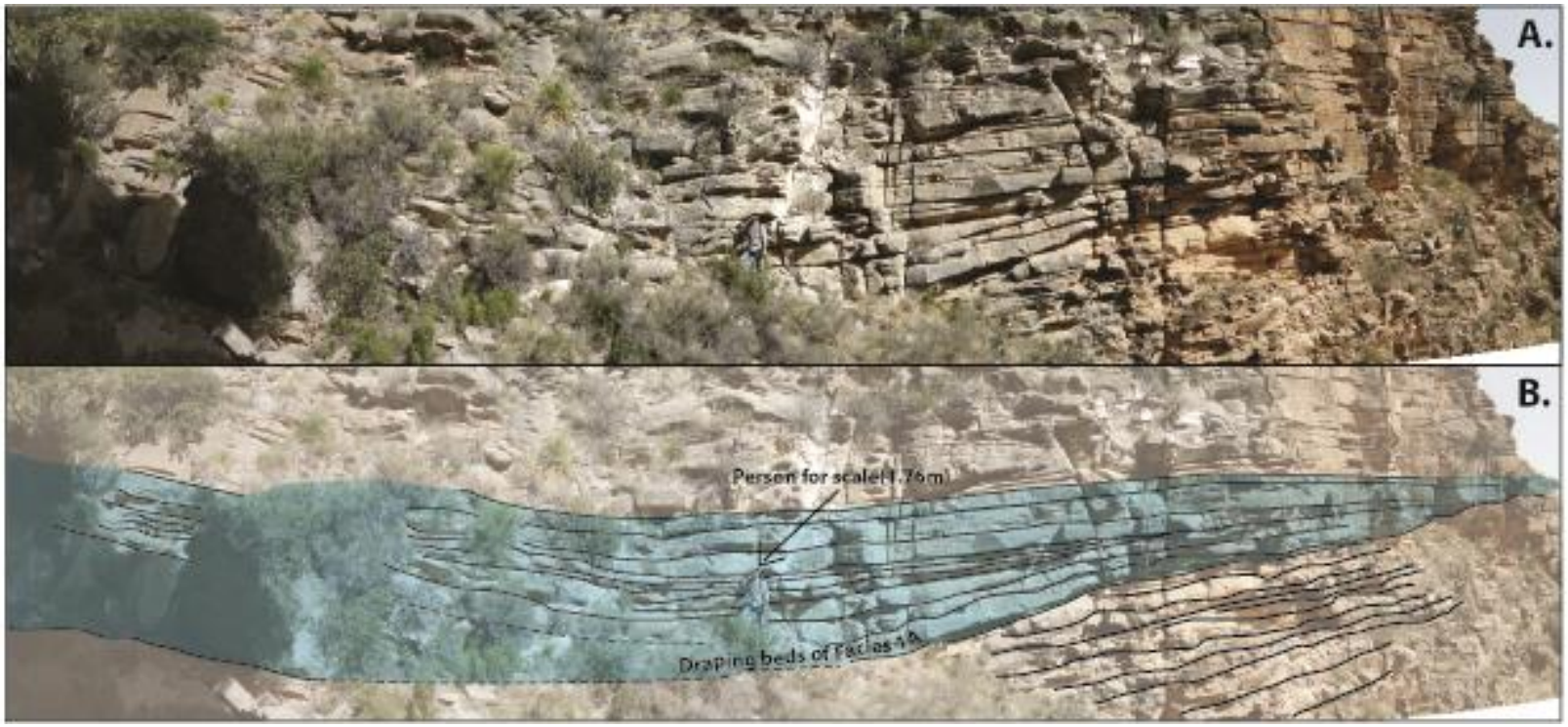

Figure 3.6: Photograph (A) and line drawing (B) of geometries associated with thickly-bedded, fine- to medium-grained, structureless sandstones of Facies 1A, which drape a scour ~2.5m deep and thin at the margins

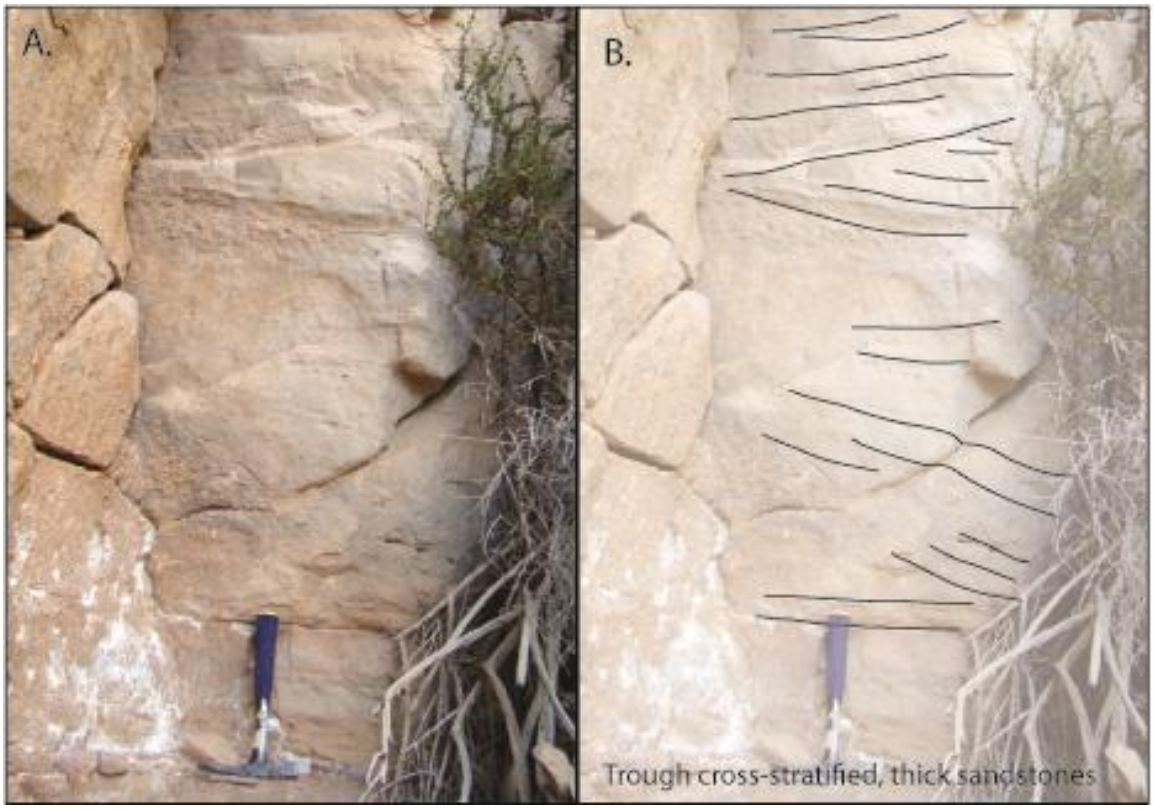

Figure 3.7: Photograph (A) and line drawing (B) of thickly-bedded, trough cross-stratified fine- to medium-grained sandstones of facies 1A.

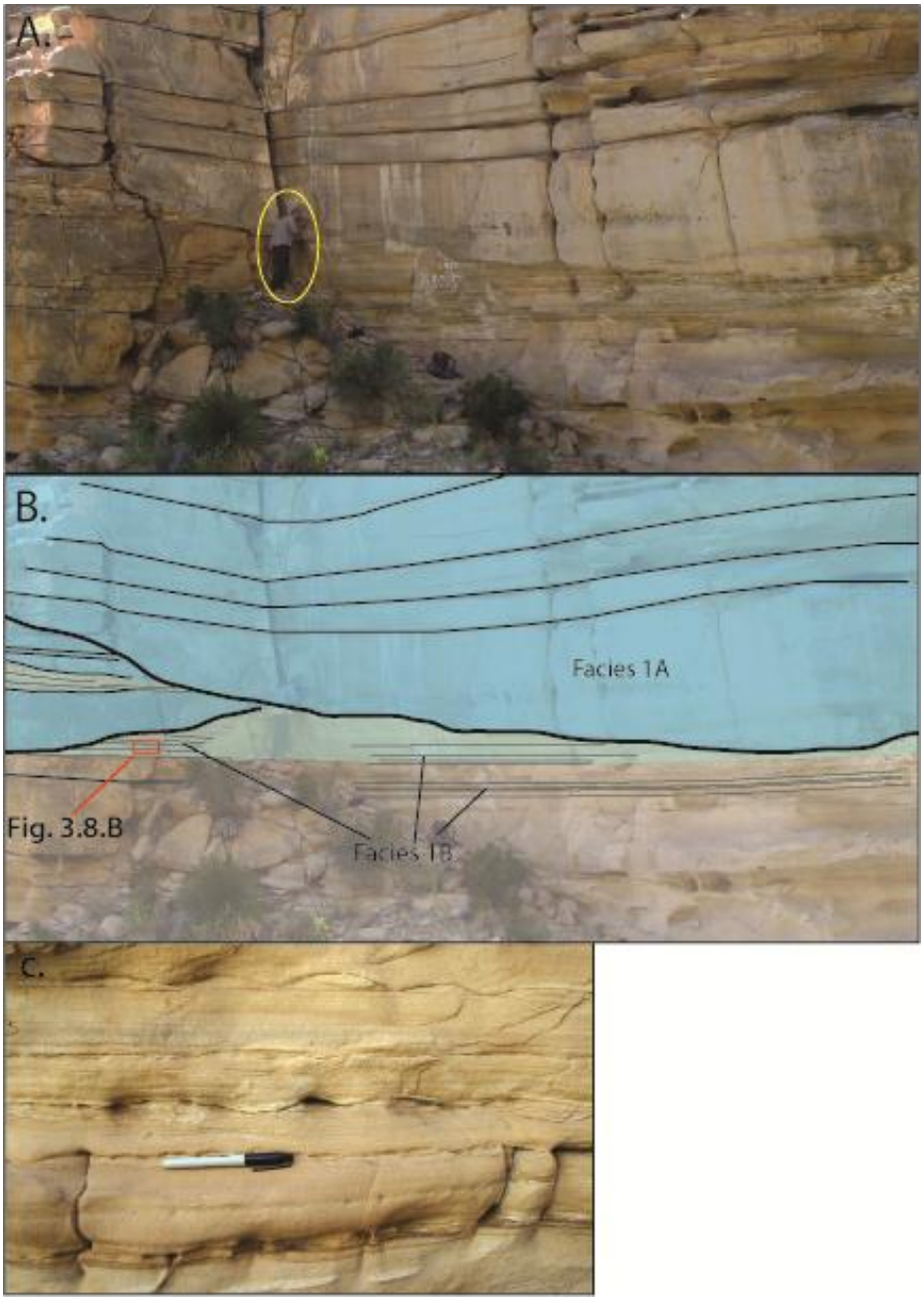

Figure 3.8: Photograph (A) and line drawing (B) showing the interbedded units of Facies 1A and 1B. Person for scale indicated in the yellow ellipse. Thinly-bedded, planar-stratified and ripple-laminated sandstones of Facies 1B (C).

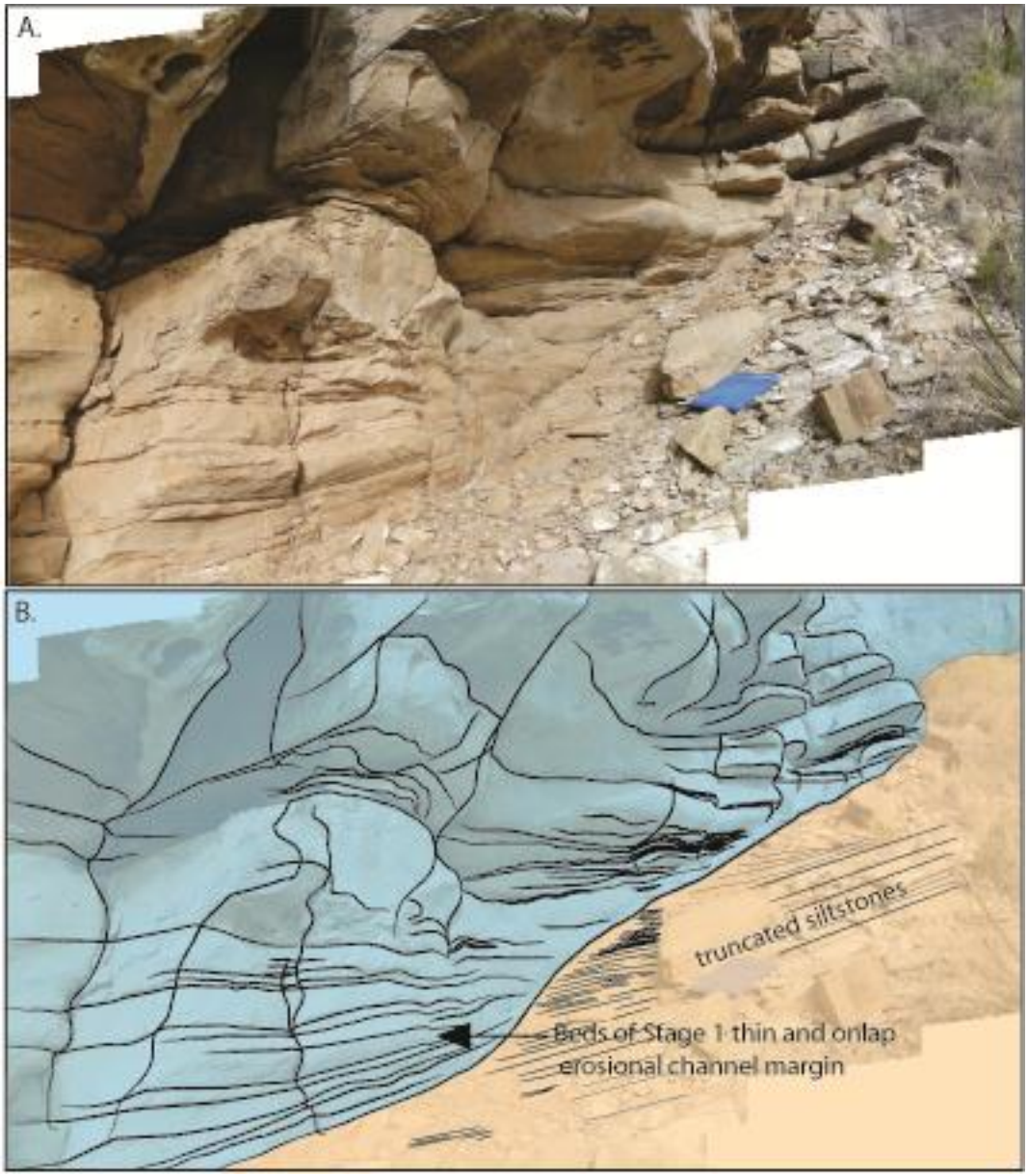

Figure 3.9: Photograph (A) and line drawing (B) of outcrop geometry at location shown in Figure 3A. The line diagram shows the thinning of thick beds of Facies 1A as they transition into thinly bedded Facies 1B and tangentially onlap against the channel margin in North Schumard. The erosional margin truncates siltstones associated with the first sandy channel fill underlying CC1.

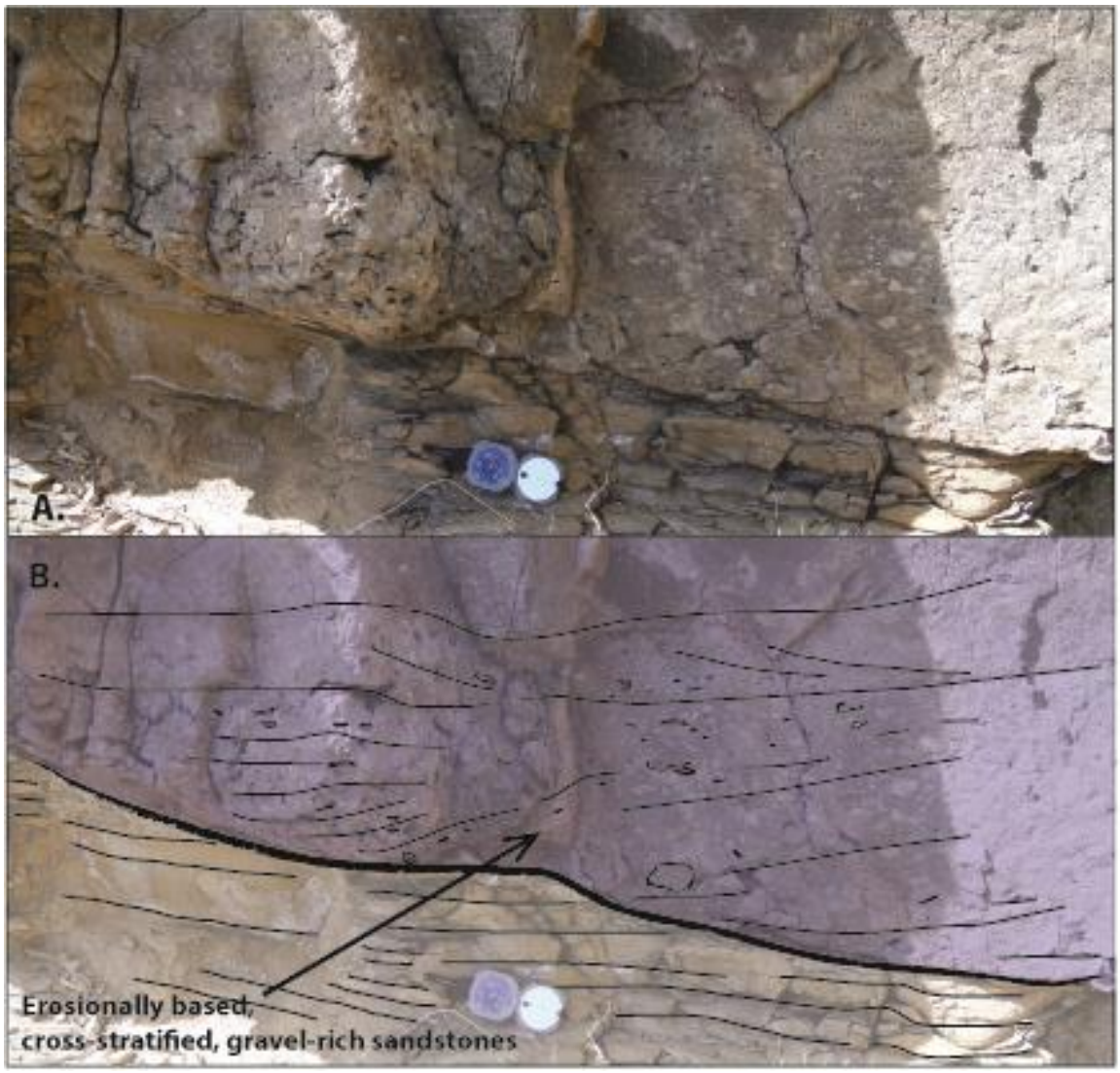

Figure 3.10: Photograph (A) and line drawing (B) of erosively based, cross-stratified, gravel rich sandstones of Facies 1 C.

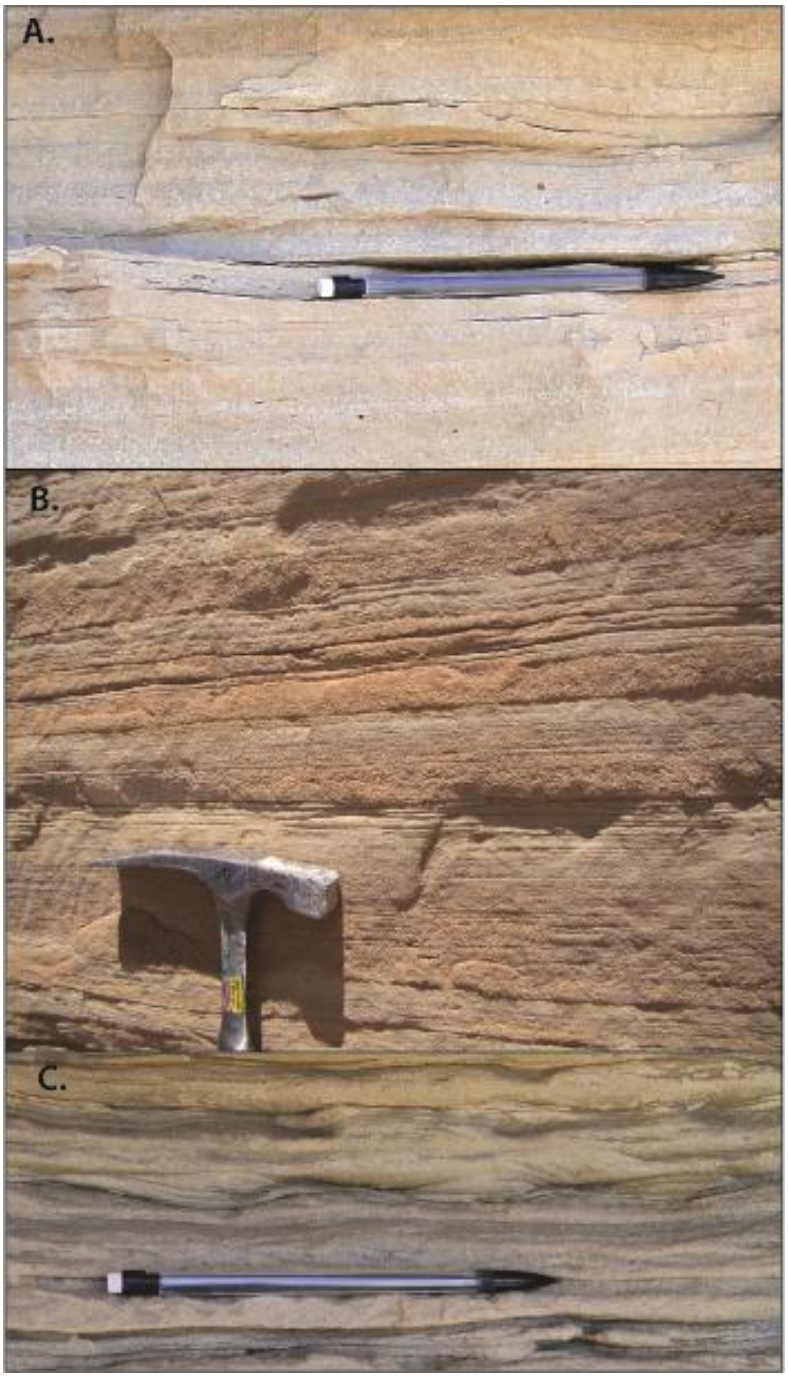

Figure 3.11: A) Planar-stratified, fine-grained sandstones of Facies 2C, with visible internal laminations. B) Planar-stratified, sandstones of Facies 2C, with layers of upper fine sandstone alternating with lower fine sands. C) Poorly-defined ripples with mud drapes, in Facies 2A.

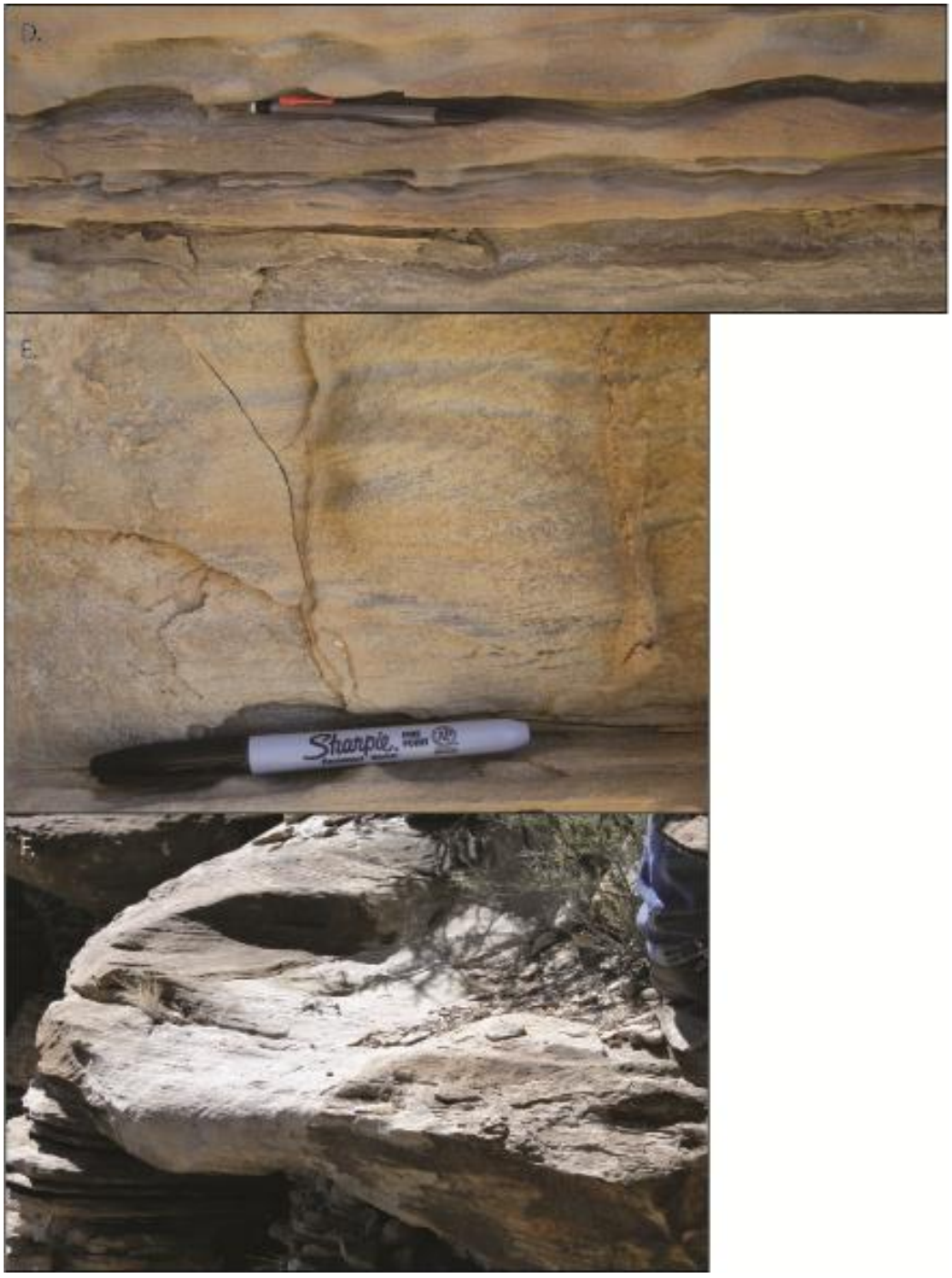

Figure 3.11 (continued): D) Alternations of planar-stratified, thin beds with climbing-ripple laminated tops in Facies 2 A. E) Super-critically climbing ripple-laminated sandstones. F) Medium-bedded, trough cross-stratified sandstones.

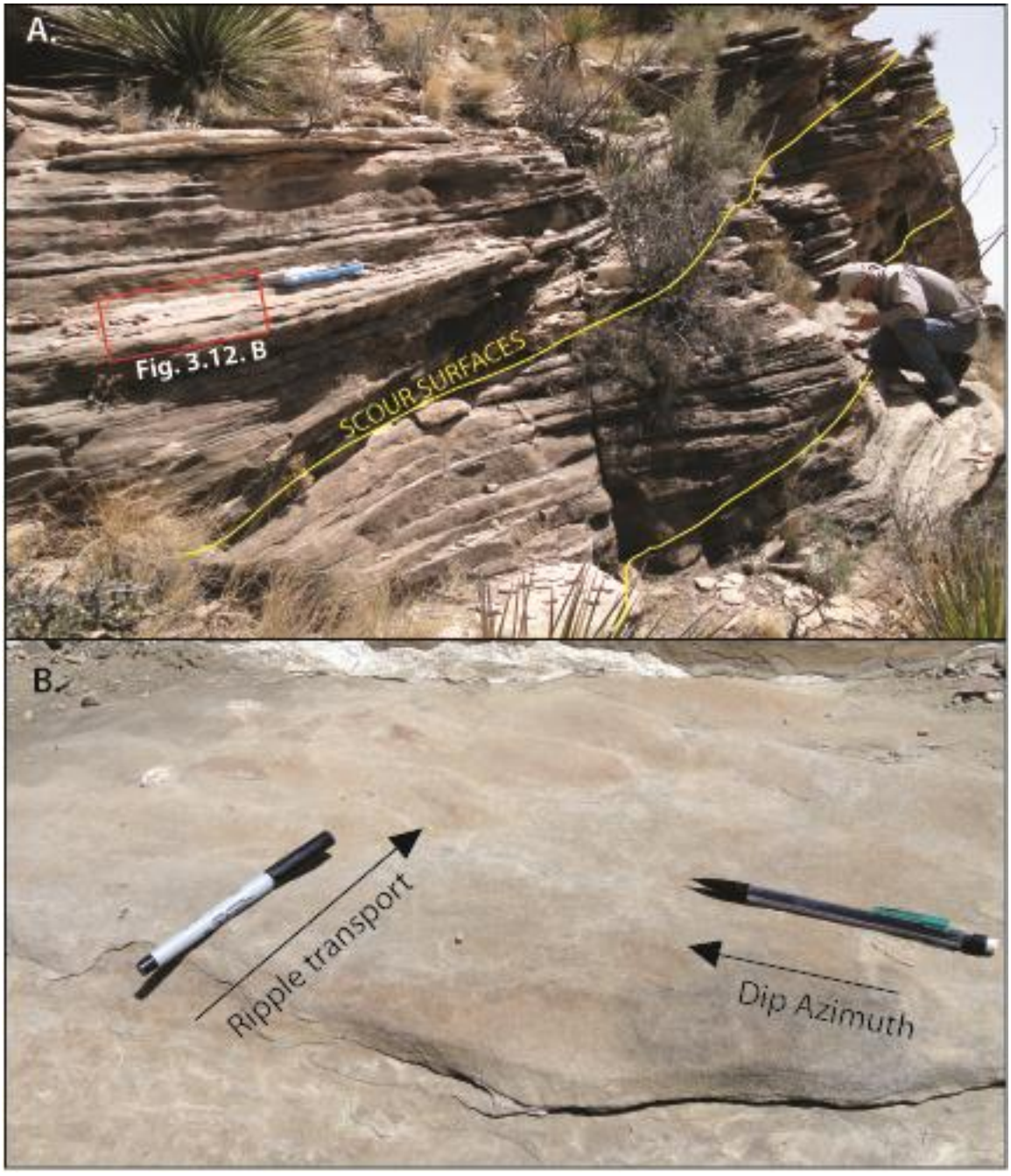

Figure 3.12: A) Steep scour surfaces within interpreted bar deposits of Stage 2. Photograph shows thinly-bedded planar-laminated or ripple-laminated sandstones draping or tangentially onlapping the scour surfaces. B) The bedding surface at the location shown by the red box in 14A show ripple transport directions that have high angles to the dip azimuth of beds.

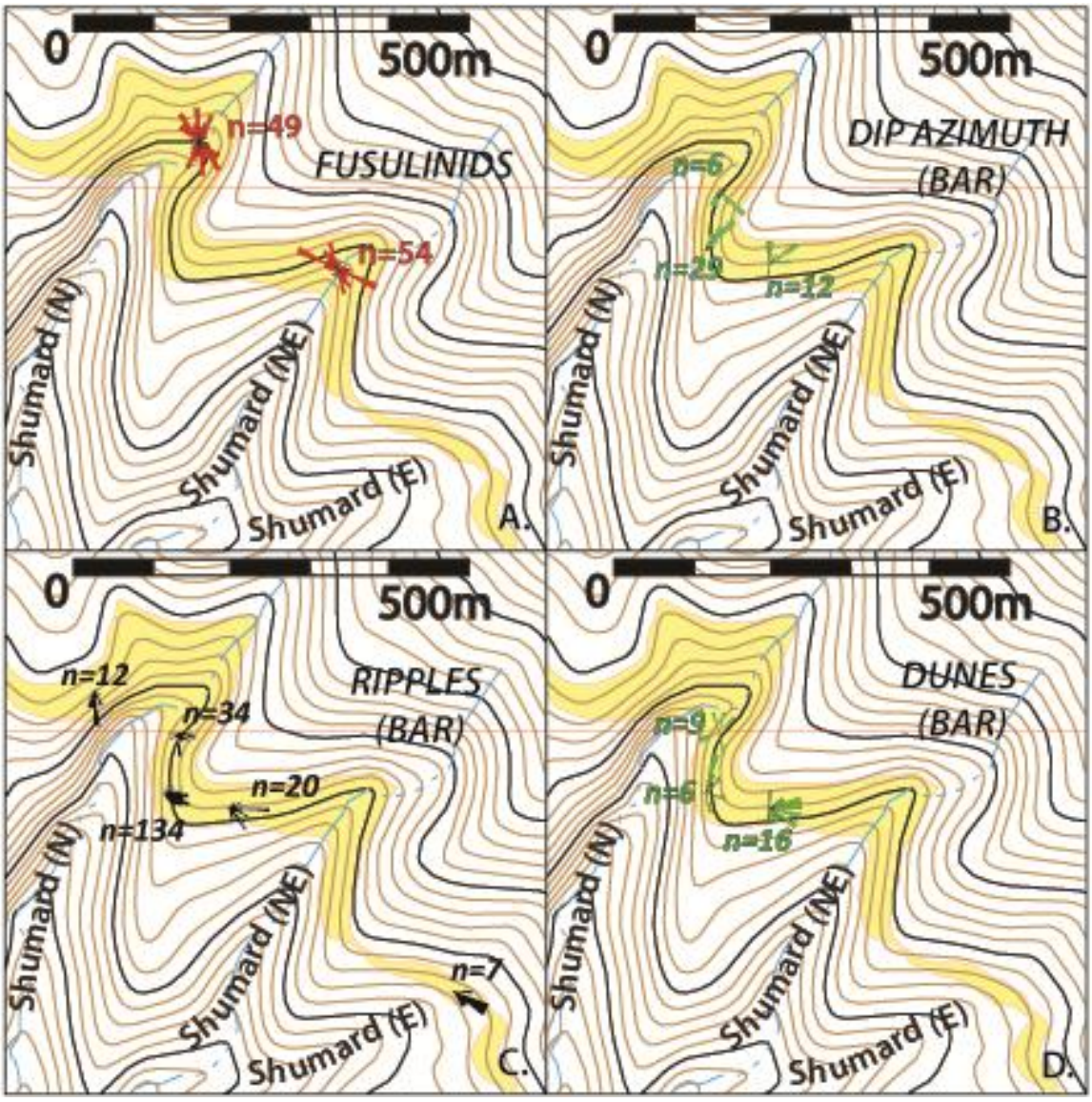

Figure 3.13: A) Fusulinid long axes orientations from within Facies 1A and 1C show a southeasterly trend to transport in Stage 1. B) Bedding dips from facies association 2 are mostly oriented north-east, but some south-easterly diping beds in North Shumard suggest that bar shape was complex. C) Ripple transport directions from facies association 2 indicate transport at high angles to bedding dips. D) 3D-dune migration directions from trough orientations in facies association 2 show a wide range of orientations (10-180m degrees).

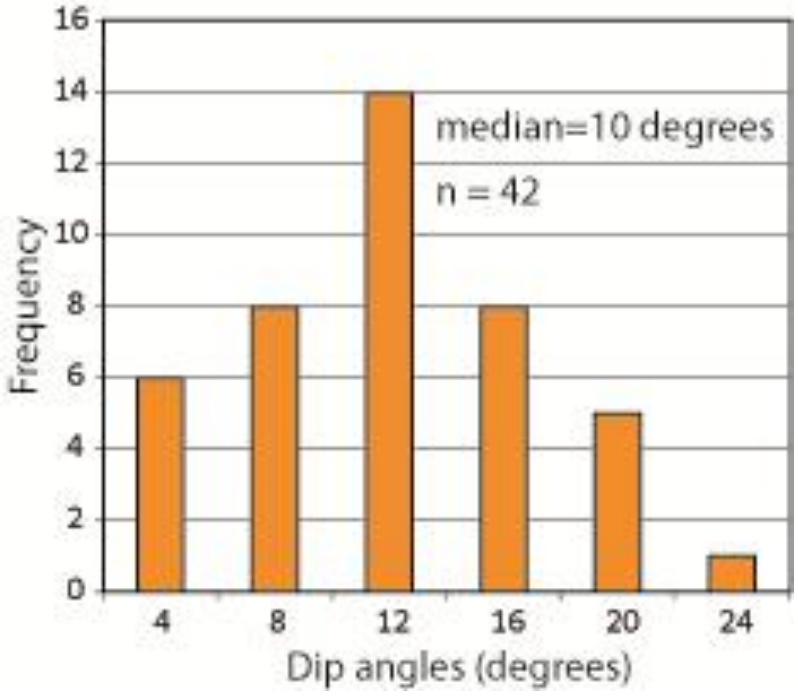

Figure 3.14: A histogram shows a median value of 10 degrees from 42 measured dips in Facies Association 2.

Figure 3.15: Prominent thin, sandier beds (A) of Facies 3B, within laminated siltstones (A,B) of Facies 3A at the margins of CC1 are interpreted as overbank deposits.

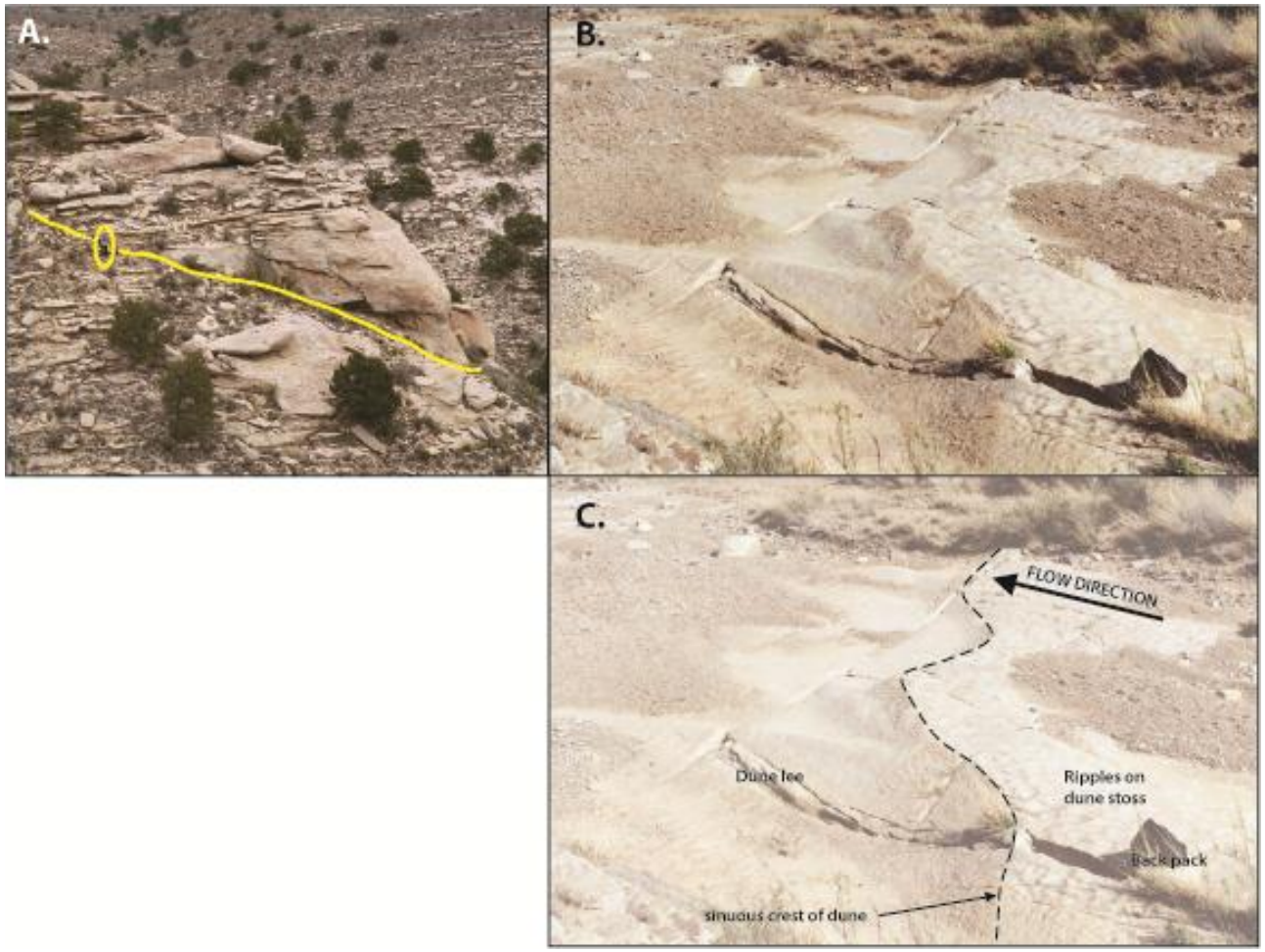

Figure 3.16: Thick, channel-plugging sandstones (A) of Facies 4 filling a channel on the proximal basin floor. Person for scale is indicated in yellow cirlce. Photograph (B) and sketch (C) of an exposed sinuous-crested dune in Facies 4 with ripples migrating up the stoss side of the dune.

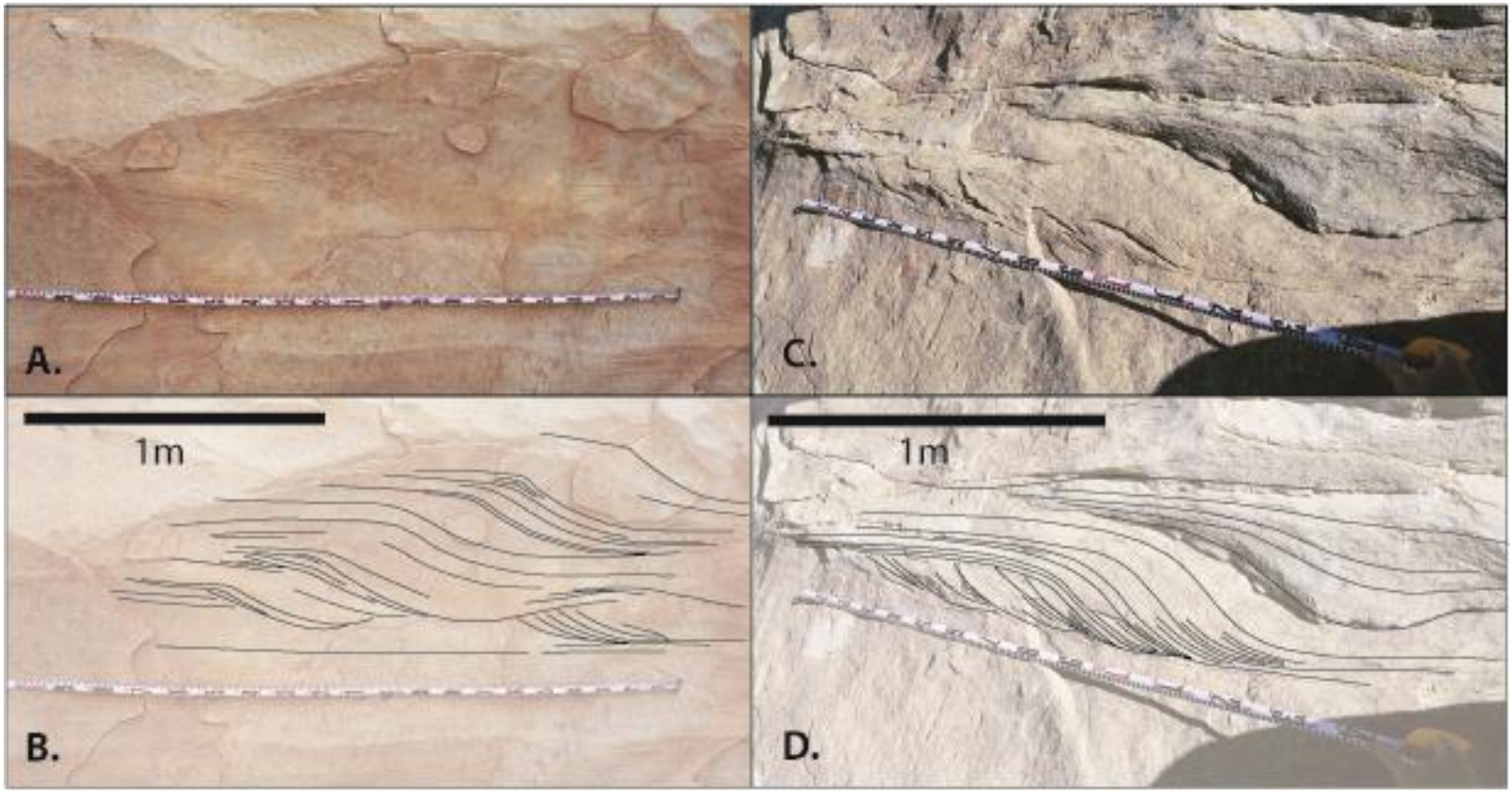

Figure 3.17: Photographs (A, C) and accompanying sketches (B, D) of dune-stratified, fine-grained sandstones showing sub- to super-critical climb angles in thickly-bedded, channel filling deposits at the toe-of-slope.

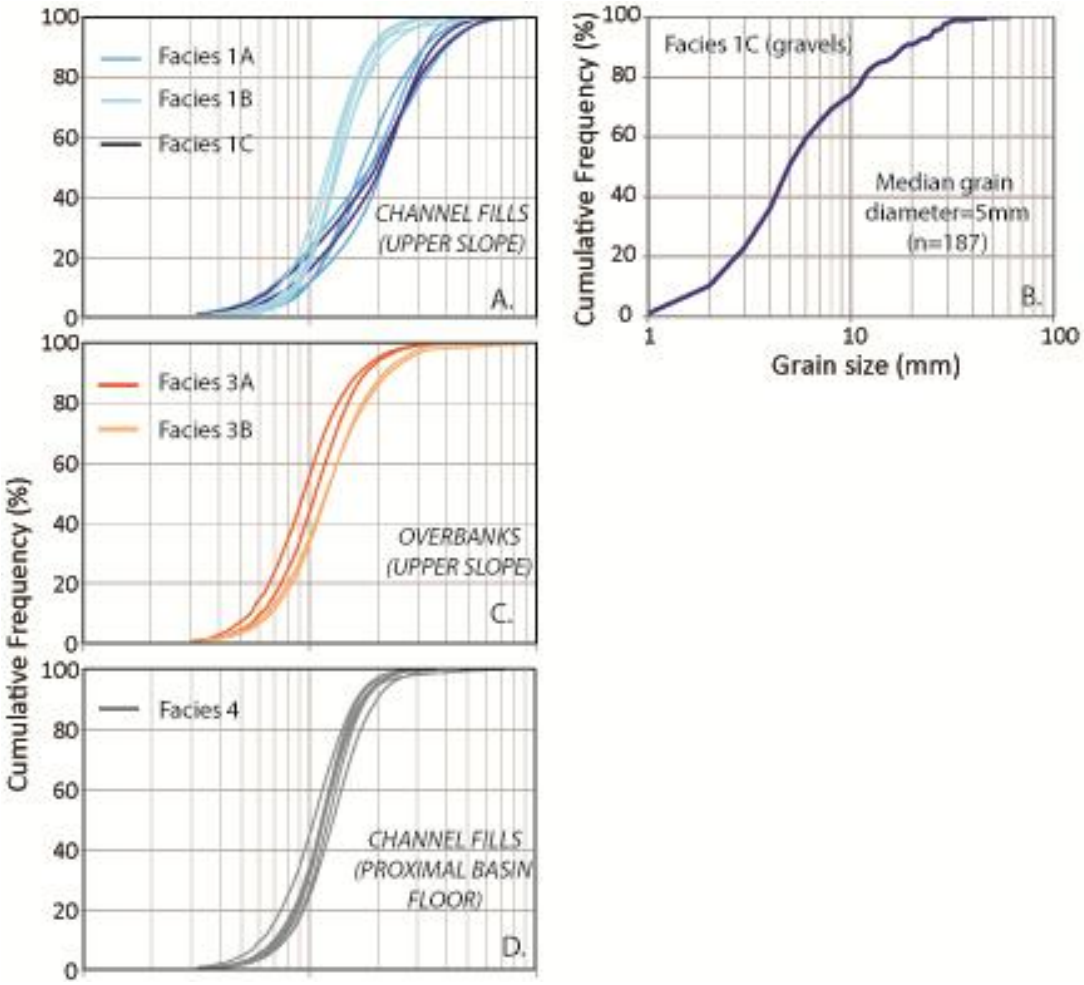

Figure 3.18: Grain-size distributions of all facies. A) Note that thin-beds of Facies 1 B are distinctly finer grained than the thicker beds of Facies 1 A and B) 187 measurements of gravel clast long axes have a median length of 5mm. C) Grain-sizes present in the overbank show a slight coarsening in the thicker, more prominent beds of Facies 3B. D) Channel fills on the basin floor show a narrow range of grain sizes. E-J) Grain sizes preserved in upper slope bar show very litle internal variation. Two modes are sometimes present, at 120 and 210 microns respectively. L) Grain sizes present in the upper slope bar and channel fills are compared to grain-sizes in basin floor channel fills. Sizes coarser than 250 micron are absnet from the bar and basin floor. These are interpreted to have been travelling near the channel bed and removed from transport on the upper slope. Grain sizes in basin floor channel fill are well represented in the bar on the upper slope. Note that the coarse fractions present in the bar deposits (E, G, I) are similar to the coarser-fraction present in the over banks, sugesting that these grain-sizes were well-suspended.

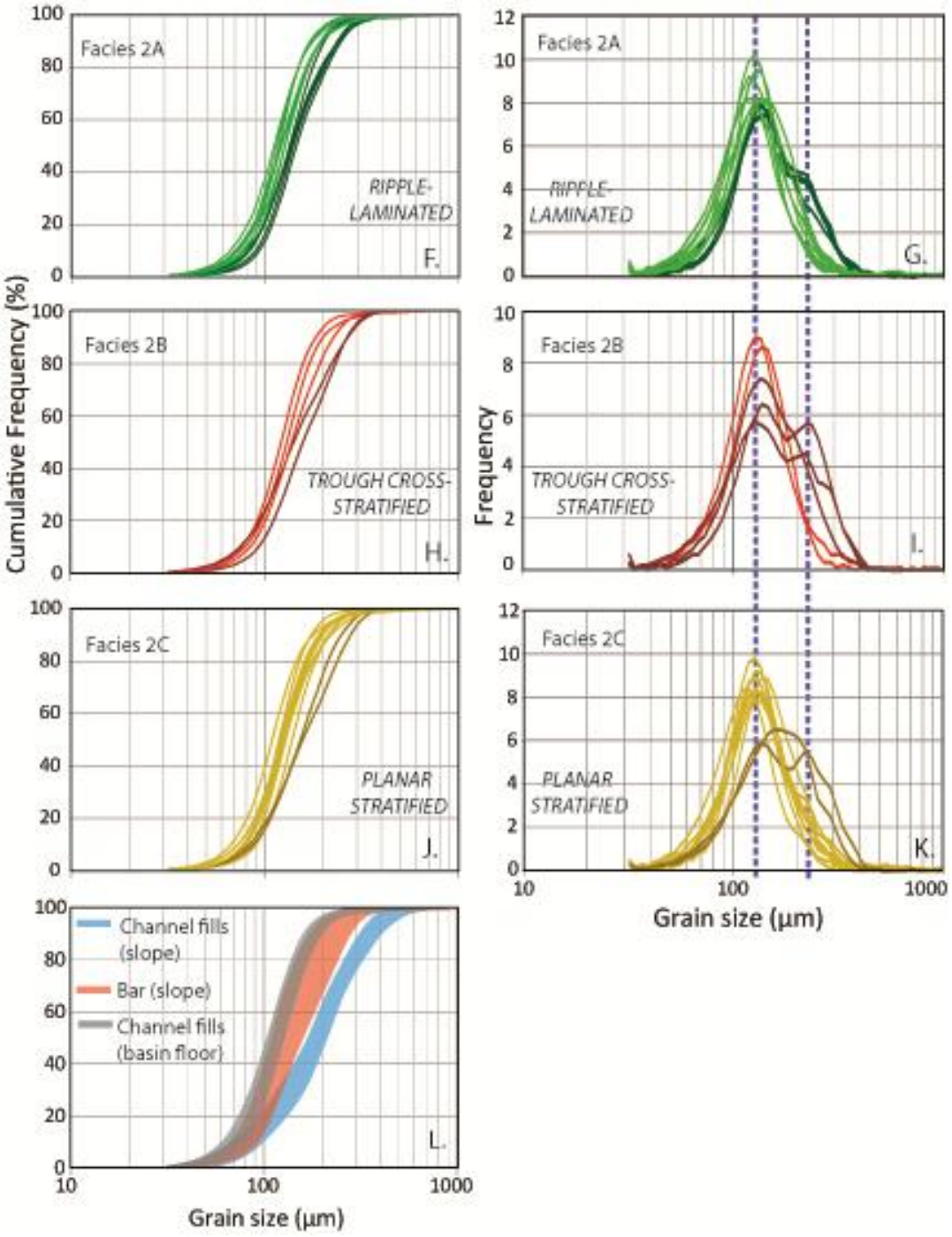
Facies 2A
RIPPLE-LAMINATED
F.
Facies 2A
RIPPLE-LAMINATED
G.
Facies 2B
TROUGH CROSS-STRATIFIED
H.
Facies 2B
TROUGH CROSS-STRATIFIED
I.
Facies 2C
PLANAR STRATIFIED
J.
Facies 2C
PLANAR STRATIFIED
K.
Channel fills (slope)
Bar (slope)
Channel fills (basin floor)
L.
Cumulative Frequency (%)
Frequency
Grain size (µm)
Grain size (µm)

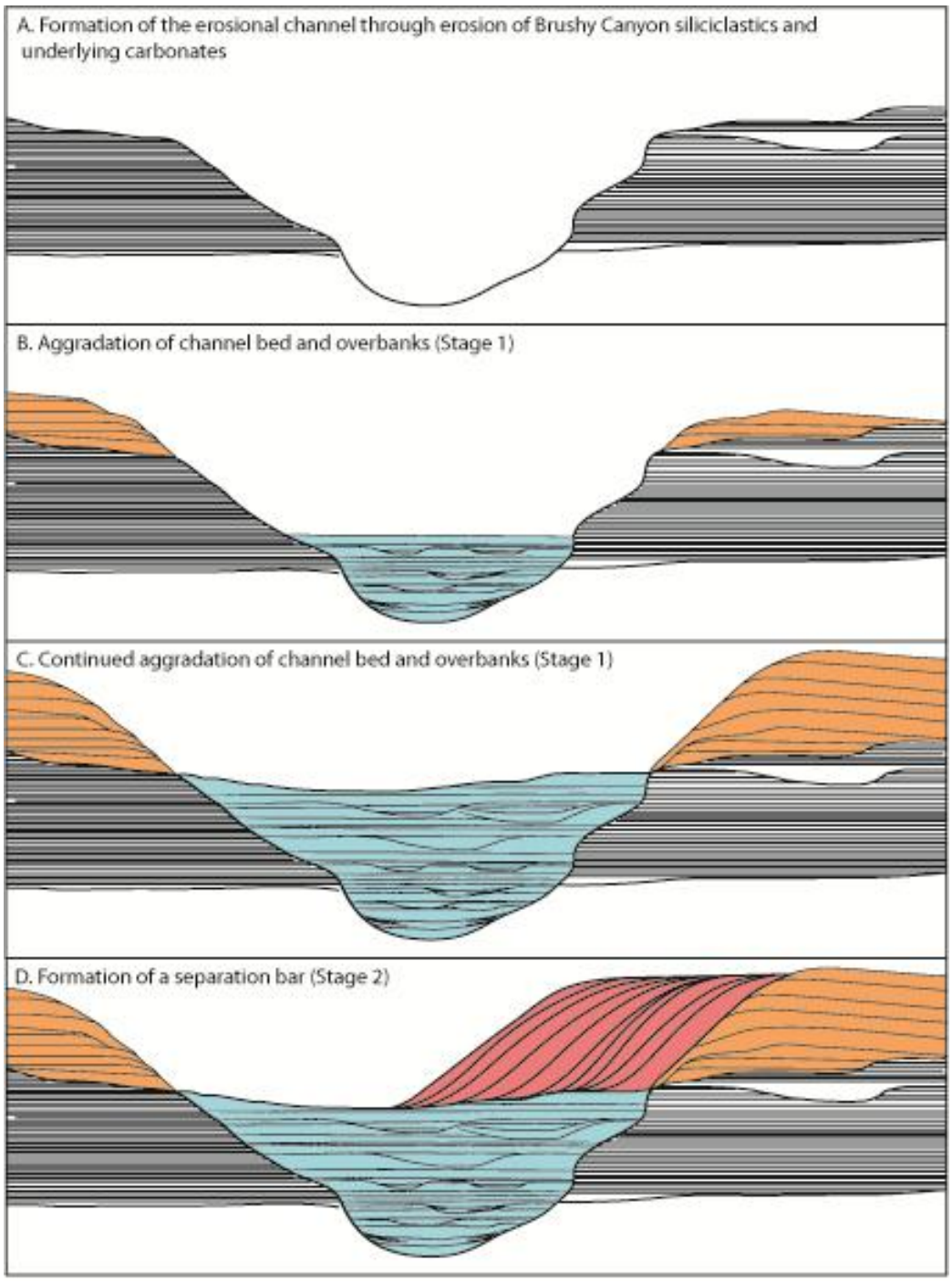

Figure 3.19: Stages in the development of Channel Complex 1. Shading represent interpreted facies. Facies Association 1 (blue), Facies Association 2 (pink), Facies Association 3 (peach).

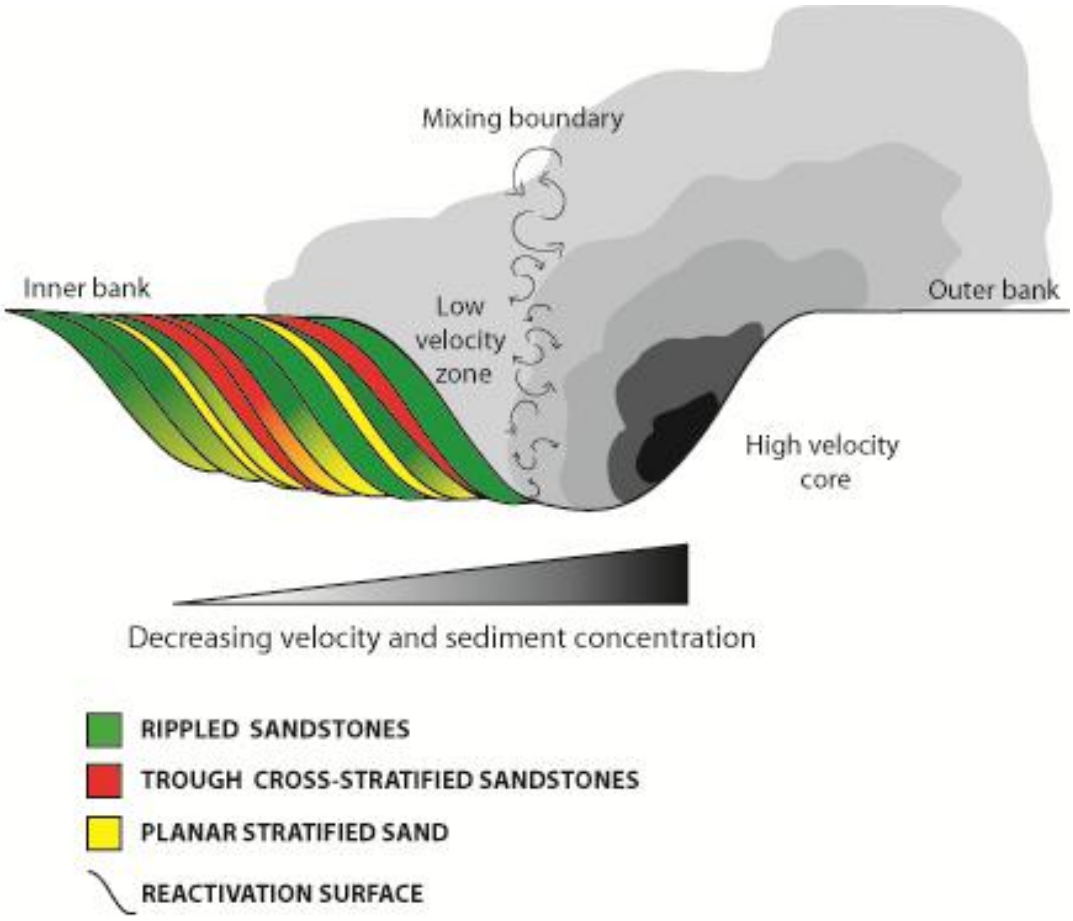

Figure 3.20: The facies model for a bank-attached bar built from suspended sediment in a low-velocity flow separation zone.

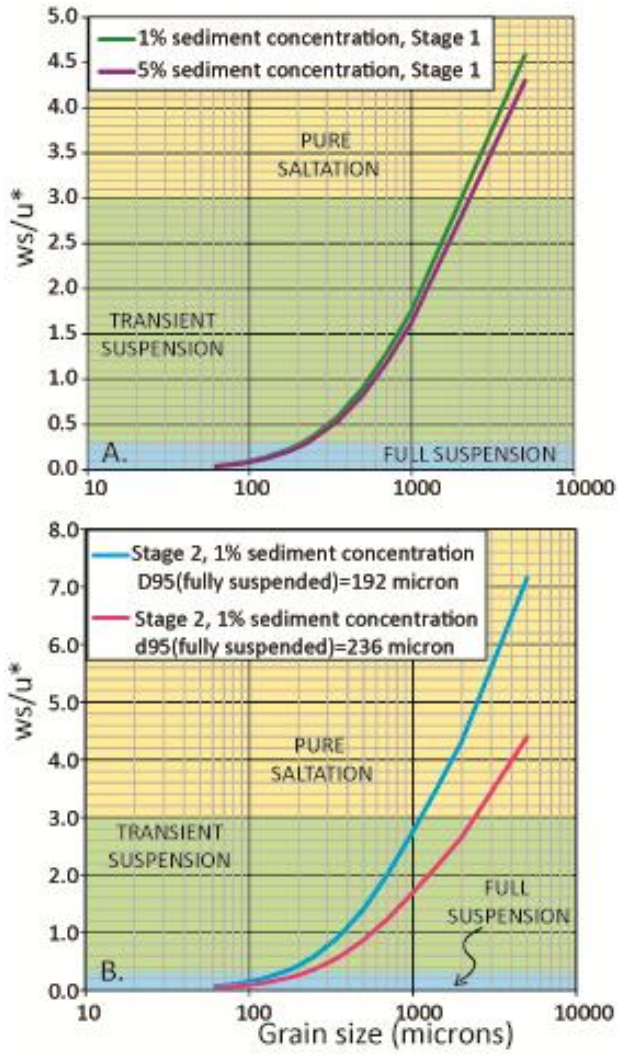

Figure 3.21: A) Paleotransport estimates for Stage 1 show that flows with a 5% sediment concentration would have transported particle sizes 241 microns and finer as fully suspended load while fractions coarser than 241 microns were transported as bedload or transiently suspended load. Flows with a 1% sediment concentration tansported particle sizes 227 microns and finer as fully suspended load while fractions coarser than 227 microns were transported as bedload or transiently suspended load. Upper-fine or medium sands deposited in medium to thick beds associated with Stage 1 were sourced from bedload or transiently suspended load. B) Turbidity currents associate with Stage 2 transported particle sizes coarser than 236 microns as incipiently suspended load and particle sizes coarser than 1-2.5mm as pure bedload.

Chapter 4: Patterns of Erosion and Deposition in Incisional Sub-aqueous Channel Bends

INTRODUCTION

Channels and canyons are important elements of landscapes on Earth, as well as on other planets and moons (Bray et al., 2007; Jobe et al., 2011; Perron et al., 2006; Whipple, 2004; Williams-Jones et al., 1998; Wynn et al., 2007). Incisional channels and canyons have been identified on many modern and ancient continental margins around the world. However, direct measurements of currents through these submarine channels are sparse (Hay, 1987; Khripounoff et al., 2003; Xu et al., 2009) and dynamic measurements resolving how currents evolve erosional channels do not exist. This has adversely affected our ability to interpret the well-preserved stratigraphic record in the deep-ocean and model past environments on Earth.

Physical models have been used to study submarine systems at reduced spatial and temporal scales. They have offered insight into the morphodynamics of submarine channels and landscapes. With a few notable exceptions (Amos et al., 2010; Metivier et al., 2005), these models have primarily focused on the morphodynamics of strongly depositional turbidity currents. The current work presents a suite of physical models of erosional turbidity currents modifying the shape sinuous subaqueous channels. We use three experimental series to evaluate patterns of net erosion where: 1) saline density currents eroded a cohesionless sediment bed and erosion was limited by the currents

ability to transport and remove sediment, 2) saline density currents eroded a weakly cohesive sediment bed and erosion was limited by the strength of the substrate, and 3) sediment-charged saline density currents eroded a weakly cohesive bed and erosion was limited by the strength of the substrate and the ability of the current to transport sediment out of the system. Our data offers insight into the evolution of erosional channel- and bed-morphology in response to variable initial substrate properties and current properties, where transporting flows have a very low excess density relative to the ambient fluid.

Deposits within many erosional submarine channels on Earth's ancient continental margins contain large volumes of hydrocarbon reserves (Wynn et al., 2007). The processes affecting connectivity of deposits within erosional submarine channels are poorly understood. As deposit connectivity strongly influences reservoir productivity, results from physical experiments are directly relevant to the energy industry. Connections between morphology of incisional channels and the processes that modify channel shape offer crucial information for accurate environmental reconstructions in the deep-water channel systems and channelized deposits on other planets and moons. Channelized deposits on Venus and Titan are believed to have been formed by flows which had excess densities that were intermediate between that of transporting flows in rivers and submarine channels on Earth (Straub et al., 2011). Studies of the similarities and differences in how flows interact with submarine and subaerial channel forms on Earth enable us to develop valuable intuition applicable to these remote landscapes.

Incisional channels

The study of incising channels on landscapes has primarily been connected to rivers. In the current work, incisional subaqueous channels are systematically compared to ones from the terrestrial environment. The dynamics of river channels eroding into bedrock have been modeled using: a) a detachment-limited model in which the resistance of the substrate is the limiting factor that controls the rate of incision, and b) a transport-limited model where incision is limited by the ability to transport the eroded sediment (Howard, 1980; Howard, 1994; Whipple, 2004). The topographic evolution of detachment-limited channels show a high degree of sensitivity to local conditions rather than reach-averaged conditions (Johnson and Whipple, 2007). Erosion generally takes place through abrasion and wear by the impacts of sediment being transported by the flow. These channels are characterized by knickpoints, inner channels, scour holes, grooves, and sculpted bedforms (Whipple, 2004). As erosion is dependent on sediment impacts, channel incision models for sub-aerial bedrock rivers show a strong dependence on sediment flux (Gasparini et al., 2006; Sklar and Dietrich, 2004, 2006). In order to incise, the channels must be efficient at removing sediment that has been transported in from upstream as well as entraining material from the bed. The 'saltation-abrasion' model links the rates of bed erosion to the supply of saltating bedload. A small sediment supply results in fewer impacts upon the bed (the 'tools-effect') and a low incision rate, while large quantities of sediment results in deposition (the 'cover-effect') which shields the bed from further erosion (Johnson et al., 2009). Transport-limited systems, which fall in the cover-dominated portion of parameter space, are characterized by a downstream

reduction in transport capacity. They respond to input conditions from upstream rather than local conditions (Whipple, 2004). Eroding bedrock river channels are likely to evolve towards transport-limited or covered conditions (Johnson and Whipple, 2007; Shepherd and Schumm, 1974; Sklar and Dietrich, 2004; Wohl and Ikeda, 1997). Evolving roughness on the bed and walls of a bedrock channel causes a dissipation of flow energy associated with increased form drag (Wohl, 1998). Thus, incisional bedrock channels which display a high degree of bed roughness can behave in a transport limited way even if sediment starved (Johnson and Whipple, 2007). Sediment accumulations in subtle topographic lows associated with bed roughness (Johnson and Whipple, 2007; Sklar and Dietrich, 2004) are interpreted as the result of a reduction in local transport capacity.

Partially alluviated channels which incise into bedrock have been identified as important elements in depositional landscapes (Edmonds et al., 2011; Nittrouer et al., 2011). Cover effects are particularly evident in channels on the Mississippi river delta. Where channel beds are devoid of alluvial cover, bed morphologies show that they are actively incising. Nittrouer et al. (2011) have shown that these morphologies are commonly associated with channel bends where spatial accelerations promote suspension of sand particles otherwise partially travelling as bedload. As all natural erosional channels must evolve in response to conditions imposed from upstream (eg: sediment supply) and local conditions (eg: bed roughness, flow structure, turbulence), they will thus display characteristics that are intermediate between detachment-limited and transport-limited conditions (Whipple, 2004).

Deeply incised channel bends

All meandering rivers that incise into bed rock are termed 'incised meanders' (Rich, 1914). These include: 1) intrenched meander bends that are the product of near-vertical incision, and 2) ingrown meanders that are those bends which continue to laterally migrate during incision (Ikeda et al., 1981; Stark et al., 2010). Lateral migration rates are functions of flow velocity, the flux of particles impacting channel walls, bedrock weakness, and the intensity and duration of rainfall which affects bedrock stability (Stark et al., 2010). Shear stresses directed towards the outer bank of river bends erode the outer walls very close to the channel bed, producing overhanging banks that are unstable and prone to failure.

EXPERIMENTAL SET UP

The experiments focused on the development of incisional subaqueous channel bends by turbidity currents. A goal of these experiments was to examine how bed morphology evolved in cases where the bed strength and the flow's capacity for erosion varied. The main components of the experimental design are compiled in Table 4.1. The significant differences between the three series were the cohesion of the erodible substrate, the downstream slope along the channel axis and the sediment concentration within the undercurrents. In all cases, density currents were released into an experimental channel through a momentum extraction box that ensured the currents would behave in a

similar manner to sediment-laden plumes. Channels were built across a tank floor with deep moats around its edges that extracted fluid from both experimental tanks and prevented currents from reflecting off the tank walls. Experiment 1 was conducted in the experimental basin at the M. I. T. Morphodynamics Laboratory. A saline density current (excess density = 3.32%) was released through the experimental channel which consisted of a cohesionless, 2-cm thick bed of acrylic particles (specific gravity = 1.15) draped over a sinuous channel form built of weak concrete. The down-stream slope along the channel centerline was 2 degrees. Experiment 2 was conducted in a channel built entirely out of a weakly cohesive mix of acrylic particles (specific gravity = 1.15) and clay positioned on top of a sloping ramp in the Deep-water Basin of the University of Texas Morphodynamics Laboratory. The down-channel slope was ~7 degrees. Thickness of the erodible sediment layer on the channel bed was 5 cm. Two saline density currents (excess density = 4%) were released through the experimental channel. During Experiment 3, three density currents carrying a 2% volumetric concentration of suspended sediment were passed through the same channel form that was modified during Experiment 2. In Experiment 1, a lower background slope, lower excess density and loose sediment on the bed created a condition where erosion was dependent on the ability of the current to transport the sediment. In Experiment 2 a high background slope, high excess current density and the substrate cohesion created a condition where erosion was limited by the strength of the substrate. Experiment 3 tested the reduction of local erosion due to entrained sediment eroded.

Table 4.1: The initial conditions used in Experiments 1, 2 and 3 are tabulated.

	Experiment 1	**Experiment 2**	**Experiment 3**
basin dimensions in meters (length x width x depth)	5 x 5 x 1.2	8 x 6 x 2.5	
number of flows	1	2	3
channel sinuosity	1.28	1.054	1.054
number of bends	3	1+0.5+0.5	
substrate composition	acrylic (SG: 1.15)	acrylic (sg=1.15) + kaolinite (10:1 by volume)	
substrate strength	non-cohesive	weakly-cohesive	
sediment grainsize distribution (micron)	D1=49 , D10=88 , D25=127, D50=146, D75=205, D90=243, D99=340	D1=49 , D10=88 , D25=127, D50=146, D75=205, D90=243, D99=340	
excess density	3.30%	4%	
sediment concentration (by volume)	0%	0%	2%

Table 4.2: Geometries and dynamics of experimental channels scaled to natural systems

		Experiment 1	Natural channels	Experiment 2	Experiment 3	Natural channels
Geometric Scaling	**channel depth**	0.09m	400m	0.15m		50m
	channel width	0.40m	40m	0.50m		500m
	Down-channel slope	2 degrees	0.9 degrees	7 degrees		2.3 degrees
Dynamic Scaling	**depth averaged velocity**	0.045m/s	0.94m/s	0.10m/s		1.83m/s
	shear velocity	0.109m/s	0.042m/s	0.0412m/s		0.0816m/s
	Frd	0.24		0.41		
	Re	4050		15000		
	sediment grainsize distribution (microns)	D1=49 , D10=88 , D25=127, D50=146, D75=205, D90=243, D99=340	D1=9 , D10=15 , D25=21, D50=24, D75=32, D90=37, D99=51	D1=49 , D10=88 , D25=127, D50=146, D75=205, D90=243, D99=340		D1=19 , D10=33 , D25=47, D50=55, D75=75, D90=89, D99=124
	flow duration	6 min.	2.11 hours	25min	Flow 1,3: 40min; Flow 2: 72min	2-21 hours
	current thickness	~0.09m	36m	~0.10m		33m

Data and Methods

Data collected during each experiment included (1) high-resolution bathymetry maps built using a submerged laser distancing system (vertical resolution ~100 microns), (2) time lapse photographs, (3) video, (4) bulk suspended-sediment concentrations for the eroding currents, and (5) current velocity profiles. A Vectrino Acoustic Doppler Profiler (measurement window = 12cm, bin size = 1.6cm, Sampling Rate = 4Hz) was used to measure the velocity of currents in experiment 1 and a Vectrino Acoustic Doppler Velocimeter Profiler (ADVP) was used in experiment 2 and 3 (measurement window = 3cm, bin size = 0.1cm, Sampling rate=75Hz) (Fig. 4.01).

The laboratory experiments can be roughly compared to natural systems through the scaling of three dimensionless variables, the densimetric Froude number (Fr_d), the Reynolds number (Re) and the ratio of particle fall velocity to current shear velocity (w_s/u^*). An approximate dynamic similarity was assumed by setting $Fr_{d\ (model)} = Fr_{d\ (nature)}$ (Graf, 1971). Resulting prototype values of depth averaged velocity, current thickness and flow duration are compiled in Table 4.2. Sediment transport properties are compared between systems by setting the ratio $w_s/u_{*(lab)}$ equal to $w_s/u_{*(nature)}$. Values for w_s were computed using the empirically derived relationship of (Dietrich, 1982). Shear velocities for the experimental currents were estimated by fitting The Law of the Wall measured down-channel velocities plotted against the natural log of elevation above the bed (Altinakar et al., 1996). Only the lower portions of the velocity profiles measured at the channel inlets were used for these calculations (Fig.4.1, A and B). In this formulation, the slope of the best fit line is equal to κ/u^*, where κ is von Karman's constant= 0.407 and

u* is the shear velocity. The estimated sediment transport conditions are also compiled in Table 4.2.

EXPERIMENTAL RESULTS

The presented data is intended to emphasize trends in the evolution of subaqueous channel topography in response to the passage of eroding turbidity currents.

Experiment 1

Sediment on the bed was reworked into a continuous field of bedforms. (Fig. 4.2, A, B, C). To analyze the change in channel topography, channel curvature was calculated at every 16mm along the channel centerline (Fig. 4.3, A, C). The amount of sediment both deposited and eroded to produce the net change in channel topography was measured at cross sections generated perpendicular to the evolving channel centerline every 24mm (Fig. 4.3C). Topographic change was measured at points spaced 24mm apart along each of these cross-sections. Down-channel trends are plotted in Figure 4.3B. The net removal of sediment at any particular location was connected to channel curvature and occurred in a diffuse manner at and just downstream of bend apices (Fig. 4.2, A,B, C). At the outer wall of bends, sediment removal exposed the underlying concrete in the troughs between the starved ripples (Fig. 4.2 C, Fig. 4.4B). Sediment was deposited at the inner bank beginning just upstream from the points of maximum curvature through cross-stream bedload transport. (Fig. 4.2; Fig. 4.3 A, Fig. 4.4). Individual point bars were connected through continuous sedimentation across inflection points between bends (Fig.

4.2; Fig. 4.3; Fig. 4.4). An overall reduction in the mean erosion was observed in the downstream direction. (Fig. 4.2, C).

Experiment 2

Extreme run-up of currents onto the outer walls of channel bends resulted in both a small portion of each flow leaving the channel at each bend and the formation of a low-velocity zone at the inner bank each bend (Fig. 4.5). These inner-bank zones received very little current. Erosion on the channel bed correlated strongly with the pathway of the high velocity core of each current (Fig. 4.6; Fig. 4.7). Erosion on the bed occurred through wear by abrasion and plucking. The channel bed evolved into a series of grooves, pits and larger scour holes (Fig. 4.6; Fig. 4.7). A small breach which formed in the channel wall during flow 1, continued to enlarge during flow 2 (Fig. 4.7, B), and resulted in an ever greater fraction of the current leaving the channel at this location during subsequent flows. The outer banks of bends displayed sets of superimposed grooves with different orientations which later developed into scalloped erosional bedforms (Fig. 4.8).

Channel curvature, calculated at every 24mm along the channel centerline is shown in Figure 4.9A and C. Mean topographic change was evaluated at cross-sections generated perpendicular to the channel centerline at every 20mm (Fig. 4.9,B, C). Large erosional pits that initiated at the outer banks of bends during flow1 were then propagated downstream during flow 2 (Fig. 4.6; Fig. 4.7; Fig. 4.9). Other sites of developing roughness in the bed became sites of continued erosion during flow 2 (Fig. 4.9). Bend

areas developed topography similar to a deeply entrenched inner channel that was one-third to one-half the original channel width. (Fig. 4.10). Straight reaches between bends showed a lesser degree of erosion (Fig. 4.9). Inner bank areas are sites of no erosion or even weak sediment deposition (Fig. 4.7). Deflection of the eroding currents around these inner bend areas resulted in the formation of raised benches near the inner bank (Fig. 4.6; Fig. 4.7; Fig. 4.10). Erosion decreased in the downstream direction, though the channel stayed net-erosional (Fig. 4.9). Abrupt topographic alterations were common during each flow due to sustained erosion or intermittent plucking of blocks from the up- or down-stream rough edges of scour holes. Locations of enhanced bed roughness associated with variance in the local bed topography became sites of continued erosion (Fig. 4.9). Fresh edges became sources for the continuous release of sediment. These blocks and fragments traveled along grooves on the bed and probably acted as tools for enlarging existing grooves or creating more. These ripped up fragments from the bed usually disintegrated rapidly as they bounced and rolled down the channel (See Movie in supplementary materials). The maximum depth of scours in this experiment was limited by the substrate thickness, which was 5cm along the channel centerline.

Experiment 3

Three currents were released during experiment 3 through the channel that evolved from flows in experiment 2 (Fig. 4.6 C). Mean topographic change was evaluated along cross-sections spaced at 20mm increments along the channel centerline.

Topographic change was measured at points spaced at 20mm along each cross-section (Fig. 4.13). The three currents were still net erosional but the magnitude of erosion was far less than in experiment 2 (Fig. 4.12; Fig. 4.13). Some topographic lows which formed during experiment 2 became sites that shifted dynamically between sedimentation during one flow and erosion during the next, while elsewhere scours were smoothed over by trapped sediment (Fig. 4.12, Fig. 4.13). Rough surfaces in the system continued to be sites of pronounced erosion and the outer banks of bends were sites of the strongest erosion (Fig. 4.10, C, D, E; Fig. 12; Fig. 4.13).

Near-bed flow-fields in subaqueous channel bends of experiment 2 and 3

Data collected during experiment 2 and 3 defines the cross-stream structure in flow velocity and flow thickness at channel bends. Velocity profiles were collected every 5cm in the cross-stream direction. Velocity profiles were measured in vertical bins spaced 1mm apart (Fig. 4.14). These measurements show a low velocity zone near the inside of the bend and a zone of high velocity up against the outer channel bank.

The hand off between horizontal and vertical velocities near the channel sidewall can be seen in Figure 4.14 C and E. At positions closest to the outer bank, a positive value for the vertical component of velocity indicates upward-directed flow. In contrast, other parts of the velocity field are negative or zero values indicating that in these regions flow is predominantly downslope. The maximum upward-directed velocity at the outside

of the bend is roughly an order of magnitude less than the maximum downstream directed velocity elsewhere in the channel.

Erosion on the channel bed versus erosion on the sidewalls

In experiment 2 and 3, side-wall erosion took place through under-cutting and sidewall collapse at the outer wall of channel bend 1 and through steady abrasion of the outer channel walls at bends 2 and 3. Currents running up the outer walls of bends often carried ripped-up blocks of substrate up the outer banks and these blocks acted as erosional tools. Figure 4.15 shows that the relative contributions of side-wall erosion and basal incision are comparable in magnitude in experiment 2 and 3, except when under-cutting and wholesale collapse of the sidewall occurs.

DISCUSSION AND INTERPRETATION OF RESULTS

Substrate control on erosion by turbidity currents

The channel in Experiment 1 showed a pattern of evolution similar to incising alluvial rivers characterized as transport-limited. On the other hand, erosional patterns observed in the Experiment 2 channel were more similar to detachment-limited bedrock rivers where erosion occurs through wear by abrasion and plucking. In Experiment 3, a hybrid condition was achieved where erosion is limited by both the capacity of the flow to transport sediment and by the resistance of the substrate to erosion. Most natural systems display loose sediment cover at places on the channel bed (Johnson et al., 2009;

Nittrouer et al., 2011) or reduced local shear stress due to drag effects from the rough bed (Johnson and Whipple, 2007). Thus, they are likely to exhibit a hybrid suite of properties associated with both end members. All three series of experiments show a reduction in the degree of net erosion in the downstream direction. This is attributed to a net reduction in the local boundary shear stress due to energy expended on both maintaining entrained sediment in motion and continued interaction with a rough bed. Our observations in subaqueous incisional channels reinforce the hypotheses that most natural erosional channels tend towards transport limited conditions (Johnson and Whipple, 2007; Johnson and Whipple, 2010; Sklar and Dietrich, 1998; Sklar and Dietrich, 2004; Wohl and Ikeda, 1997) because of momentum extracted by sediment transport or by drag on the bed.

The key difference between the detachment and transport limited erosional channels is the morphology and continuity of erosion through the successive channel bends. Erosion was diffuse and discontinuous, in the transport-limited case, producing reworked deposits that were connected from bend to bend (Fig. 4.2, C). On the other hand, the detachment-limited erosion was highly focussed in certain positions and strongly correlated with local planform and surface roughness (Fig. 4.7; Fig. 4.12).

Erosion and deposition related to planform and bed roughness

The evolution of the experimental channels showed that erosional turbidity currents are highly responsive to local conditions such as channel curvature and bed

roughness. Erosion of the smooth bed in Experiments 2 and 3 was strongest in the vicinity of bend apices (Fig. 4.2, C; Fig. 4.7). Local flow accelerations associated with bend curvature thus played an important role in facilitating the entrainment of sediment from a smooth bed. On the other hand, continued erosion of the cohesive bed in Series 2 and 3 showed consistent erosion at sites where topographic roughness developed (Fig. 4.7; Fig. 4.9; Fig. 4.12; Fig. 4.13). Sites of focused erosion and developing roughness propagated downstream (Fig. 4.9; Fig. 4.13). Vertical velocities associated with near-bed turbulence from fluid shear on the rough bed and from interaction with the bend itself, is interpreted to have contributed towards efficiently advecting entrained particles away from the bed and into the interior of the current. This high degree of sensitivity to local conditions that is displayed by erosional turbidity currents contrasts considerably with the remarkable insensitivity displayed by strongly depositional currents (Straub et al., 2008). Straub and others (2008) showed that patterns of topographic change produced by depositional turbidity currents are not really influenced by local accelerations or decelerations. For these depositional currents the changes in bed elevation are simply correlated with the pathway of the high velocity core of the current which had the highest sediment concentrations. While conditions imposed from upstream (sediment supply & momentum extraction by the rough bed) remains an important factor in the magnitude of reached-averaged incision, the magnitude of local erosion is strongly dependent on local roughness and channel curvature.

Sculpted morphologies on the bed and walls of bedrock rivers have often been interpreted as the result of abrasion associated with flow vortices carrying suspended sediment (Alexander, 1932; Whipple et al., 2000; Wohl et al., 1999). Johnson and Whipple (2006) hypothesize that these erosional bedforms may also result from the impacts of incipiently suspended sediment affected by local turbulence. Turbidity currents in experiments 2 and 3 transported sediment in incipient or full suspension. In this case, therefore, impacts from suspended material were likely to have been responsible for the sculpted forms observed. Crescentic or scalloped erosional bedforms which evolve within the eroding inner channel at bend 3 (Fig. 4.8) have a similar shape and form to bedforms documented in the proximal reaches of the Monterey Canyon (Paull et al., 2010; Smith et al., 2007; Smith et al., 2005; Xu et al., 2008). These features have been hypothesized as associated with slumping or down-channel migration of loose sediment. Observations from experiment 2 and 3 suggest that these features are erosional bedforms in cohesive channel-bottom deposits.

Deposits preserved in Experiments 2 and 3 were highly discontinuous and separated by wide areas of erosion (Fig. 4.7; Fig. 4.12). Flow traveling around bends in this channel showed a high degree of runup at the outer banks and as a result a wide zone of flow separation was formed near the inner banks (Fig. 4.5). As the highest velocities and sediment concentrations were associated with the main current at the outside of the bend, these inner bank areas were exposed to very low concentrations and extremely sluggish flow (Fig. 4.5; Fig. 4.14). Inner bank separation zones were sites of persistent, weak sediment accumulation, surrounded by a swath of erosion (Fig. 4.7; Fig. 4.12).

Sediment transported within the high velocity portions of the current traveled chiefly as suspended load and these inner bend areas were the only locations with sufficiently low velocities to permit sedimentation and preclude remobilization of deposited material.

During Experiment 3, topographic lows associated with deep scours became sites for temporary or long term sediment storage (Fig 4.12, A, B, C). These locations were in close proximity to areas that had previously undergone erosion. Deposits are localized and scours are believed to have collected material which travelled as transiently suspended load, and responded to a local reduction in transport capacity. We interpret that the trapped material was travelling close to the bed, routed through topographic lows and with characteristic excursion lengths less than those associated with topographic roughness elements. Bedload and incipiently suspended load are more sensitive to topographic variability and the accompanied variability in local flow conditions, unlike well suspended sediment load. Once deposited, this material probably served to protect the bed from further erosion in a similar manner to bed armoring observed in natural channels (Johnson et al., 2009; Sklar and Dietrich, 1998).

The cohesionless sediment bed in Experiment 1 showed the reworking of the sediment cover on the bed into a continuous bedform field, except at the eroded outer banks of bends (Fig. 4.2, C). In contrast to Series 2 & 3, a large fraction of sediment load was transported as bedload. Inner bank bars were built from bedload and were connected across inflection points between bends. Low rates of sediment removal thus resulted in a higher degree of connectivity between the deposits. In contrast, the inner bank deposits in the cohesive bed case were isolated from deposits at other bends (Fig. 4.7; Fig. 4.12).

Terraces and inner channels in submarine channel bends

Carved terraces near the inner banks of incising submarine channels have been documented in a number of submarine channels and canyons(e.g.; Congo channel, (Babonneau et al., 2009); Monterey canyon, (Shepard, 1966); La Jolla canyon, (Shepard and Buffingt.Ec, 1968) and the Lucia Chica channel system,(Maier et al., 2012). Carved inner-bank terraces observed in Series 2 and 3 (Fig. 4.5, Fig. 4.6, Fig. 4.10, Fig. 4.11, Fig. 4.12), coincide with the boundary of the low velocity zone documented by our Accoustic Doppler Velocimeter Profiler measurements (Fig. 4.14). These observations suggest that inner bank terraces in natural systems are also likely to form in a similar way, at the boundary between high-velocity down-channel flow and sluggish separated flow. Regions of separated flow experience no erosion and weak sedimentation (Fig. 4.13). Multiple steps documented at the inner banks of submarine channels might therefore mark the boundary of the flow separation zone through time as the incisional channel bends migrated outwards.

The downstream propagating scours in our Experiments 2 and 3 resulted in a final semi-continuous series of deep scours. We have loosely termed the resulting erosional form an incised “inner channel”. The cross-sectional geometry of the inner channel that developed through experiment 2 and 3 is similar to the inner channel observed in the deeply entrenched Congo channel. The cross sections through the experimental inner channel at bend apices show that it occupies roughly 26-36% of the larger channel depth

and 22-30% of the larger channel width. The entrenched inner channel in the Congo shows a width that is approximately 25-33% of the larger channel width and roughly 50% of the larger channel depth. Evidence of incision during channel migration is preserved in the Congo channel, where multiple terrace-like steps are associated with one channel bend (Babonneau et al., 2009). Seismic lines presented by Babonneau et al. (2010), and Maier et al. (2012) through inner bank benches suggest that these morphologies are likely to be the result of both bench-carving and sedimentation. Our experiments showed more incision than lateral migration and weak deposition on the tops of the carved benches. I suggest that these observations document the dynamic processes contributing towards the formation of stepped, inner-bank benches in incisional, sinuous submarine channels.

Incisional subaqueous and subaerial channel bends

The presented results show that there are a few important differences in the processes which evolve incised subaqueous and subaerial channel bends. The extreme run-up observed with turbidity currents traversing channel bends brings the high velocity core of the current far up onto the outer banks (Straub et al., 2011). The associated high basal shear stresses and sediment concentrations are thus available at high elevations along the outer channel wall and the area of outer wall erosion is expanded. Grooves present high up along the outer wall of the channel attest to the contribution of abrasion to outer wall erosion.

In contrast, the highest shear stresses and sediment concentrations are located low down in the flow in incising river channel bends. River bends thus experience erosion closer to the base of the channel. In the river case, lateral channel wall erosion is accomplished through a combination of undercutting and resultant slumping due to destabilization (Parker et al., 2011). Deeply ingrown rivers can show both the comparatively smooth inner "slip off slopes" (Blank, 1970; Harden, 1982) associated with only little variation in the relative rates of incision and lateral erosion, and the stepped morphologies of unpaired strath terraces (Finnegan and Dietrich, 2011; Shyu, 2006) associated varying relative rates of incision and lateral erosion. Inner bank separation zones are likely to exist in any submarine channel with sufficient width to permit the unrestricted meandering of the high velocity core and flow separation from the inner bank. Because of this I propose that the raised inner bank terraces which form as a result of erosion around the separation zone and sedimentation within the separation zone are likely to be under-recognized but much more common geomorphic features in incising submarine channels versus sub-aerial incisonal channels. Another noteworthy difference between sub-aerial and submarine entrenched channels is that the inner channels developed in incised rivers usually contain the whole thickness of the sculpting flows (Johnson & Whipple, 2006). Rills reported by Babonneau et al., (2010) along the tops of inner-bank terraces in the Congo channel indicate that turbidity currents may commonly extend above the inner channel, as was confirmed in Experiments 2 and 3 (Fig. 4.5, Fig. 4.14)

SUMMARY

Experimental results show that erosional turbidity currents are most sensitive to local variation in channel planform and bed topography. The magnitude of local erosion is strongly influenced by these factors, while reach-averaged erosion is only weakly dependent on upstream conditions (eg: sediment supply). This contrasts with patterns of change associated with highly depositional currents, where the magnitude of deposition correlates with the high-velocity core of currents carrying the highest sediment concentrations.

Incisional subaqueous channels tend to evolve towards a transport-limited behavior, irrespective of whether the channel bed is alluviated or exposed bedrock. In alluviated channels, sediment removal causes a downstream reduction in transport capacity. In bedrock channels, the variance in erosion and resulting form drag on the erosional bedforms also causes a downstream reduction in transport capacity.

Where currents are efficient at removing eroded material, sediment is transported predominantly as fully suspended load and bedrock is exposed to erosion. Sedimentation is limited to topographic lows in the channel thalweg and flow-separation zones at bends. Where currents are less efficient at removing the eroded material, sediment cover on the bed is relatively continuous. The channel bed is covered by a continuous bedform field that migrate down-channel at a relatively slow pace.

I documented the evolution of raised benches in flow separation zones associated with bend curvature. These benches formed as a result of erosion around inner bank areas and weak deposition within separation zones. Morphology of these inner bank benches

are comparable to those observed in the sinuous Congo channel (Babonneau et al., 2009) and in the Lucia Chica channel system (Maier et al., 2012).

My observations show that the processes associated with side-wall erosion differ in incisional submarine versus river bends. Erosion of side-walls by turbidity currents can take place over an expanded area due to the run-up of the high velocity core against the outer banks. In incisional river bends, erosion is focused closer to the channel bed and lateral erosion in channels is mainly the result of undercutting and collapse.

ACKNOWLEDGEMENTS

Jim Buttles, Michael Markowski and Liz Rinehart are thanked for their assistance in the laboratory. Constructive suggestions from Joel Johnson helped refine the conparisons to bedrock rivers. These experiments were funded by the RioMAR consortium of oil companies and the SEPM Weimer Research Grant.

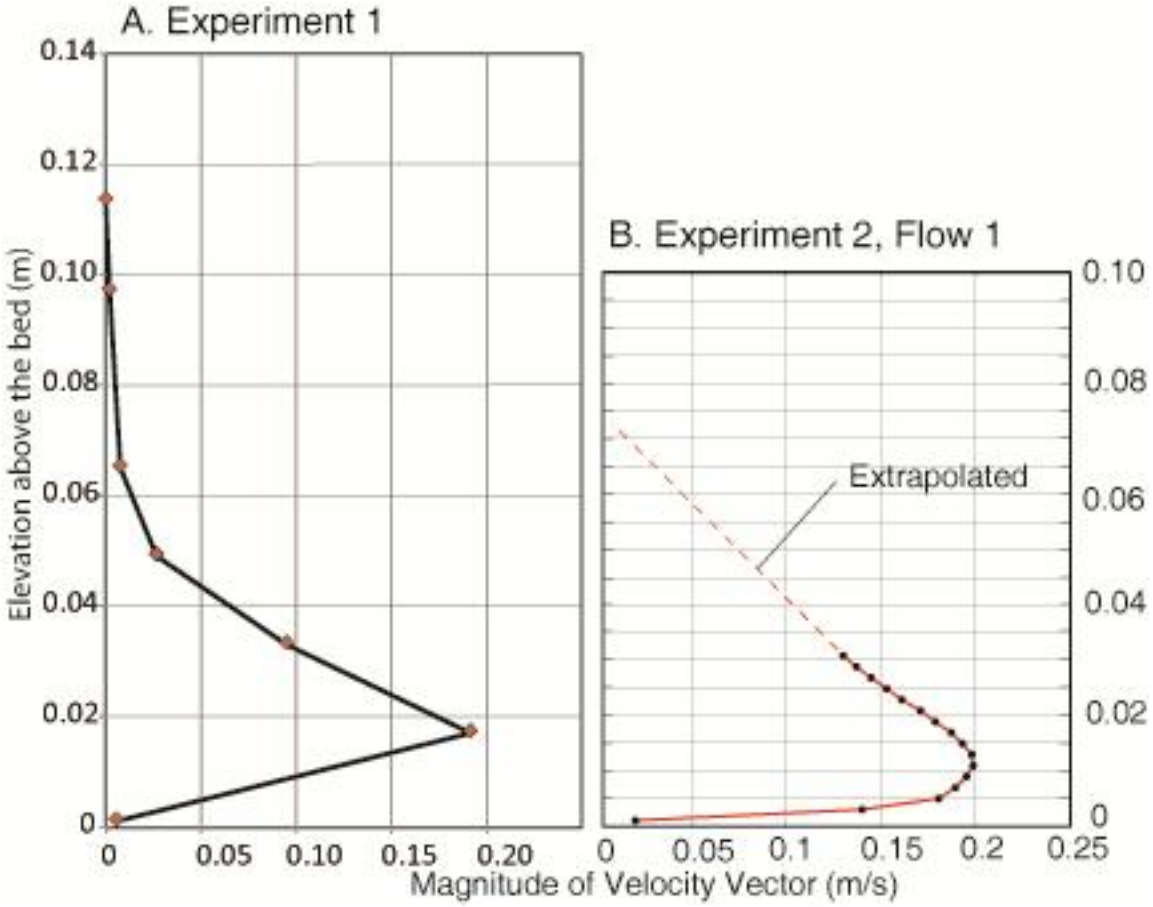

Figure 4.1: The inlet velocity profiles of the density current in experiment 1 (A) and experiment 2 (B).

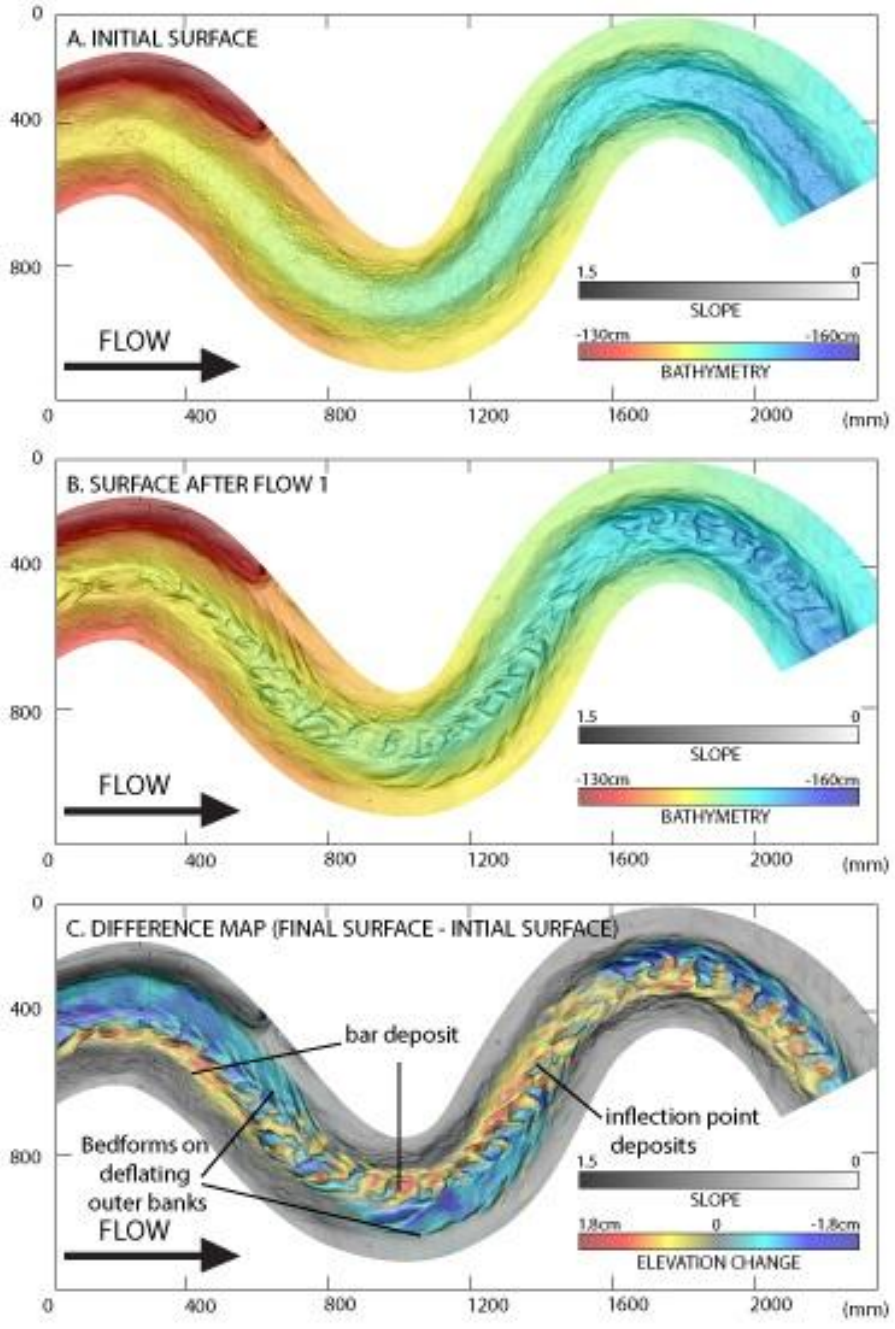

Figure 4.2: The topographic evolution of channel in experiment 1. A) Bathymetry map overlain by a dip map of the initial experimental surface. B) Bathymetry map overlain by a dip map of the final surface. Dark blue = topographically lows, red = topographic highs. C) Difference map of change to the experimental surface after Flow 1, overlain by a dip map of the final surface. Cold colors = erosion, hot colors = deposition.

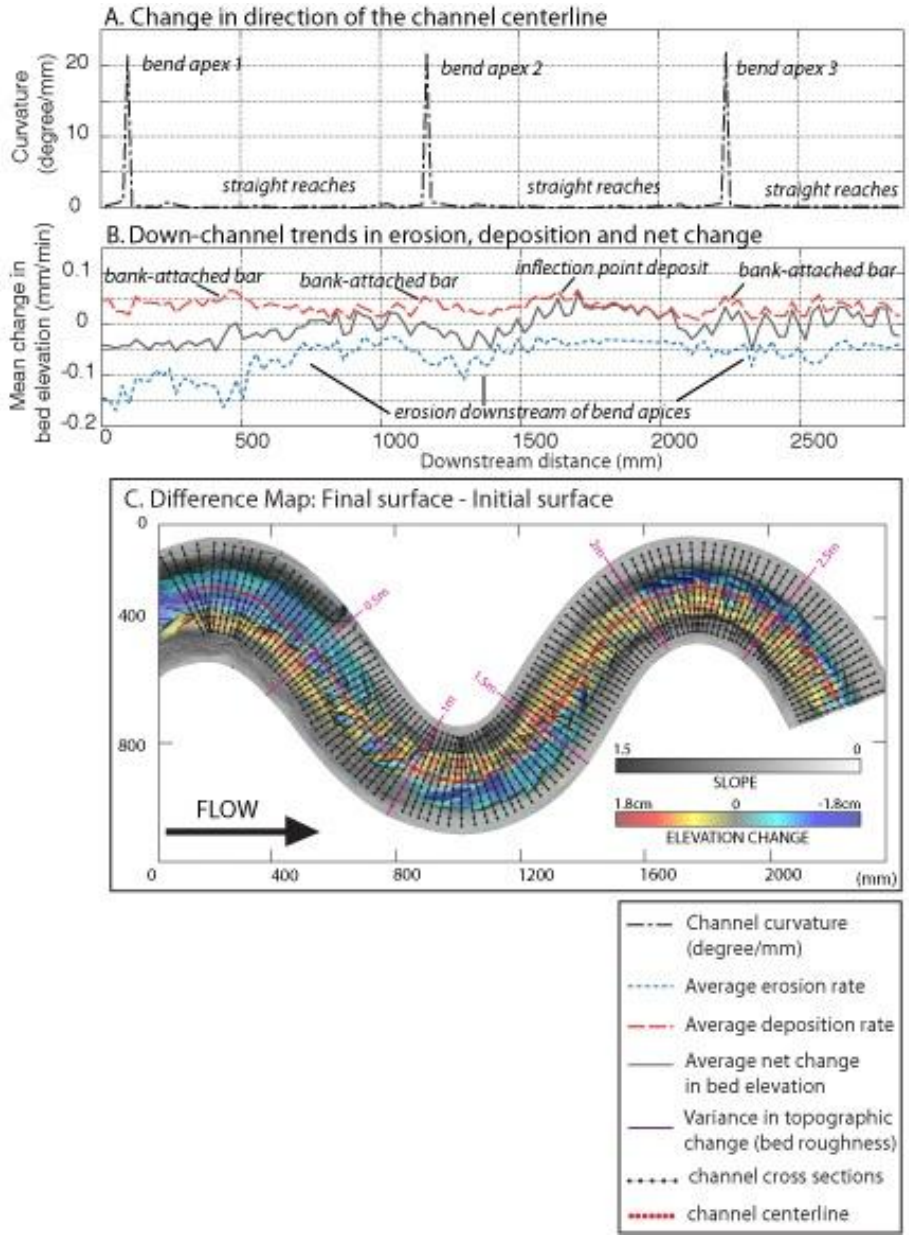

Figure 4.3: A) Downstream change in direction of the channel centerline. B) Downstream trends in mean cross-channel erosion (blue), mean cross-channel deposition (red) and mean topographic change (grey). C) Reference difference map showing: (1) the cross section along which down-channel trends were averaged (black), and (2) points at which change in centerline curvature was evaluated (red). Channel cross-sections were generated at points spaced at intervals of 24mm. Topographic change was evaluated at every 24mm along each cross-section.

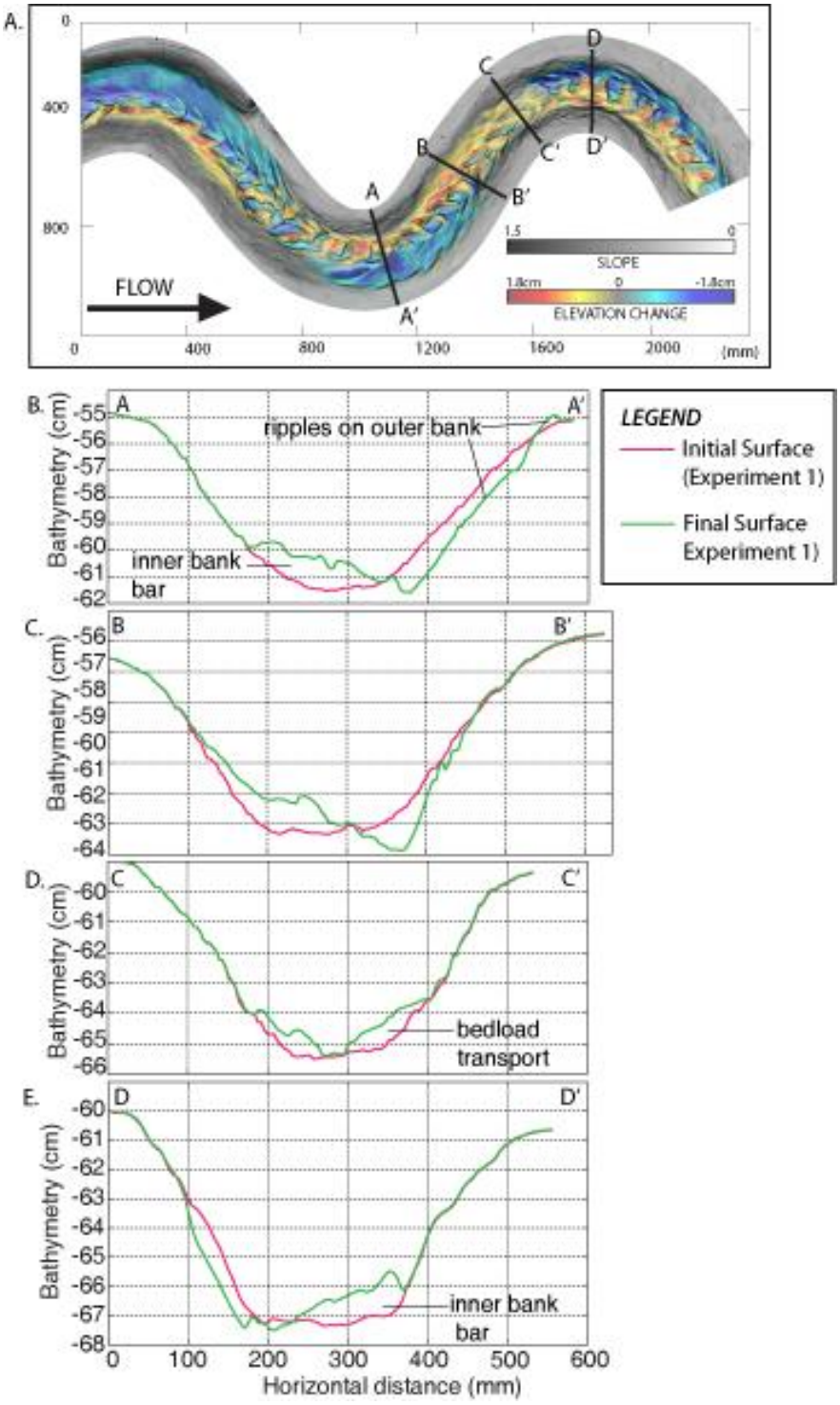

Figure 4.4: Reference map (A) and cross-sections through the channel in Experiment 1 (B, C, D, E).

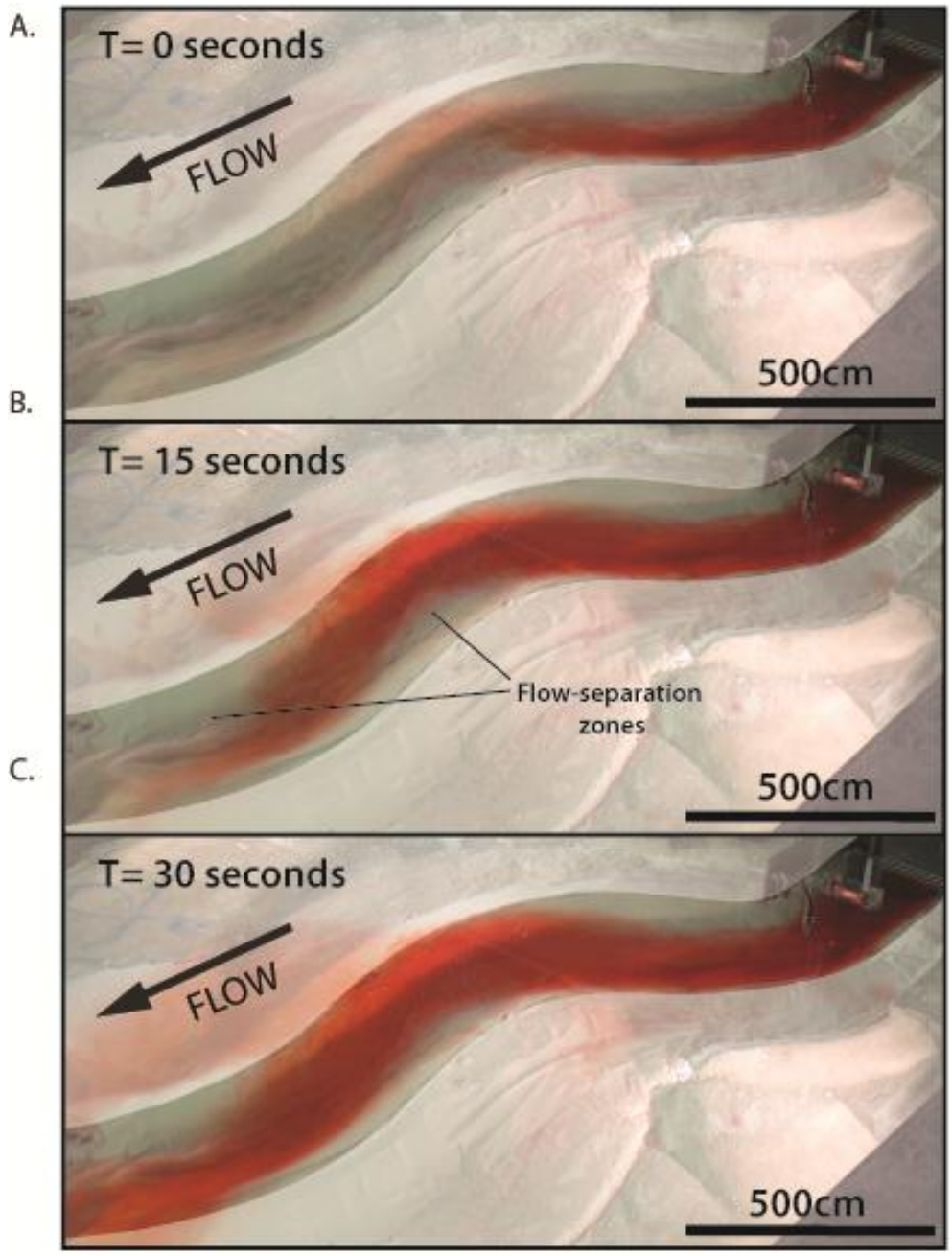

Figure 4.5: Time lapse photographs define the pathway of the high-velocity core of the current, as defined by a shot of dye in the current. Low velocity zones where flow separated from the inner banks received the dyed current later than the outside of bends and the dye intensity was always lower than the outside of bends.

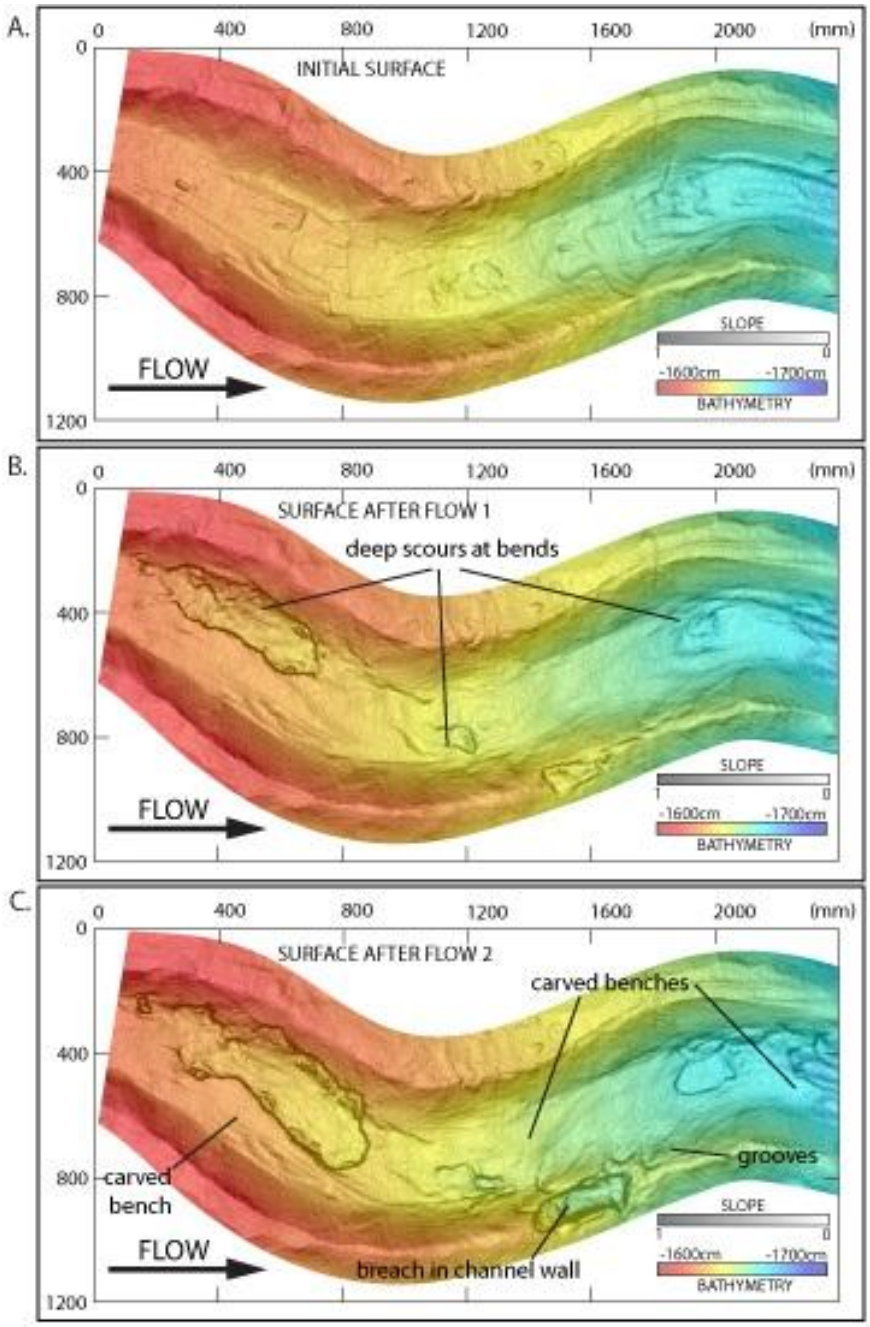

Figure 4.6: The topographic evolution of the channel in Experiment 2. Bathymetry maps of each time step are overlain by the dip map of the same surface. Hot colors indicate topographic highs, cold colors indicate topographic lows. Gark greys indicate high slopes, white indicates low slopes. A) Initial surface, B) Surface after Flow 1, C) Surface after Flow 2.

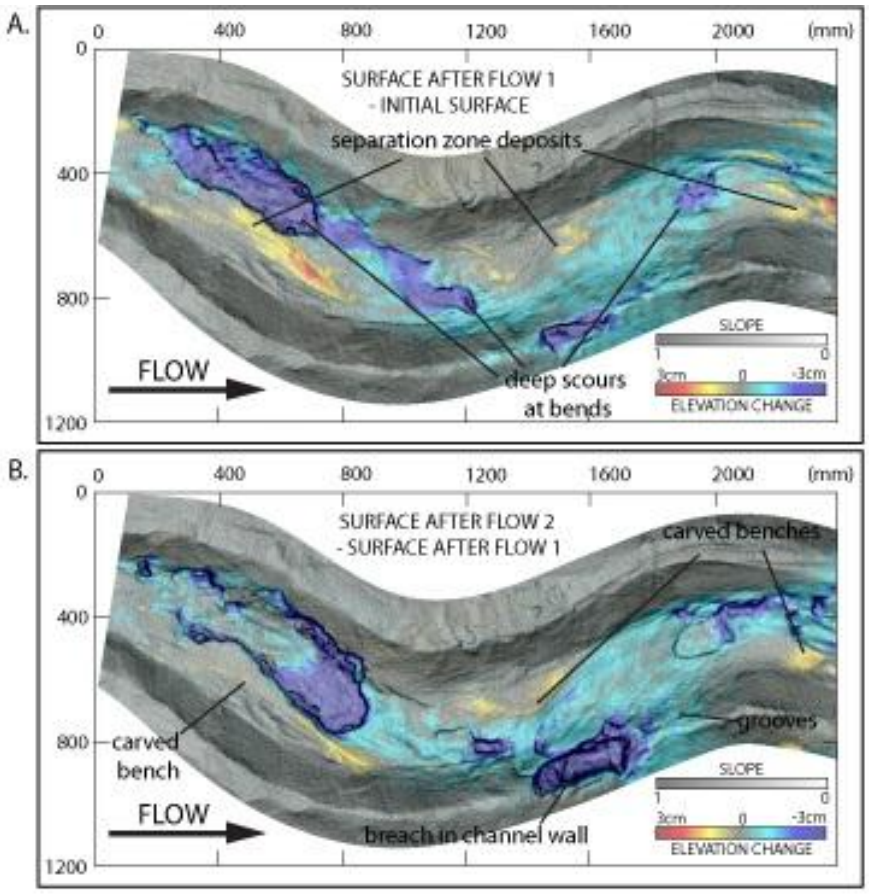

Figure 4.7: Erosion and deposition in the channel in Experiment 2. Hot colours = deposition, cold colours = erosion. The difference map showing the erosion and depositionassociated with each time step is over lain by a gray scale dip map. A) Difference map (surface after flow 1 minus initial surface), B) Difference map (surface after flow 1 minus surface after flow 2).

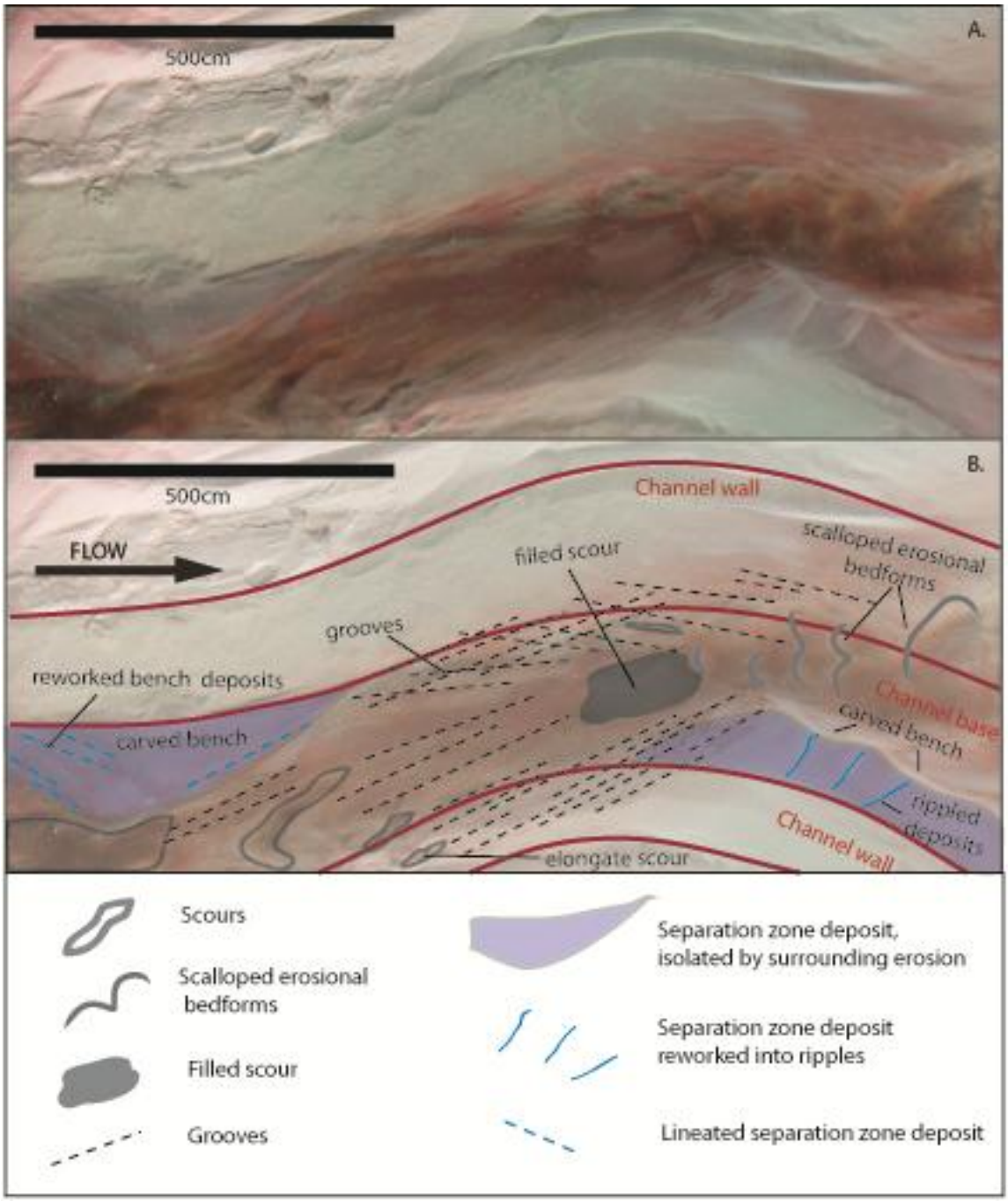

Figure 4.8: Erosional bedforms and depositional inner bank zones which evolved on the channel bed in experiment 2 and 3.

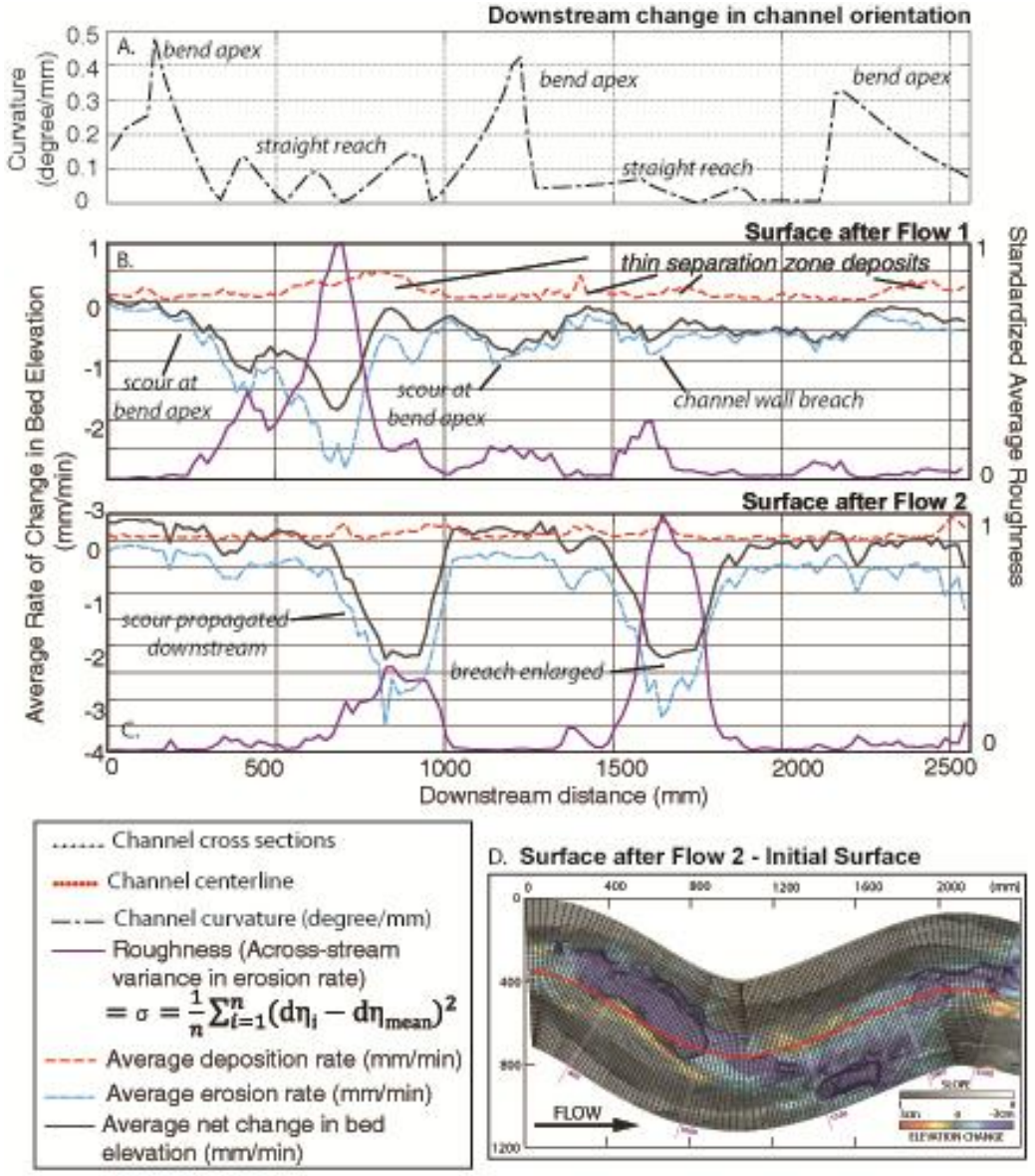

Figure 4.9: Downstream trends in: A: channel centerline curvature, mean cross-channel erosion (blue), mean cross-channel deposition (red), mean topographic change (grey) and the standardized channel bed roughness associated with Flow 1 (B) and Flow 2 (C). Erosion in the experimental channel was strongest at the outside of bends during Flow 1. Large roughness elements (deep scours), associated with erosion from Flow 1, were propagated downstream during flow 2. The reference map (D) shows the cross section along which down-channel trends were averaged (black), and points at which change in centerline direction was evaluated (red).

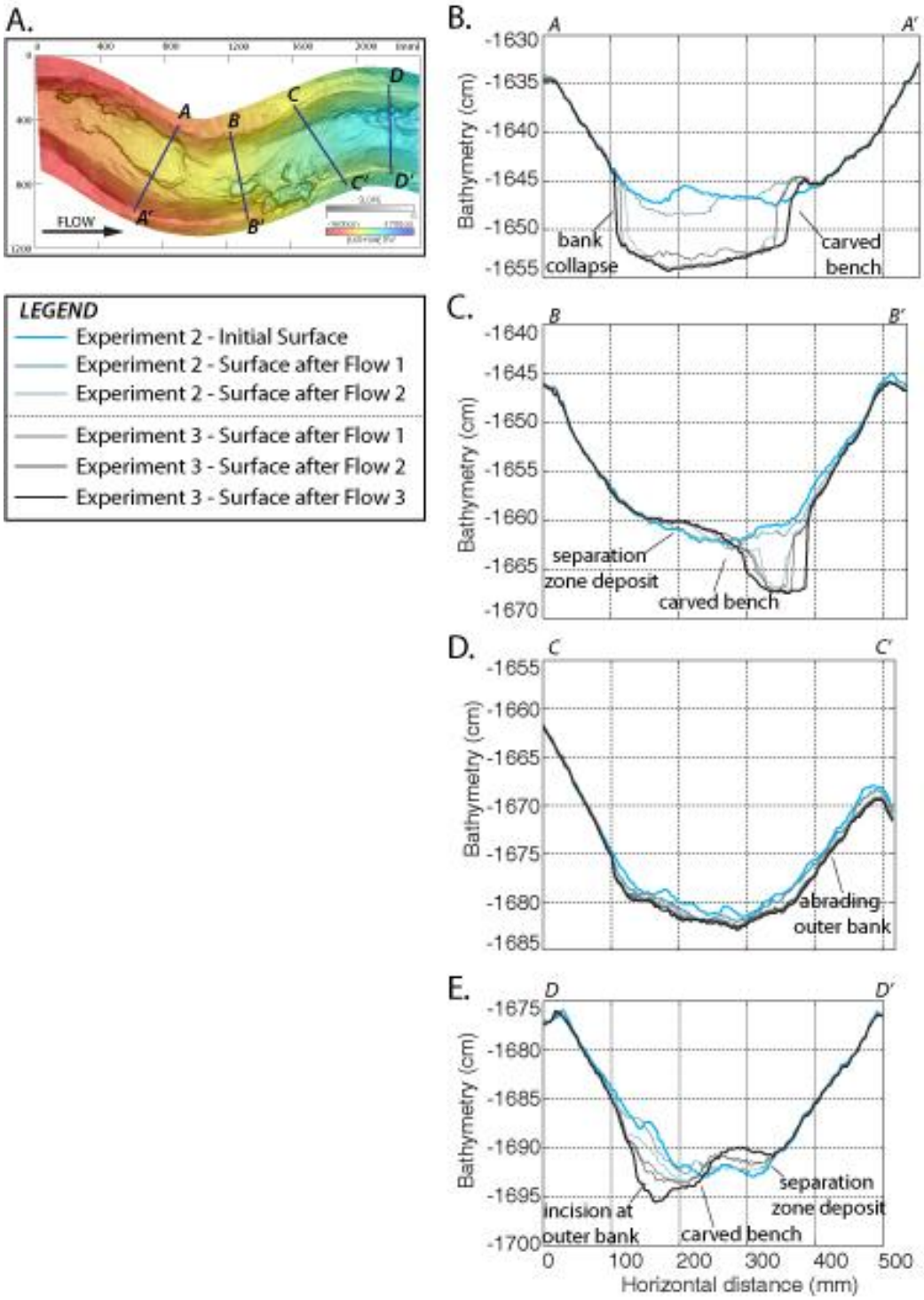

Figure 4.10: Reference map (A) and cross sections through the channel in experiment 2 and 3 (B, C, D, E)

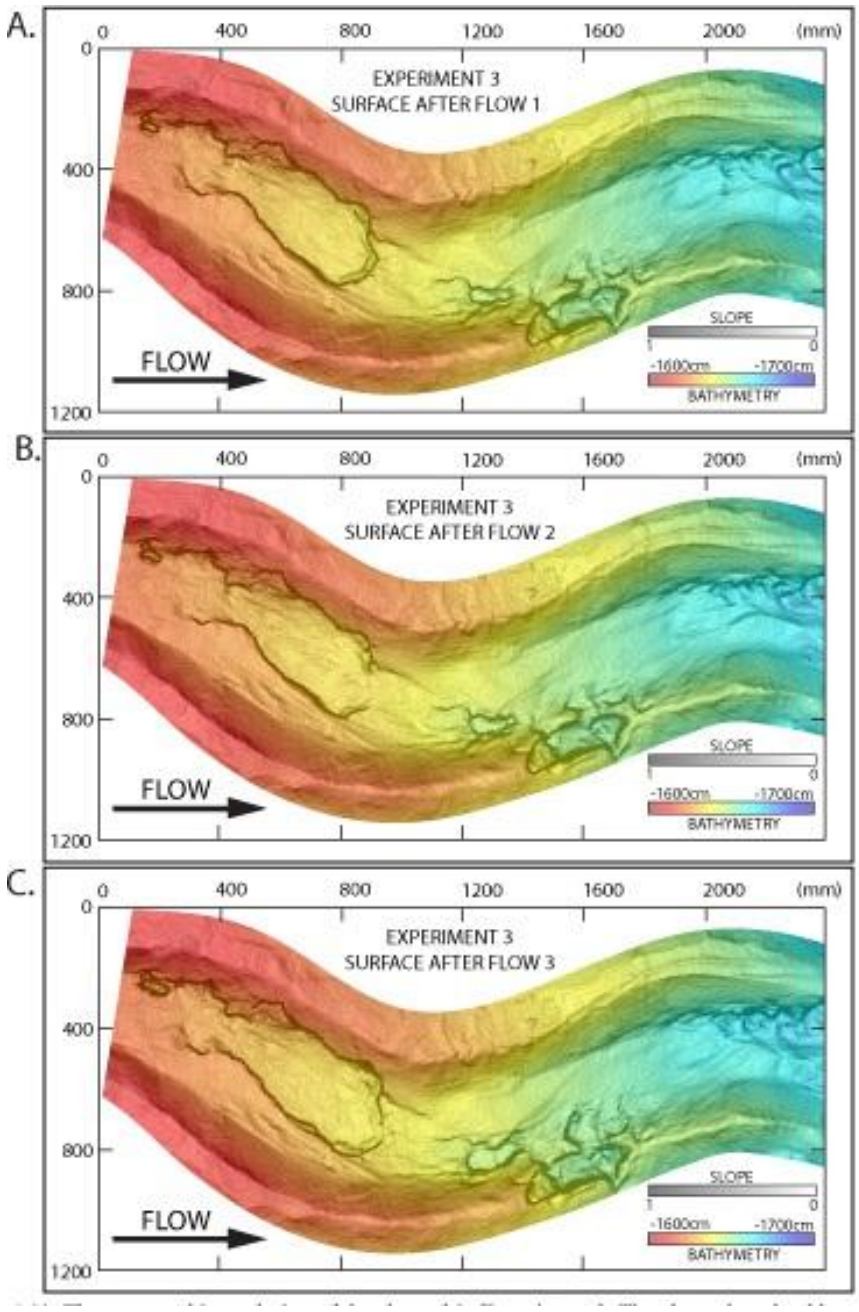

Figure 4.11: The topographic evolution of the channel in Experiment 3. The channel evolved by experiment 2 was used as the initial condition for this experiment. Bathymetry maps of each time step are overlain by the dip map of the same surface. Hot colors indicate topographic highs, cold colors indicate topographic lows. Gark greys indicate high slopes, white indicates low slopes. Surface after Flow 1, B) Surface after Flow 2, C) Surface after Flow 3.

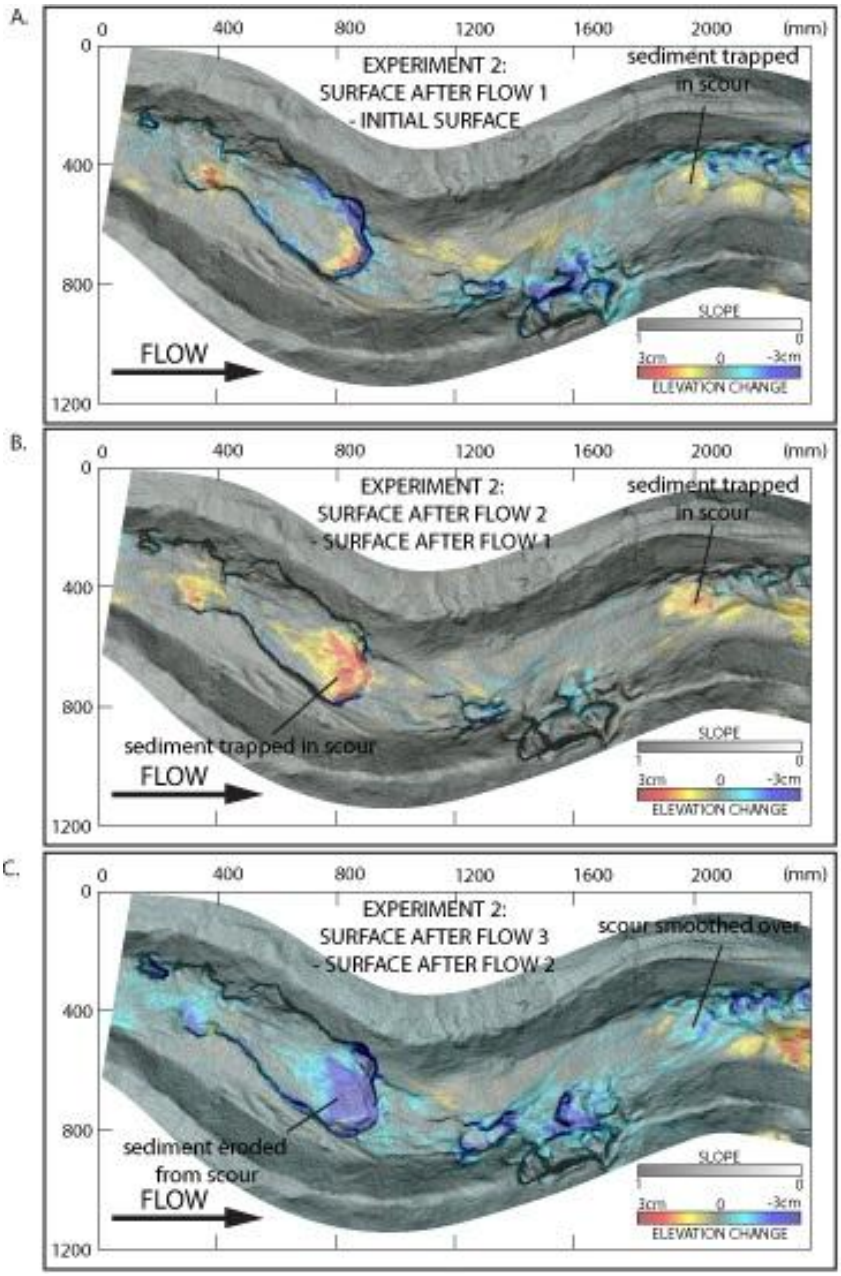

Figure 4.12: Erosion and deposition in the channel in Experiment 3. Hot colours = deposition, cold colours = erosion. The difference map showing the erosion and deposition associated with each time step is over lain by a gray scale dip map. A) Difference map (surface after flow 1 minus initial surface), B) Difference map (surface after flow 2 minus surface after flow 1), C) Difference map (surface after flow 3 minus surface after flow 2).

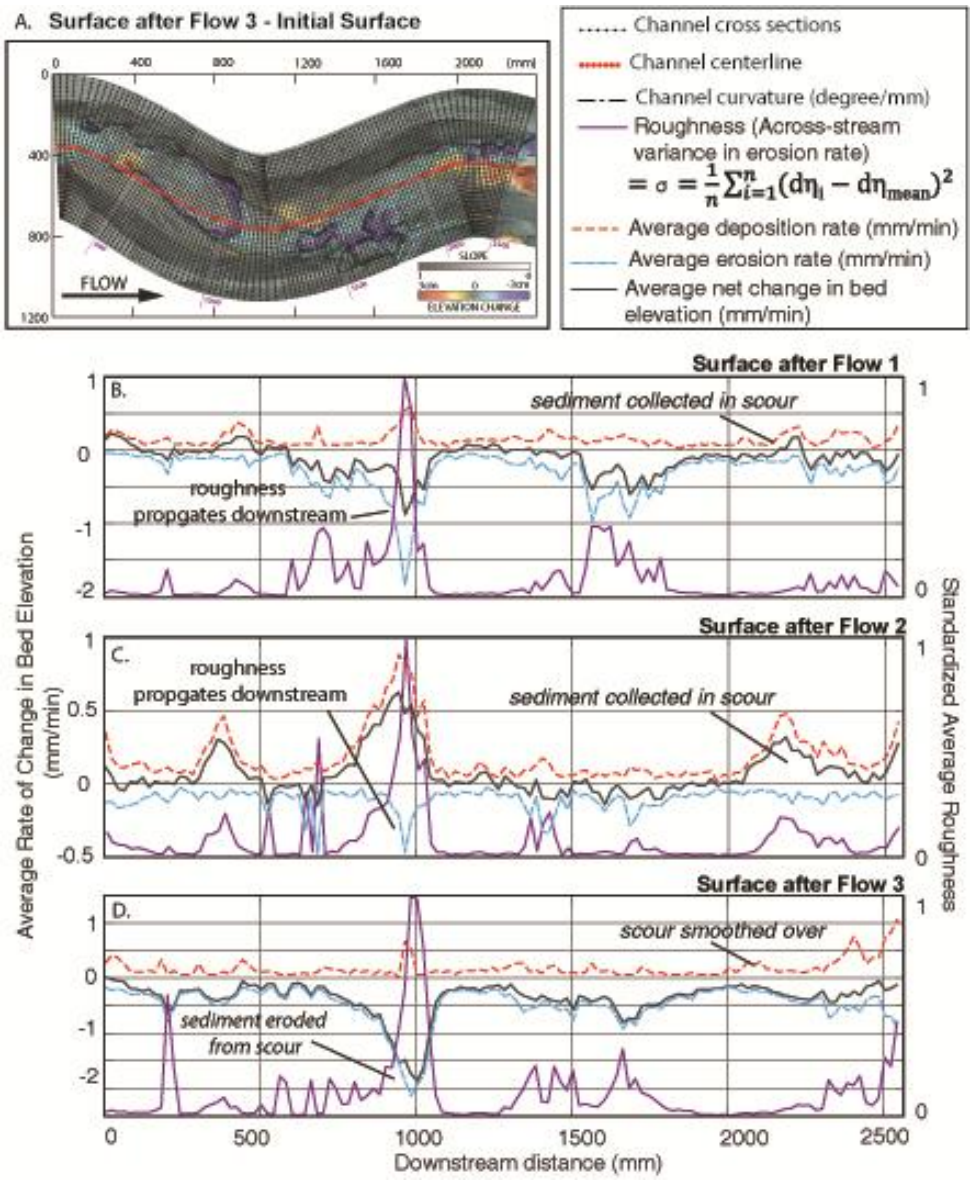

Figure 4.13: (A) Reference difference map showing: (1) the cross sections along which down-channel trends in (B, C, D) were averaged (black). Downstream trends in mean cross-channel erosion (blue), mean cross-channel deposition (red), mean topographic change (grey) and the standardized channel bed roughness associated with Flow 1 (B), Flow 2 (C), and Flow 3 (D). Roughness elements, associated with erosion from experiment 2 continued to be sites of further erosion. Topographic lows were sites of temporary or long-term sedimentation. Locations at which sediment accumulated in scours were protected from further erosion.

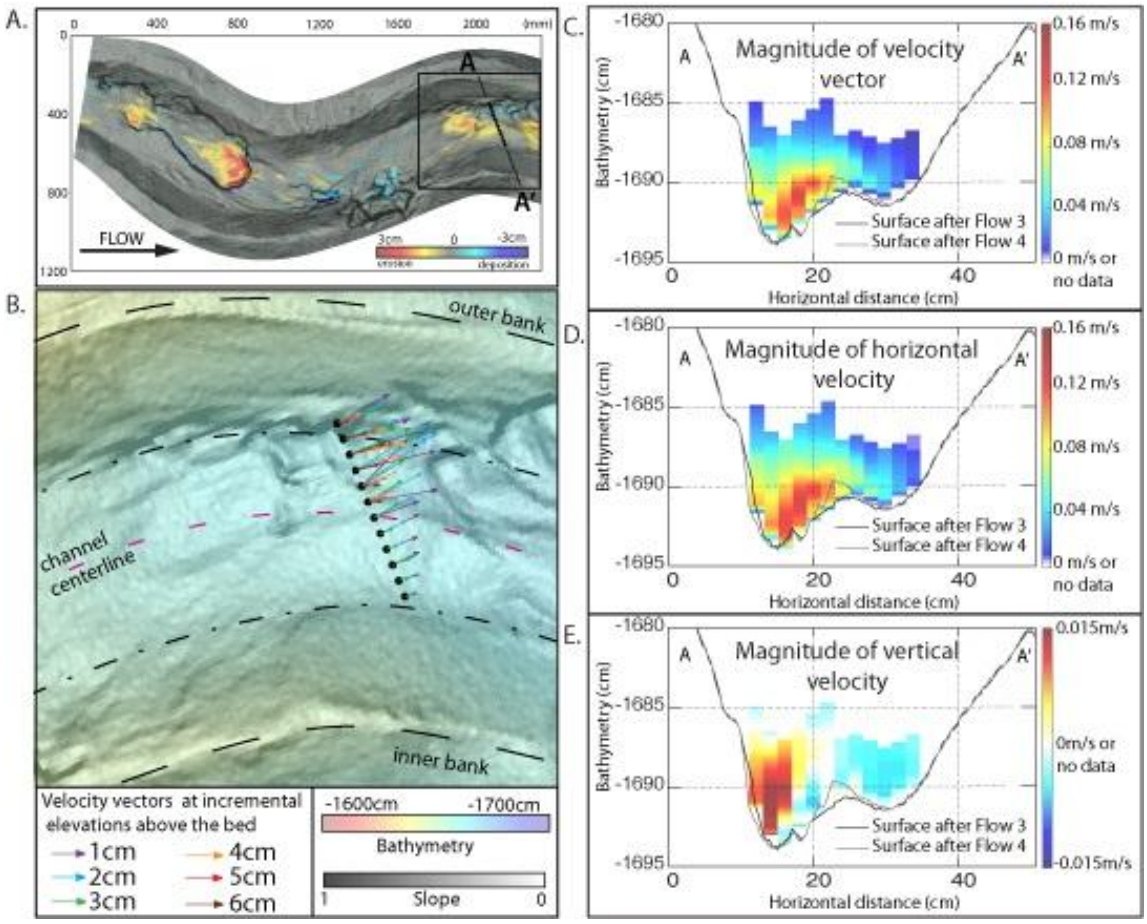

Figure 4.14: A) Reference map showing the location at which velocity profile measurements were collected during Flow 2. B) The magnitude and directions of horizontal velocity vectors along the measured cross-section at 1cm, 2cm, 3cm, 4cm, 5cm, and 6cm above the bed. C) The magnitude of the XYZ-velocity vector. D) The magnitude of the horizontal (XY) velocity vector. E) The magnitude of the vertical (Z-) velocity vector.

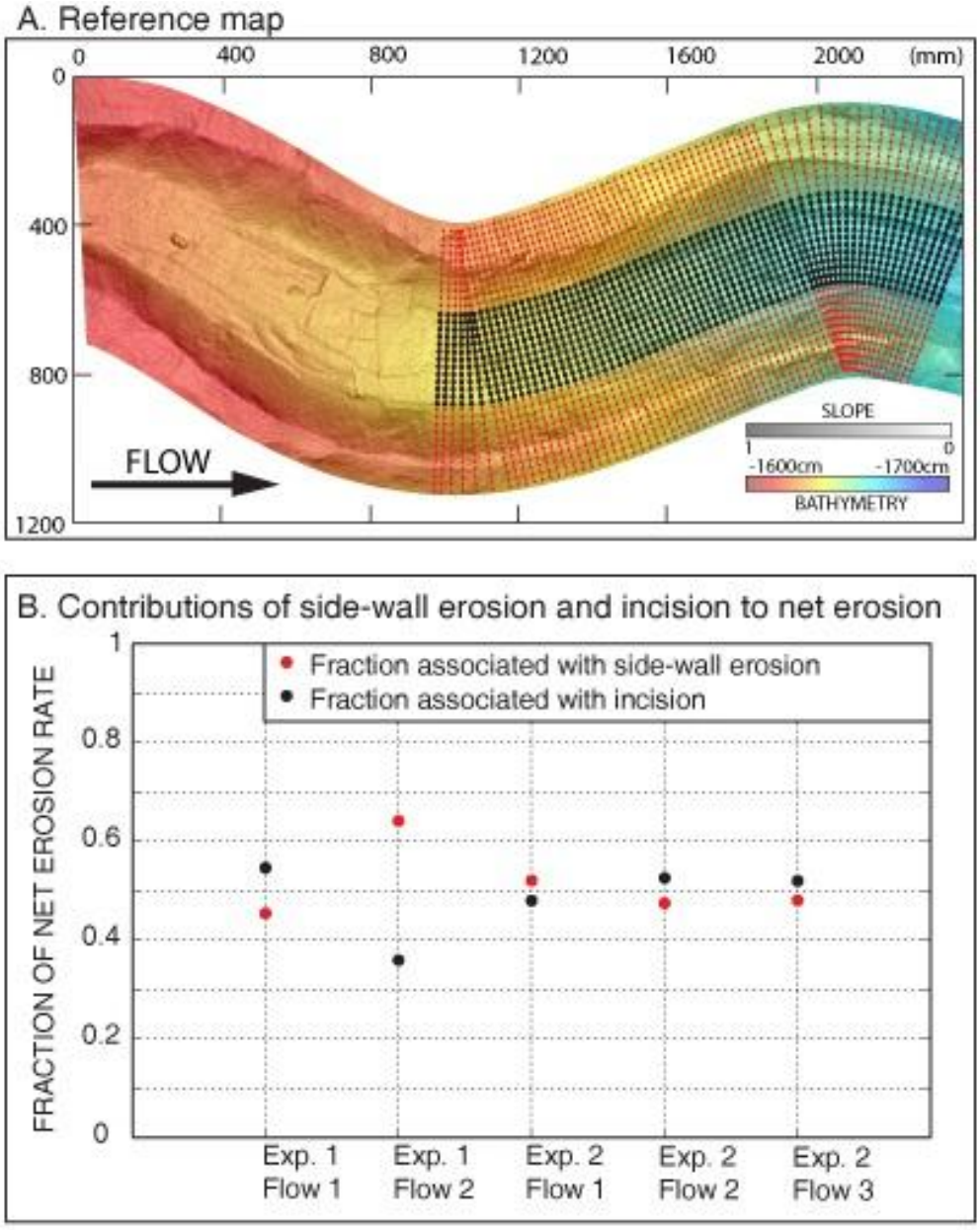

Figure 4.15: Reference map (A) shows the points over which net erosion was summed for the whole channel (red points) and for just the channel base (black points). The fraction of net erosion associated with the channel base and side-wall for each flow in experiment 2 and 3.

Chapter 5: Conclusions and Suggestions for Future Work

This dissertation has focused on understanding the interactions between turbidity currents and topography, and on their implications for the evolution of submarine landscapes and stratigraphy. Chapters Two, Three and Four addressed this problem at a range of spatial and temporal scales. Chapter Two analyzed three dimensional attributes of stratigraphic surfaces within deposits of submarine channels that were several kilometers long and evolved over many thousands of years. Chapter Three focused on the detailed physical sedimentology and stratigraphy of a single ancient submarine channel, which evolved over long time scales. Chapter Four investigated the evolution of individual subaqueous channel bends. Documented erosion and deposition connected to evolving channel shape and topography occurred at reduced timescales equivalent to a few hours in natural systems.

I have coupled well-developed models of channelized flow in rivers with my own observations and the known physics of turbidity currents to characterize the dynamic evolution of submarine channels and consequences for the construction of stratigraphy. In the following sections, I will focus on a few of the key contributions of my research to the earth sciences and discuss a few of ideas for future research directions.

THE MORPHOLOGY, SEDIMENTOLOGY AND STRATIGRAPHY OF BANK ATTACHED BARS

My research highlights a few fundamental differences in the ways that flows interact with channel bends in submarine and sub-aerial environments. Turbidity currents have very low excess densities relative to the ambient fluid (sea-water). This results in an extreme run-up of the currents at the outside of channel bends (Chapter 4; Straub et al, 2009; Straub et al., 2011). As a result, a low-velocity zone develops where flow separates from the inner bank. Chapter 2 documents that barforms in submarine channel bends generally form in low velocity zones and have shapes that indicate they are dominantly constructed from suspended sediment rather than bedload. Bedload travelling through sinuous subaqueous channels is always routed through the thalweg and never enters the flow-separation zone (Chapter 4). The facies model presented in Chapter 3 uses physical sedimentology and mapped stratal geometries from outcrop to characterize flow-separation bars. This facies model shows that a thick bank-attached bar can be constructed from fully-suspended sediment and the resulting stratigraphy contains bedforms associated with varying degrees of reworking.

Constructing and testing a predictive model that resolves the composition of separation-bar deposits from a few known conditions is the natural next step to these analyses. Straub and others (2011) suggested that ratio of the kinetic energy of moving currents to the potential energy required to overtop the relief of the outer channel bend levees is an effective indicator of the degree of channelization of currents. They observed that when this ratio approached 1, large volumes of the current left the channel and never returned. A poorly contained current will escape the channel at any high-curvature bend.

Many natural channels contain bends with moderate to high curvature. This energy balance relationship can therefore be applied to natural channels. Where channel depth is known and a range of realistic sediment concentrations is applied, current velocities and shear velocities can be estimated (Straub et al., 2011). The relationship between shear velocity and settling velocity of natural particles with different diameters (Nino et al., 2003; Smith and Hopkins, 1972) can then be used to predict the mode of transport for different particle sizes within currents in equilibrium with the channel shape. Knowing the estimated range of particle sizes travelling in suspension provides a testable hypothesis for particle sizes that will dominate bar deposits. This hypothesis can then be tested using outcrop data, core tied to seismically imaged bars or experimental data. This method is a potentially powerful predictive tool for characterizing the reservoir properties of bars where only limited lithological data is available.

The shape of a channel bend dictates the geometry of the inner bank flow separation zone i.e. the size of the flow separation zone increase as curvature increases. Bimodal grain size distributions recorded in the Brushy Canyon Formation separation bar were interpreted to be connected to locations that were proximal to the high velocity core of the current and so received input of material travelling close to the bed within the high-velocity core. Bars built in smaller flow separation zones (associated with weak sinuosity) might therefore be expected to contain larger fractions of this coarser material. Applicability of this hypothesis is easily tested using physical experiments in subaqueous channel bends with different curvature. Such a study would be effectively complemented

with a study of bar deposits in separation zones associated with different bend curvature in modern rivers.

SUBMARINE BENDS EVOLVED BY STRONGLY OR WEAKLY EROSIONAL TURBIDITY CURRENTS

My experiments (Chapter 4) with incisional subaqueous channel bends also showed that the run-up of erosional turbidity currents is tied to the development of benches at the inner bank. The relief of these benches was the combined result of weak deposition within the separation zone and continuous incision around the separation zone. Documenting the dynamic evolution of these features in my experiments allowed me to offer fresh insights into the processes which formed similar features in natural systems. I have also shown that turbidity current run-up is responsible for a higher degree of abrasion at the outer walls of bends than is usually seen in incisional bedrock river bends.

Experiments of turbidity currents in sub-aqueous channel bends have, until now, focused on channel evolution by highly depositional currents. My experiments represent the first successful attempt at studying subaqueous channels evolved by erosional currents. Modeling the stratal geometries constructed by strongly depositional currents has been shown to be relatively simple and is tied to input sediment concentrations (Lamb and Mohrig, 2009; Straub and Mohrig, 2008). In contrast, Chapter Four shows that erosional turbidity currents are strongly influenced by local conditions such as topographic roughness and planform curvature. Topographic roughness brings about localized accumulation of the material travelling close to the bed, while deposition of

fully suspended material is consistently weak and always tied to separation zones at the inner banks of bends.

My experiments have examined end member conditions where: 1. the bed was composed of only cohesionless sediment cover, and 2. the cohesive 'bed-rock' was almost always exposed to erosion. The logical next step is to evaluate channel evolution where varying amounts of sediment are allowed to travel through the system as bedload. Larger amounts of bed material are likely to armor the bed and prevent or reduce the rates of erosion (Johnson and Whipple, 2007). These experiments will probably offer valuable insights into local and input conditions associated with incision and filling of natural submarine channels.

Erosional currents in experiments presented in Chapter 4 modified the experimental channels through erosion of the bed and outer bank and through deposition at the inner bank. Overall, channel incision exceeded outer-bank erosion. Modeling migrating channels through weaker incision, pronounced side-wall erosion and higher inner bank deposition rates is a logical step forward. My experiments suggest that strongly erosional currents will deform the experimental channel at bends because weak sediment volumes accumulating at the inner bank cannot match the volume of sediment removed at the outer bank of bends. Observations of bend migration on the Powder River (Pizzuto, 1994) show that high-discharge floods increase the cross-sectional area of the channel through erosion of the outer bank and bed. During normal flow periods, accretion at the inner banks of the channel and aggradation of the bed result in a return to the original cross-sectional area. Submarine channel migration probably takes place in a

similar punctuated manner (Maier et al., 2012). Cycling between erosional and depositional turbidity currents in the laboratory will allow accretion of the inner bank of the channel to take place at a similar rate to migration of the outer bank.

Appendix A

This appendix contains a layered worksheet with grain-size data, sample weights, notes and sampling locations for all the samples collected for Chapter 3. This file is loaded in digital form with this document.

Bibliography

Abreu, V., Sullivan, M., Pirmez, C., and Mohrig, D., 2003, Lateral accretion packages (LAPs): an important reservoir element in deep water sinuous channels: Marine and Petroleum Geology, v. 20, p. 631-648.

Alexander, H.S., 1932, Pothole erosion: Journal of Geology, v. 40, p. 305-337.

Altinakar, M.S., Graf, W.H., and Hopfinger, E.J., 1996, Flow structure in turbidity currents: Journal of Hydraulic Research, v. 34, p. 713-718.

Amos, K.J., Peakall, J., Bradbury, P.W., Roberts, M., Keevil, G., and Gupta, S., 2010, The influence of bend amplitude and planform morphology on flow and sedimentation in submarine channels: Marine and Petroleum Geology, v. 27, p. 1431-1447.

Arnott, R.W.C., 2007, Stratal architecture and origin of lateral accretion deposits (LADs) and conterminuous inner-bank levee deposits in a base-of-slope sinuous channel, lower Isaac Formation (Neoproterozoic), East-Central British Columbia, Canada: Marine and Petroleum Geology, v. 24, p. 515-528.

Babonneau, N., Savoye, B., Cremer, M., Bez, M., Domzig, A., Deverchere, J., Strzerzynski, P., Yelles, K., Babonneau, N., Cattaneo, A., Mercier de Lepinay, B., Graindorge, D., Bracene, R., Kherroubi, A., Gaullier, V., and Anonymous, 2009, Sedimentary Architecture in Meanders of a Submarine Channel: Detailed Study of the Present Congo Turbidite Channel (Zaiango Project). The Algerian margin: a case study of interaction between plio-quaternary sedimentation and tectonics: Journal of Sedimentary Research, v. 80, p. 852-866.

Bagnold, R.A., 1941, The physics of blown sand and desert dunes.

—, 1960a, Flow resistance in sinuous or irregular channels; part 2, A theoretical model of energy loss in curved channels: U. S. Geological Survey Professional Paper, p. 122-130.

—, 1960b, Some aspects of the shape of river meanders, U. S. Geological Survey Professional Paper: United States, U. S. Geological Survey : Reston, VA, United States, p. 135-144.

—, 1966, An approach to the sediment transport problem from general physics, U. S. Geological Survey Professional Paper: United States, U. S. Geological Survey : Reston, VA, United States.

Beaubouef, R.T., and Pirmez, C., 1999, Mixed sand/mud submarine fan systems; comparing the Amazon Fan to intra-slope basin fans of the Gulf of Mexico: Annual Meeting Expanded Abstracts - American Association of Petroleum Geologists, v. 1999, p. A10-A10.

Beaubouef, R.T., Rossen, C.R., Zelt, F.B., Sullivan, M.D., Mohrig, D.C., Jennette, D.C., Bellian, J.A., Friedman, S.J., Lovell, R.W., and Shannon, D.S., 1999, Deep-water sandstones, Brushy Canyon Formation, West Texas, AAPG Continuing Education Course Note Series, Volume 40: United States, American Association of Petroleum Geologists. Education Department : Tulsa, OK, United States.

Blank, H.R., 1970, Incised meanders in Mason County, Texas: Geological Society of America Bulletin, v. 81, p. 3135-3140.

Bluck, B.J., 1971, Sedimentation in the meandering River Endrick: Scottish Journal of Geology, v. 7, Part 2, p. 93-138.

Bray, V.J., Bussey, D.B.J., Ghail, R.C., Jones, A.P., and Pickering, K.T., 2007, Meander geometry of Venusian canali: Constraints on flow regime and formation time: Journal of Geophysical Research-Planets, v. 112.

Bridge, J.S., and Jarvis, J., 1982, The dynamics of a river bend: a study in flow and sedimentary processes: Sedimentology, v. 29, p. 499-541.

Britter, R.E., and Linden, P.F., 1980, The motion of the front of a gravity current travelling down an incline: Journal of Fluid Mechanics, v. 99, p. 531-543.

Burge, L.M., and Smith, D.G., 1999, Confined meandering river eddy accretions: sedimentology, channel geometry and depositional processes, *in* Smith, N.D., and Rogers, J., eds., Fluvial Sedimentology Vi, Volume 28: International Association of Sedimentologists Special Publication: Oxford, Blackwell Science Publ, p. 113-130.

Burge, L.M., Smith, D.G., and Anonymous, 1996, Eddy accretion deposits in confined meandering river valleys; morphology, sedimentology, depositional processes and implications: Abstracts with Programs - Geological Society of America, v. 28, p. 277.

Chepil, W.S., 1945, Dynamics of wind erosion; Part 1, The nature of movement of soil by wind; Part 2, Initiation of soil movement; Part 3, The transport capacity of the wind; Part 4, The translocating and abrasive action of the wind; Part 5, Cumulative intensi: Soil Science, v. 60, p. 305-320.

Das, H.S., Imran, J., Pirmez, C., and Mohrig, D., 2004, Numerical modeling of flow and bed evolution in meandering submarine channels: Journal of Geophysical Research-Oceans, v. 109.

Dietrich, W.E., 1982, Settling velocity of natural particles: Water Resources Research, v. 18, p. 1615-1626.

Dietrich, W.E., and Smith, J.D., 1984, Bed load transport in a river meander: Water Resources Research, v. 20, p. 1355-1380.

Dietrich, W.E., Smith, J.D., and Dunne, T., 1979, Flow and sediment transport in a sand bedded meander: Journal of Geology, v. 87, p. 305-315.

—, 1984, Boundary shear stress, sediment transport, and bed morphology in a sand-bedded river meander during high and low flow: New York, NY, Am. Soc. Civ. Eng., 632-639 p.

Dykstra, M., and Kneller, B., 2009, Lateral accretion in a deep-marine channel complex: implications for channellized flow processes in turbidity currents: Sedimentology, v. 56, p. 1411-1432.

Edmonds, D.A., Shaw, J.B., and Mohrig, D., 2011, Topset-dominated deltas; a new model for river delta stratigraphy: Geology [Boulder], v. 39, p. 1175-1178.

Finnegan, N.J., and Dietrich, W.E., 2011, Episodic bedrock strath terrace formation due to meander migration and cutoff: Geology [Boulder], v. 39, p. 143-146.

Gasparini, N.M., Bras, R.L., and Whipple, K.X., 2006, Numerical modeling of non-steady-state river profile evolution using a sediment-flux-dependent incision model, *in* Willett, S.D., Hovius, N., Brandon, M.T., and Fisher, D.M., eds.,

Tectonics, Climate, and Landscape Evolution, Volume 398: Geological Society of America Special Papers, p. 127-141.

Graf, W.H., 1971, Hydraulics of sediment transport: United States, McGraw-Hill Book Co.; (McGraw-Hill Series in Water Resources and Environmental Engineering).

Harden, D.R., 1990, Controlling factors in the distribution and development of incised meanders in the central Colorado Plateau: Geological Society of America Bulletin, v. 102, p. 233-242.

Hay, A.E., 1987, Turbidity Currents and Submarine Channel Formation in Rupert Inlet, British Columbia.2. The Roles of Continuous and Surge-type Flow: Journal of Geophysical Research-Oceans, v. 92, p. 2883-2900.

Hickin, E.J., 1979, Concave-bank benches on the Squamish River, British Columbia, Canada: Canadian Journal of Earth Sciences = Revue Canadienne des Sciences de la Terre, v. 16, p. 200-203.

—, 1986, Concave-bank benches in the floodplains of Muskwa and Fort Nelson rivers, British Columbia: The Canadian Geographer = Le Geographe Canadien, v. 30, p. 111-122.

Howard, A.D., 1980, Thresholds in river regimes: United Kingdom, George Allen & Unwin : London, United Kingdom, p. 227-258.

—, 1994, A Detachment-limited model of Drainage Basin Evolution: Water Resources Research, v. 30, p. 2261-2285.

Ikeda, H., 1989, Sedimentary controls on channel migration and origin of point bars in sand-bedded meandering rivers: Water Resources Monograph, v. 12, p. 51-68.

Ikeda, S., Parker, G., and Sawai, K., 1981, Bend theory of river meanders. Part 1: Linear development: Journal of Fluid Mechanics, v. 112, p. 363-377.

Imran, J., Parker, G., and Pirmez, C., 1999, A nonlinear model of flow in meandering submarine and subaerial channels: Journal of Fluid Mechanics, v. 400, p. 295-331.

Jerolmack, D.J., Mohrig, D., Grotzinger, J.P., Fike, D.A., and Watters, W.A., 2006, Spatial grain size sorting in eolian ripples and estimation of wind conditions on planetary surfaces: Application to Meridiani Planum, Mars: Journal of Geophysical Research-Planets, v. 111.

Jobe, Z.R., Lowe, D.R., and Uchytil, S.J., 2011, Two fundamentally different types of submarine canyons along the continental margin of Equatorial Guinea: Marine and Petroleum Geology, v. 28, p. 843-860.

Johnson, J.P., and Whipple, K.X., 2007, Feedbacks between erosion and sediment transport in experimental bedrock channels: Earth Surface Processes and Landforms, v. 32, p. 1048-1062.

Johnson, J.P.L., and Whipple, K.X., 2010, Evaluating the controls of shear stress, sediment supply, alluvial cover, and channel morphology on experimental bedrock incision rate: Journal of Geophysical Research-Earth Surface, v. 115.

Johnson, J.P.L., Whipple, K.X., Sklar, L.S., and Hanks, T.C., 2009, Transport slopes, sediment cover, and bedrock channel incision in the Henry Mountains, Utah: Journal of Geophysical Research-Earth Surface, v. 114.

Kellerhals, R., Shaw, J., and Arora, V.K., 1975, GRAIN-SIZE FROM THIN-SECTIONS: Journal of Geology, v. 83, p. 79-96.

Kerans, C., and Fitchen, W.M., 1995, Sequence hierarchy and facies architecture of a carbonate-ramp system; San Andres Formation of Algerita Escarpment and western Guadalupe Mountains, West Texas and New Mexico, Report of Investigations - Texas, University, Bureau of Economic Geology: United States, University of Texas at Austin, Bureau of Economic Geology : Austin, TX, United States.

Khripounoff, A., Vangriesheim, A., Babonneau, N., Crassous, P., Dennielou, B., and Savoye, B., 2003, Direct observation of intense turbidity current activity in the Zaire submarine valley at 4000 m water depth: Marine Geology, v. 194, p. 151-158.

King, P.B., 1942, Permian of west Texas and southeastern New Mexico, Part 2 of DeFord and Lloyd, eds., West Texas-New Mexico symposium: Bulletin of the American Association of Petroleum Geologists, v. 26, p. 535-763.

Kocurek, G., and Kirkland, B.L., 1998, Getting to the source: aeolian influx to the Permian Delaware basin region: Sedimentary Geology, v. 117, p. 143-149.

Kolla, V., Posamentier, H.W., and Wood, L.J., 2007, Deep-water and fluvial sinuous channels - Characteristics, similarities and dissimilarities, and modes of formation: Marine and Petroleum Geology, v. 24, p. 388-405.

Kostic, S., Parker, G., and Marr, J.G., 2002, Role of turbidity currents in setting the foreset slope of clinoforms prograding into standing fresh water: Journal of Sedimentary Research, v. 72, p. 353-362.

Labourdette, R., 2007, Integrated three-dimensional modeling approach of stacked turbidite channels: Aapg Bulletin, v. 91, p. 1603-1618.

Labourdette, R., and Bez, M., 2010, Element migration in turbidite systems: Random or systematic depositional processes?: Aapg Bulletin, v. 94, p. 345-368.

Lamb, M.P., and Mohrig, D., 2009, Do hyperpycnal-flow deposits record river-flood dynamics?: Geology, v. 37, p. 1067-1070.

Laursen, E.M., 1958, The total sediment load of streams, Proceedings of the American Society of Civil Engineers, Volume 84, Part 1: United States, [American Society of Civil Engineers] : [New York, NY], United States.

Leeder, M.R., and Bridges, P.H., 1975, Flow separation in meander bends: Nature, v. 253, p. 338-339.

Leopold, L.B., Bagnold, R.A., Brush, L.M., Jr., and Wolman, M.G., 1960, Flow resistance in sinuous or irregular channels., U. S. Geological Survey Professional Paper: United States, U. S. Geological Survey : Reston, VA, United States, p. 111-134.

Maier, K.L., Fildani, A., McHargue, T.R., Paull, C.K., Graham, S.A., and Caress, D.W., 2012, Punctuated deep-water channel migration; high-resolution subsurface data from the Lucia Chica channel system, offshore California, U.S.A: Journal of Sedimentary Research, v. 82, p. 1-8.

Mayall, M., Jones, E., and Casey, M., 2006, Turbidite channel reservoirs - Key elements in facies prediction and effective development: Marine and Petroleum Geology, v. 23, p. 821-841.

Metivier, F., Lajeunesse, E., and Cacas, M.-C., 2005, Submarine canyons in the bathtub: Journal of Sedimentary Research, v. 75, p. 6-11.

Mohrig, D., and Buttles, J., 2007, Deep turbidity currents in shallow channels: Geology, v. 35, p. 155-158.

Nanson, G.C., and Hickin, E.J., 1983, Channel migration and incision on the Beatton River: Journal of Hydraulic Engineering, v. 109, p. 327-337.

Nino, Y., Lopez, F., and Garcia, M.H., 2003, Threshold for particle entrainment into suspension: Sedimentology, v. 50, p. 247-263.

Nishimura, K., and Hunt, J.C.R., 2000, Saltation and incipient suspension above a flat particle bed below a turbulent boundary layer: Journal of Fluid Mechanics, v. 417, p. 77-102.

Nittrouer, J.A., Mohrig, D., Allison, M.A., and Peyret, A.-P.B., 2011, The lowermost Mississippi River; a mixed bedrock-alluvial channel: Sedimentology, v. 58, p. 1914-1934.

Normark, W.R., Piper, D.J.W., and Stow, D.A.V., 1983, Quaternary development of channels, levees and lobes on Middle Laurentian Fan: Aapg Bulletin-American Association of Petroleum Geologists, v. 67, p. 1400-1409.

Page, K., and Nanson, G., 1982, Concave-bank benches and associated floodplain formation: Earth Surface Processes and Landforms, v. 7, p. 529-543.

Page, K.J., Nanson, G.C., and Frazier, P.S., 2003, Floodplain formation and sediment stratigraphy resulting from oblique accretion on the Murrumbidgee River, Australia: Journal of Sedimentary Research, v. 73, p. 5-14.

Paola, C., and Mohrig, D., 1996, Palaeohydraulics revisited: palaeoslope estimation in coarse-grained braided rivers: Basin Research, v. 8, p. 243-254.

Parker, G., Imran, J., and Pirmez, C., 2001, Transverse slope of bed and turbid-clear water interface of channelized turbidity currents flowing around bends: Berlin, Springer-Verlag, 119-139 p.

Parker, G., Seminara, G., and Solari, L., 2003, Bed load at low Shields stress on arbitrarily sloping beds; alternative entrainment formulation: Water Resources Research, v. 39.

Parker, G., Shimizu, Y., Wilkerson, G.V., Eke, E.C., Abad, J.D., Lauer, J.W., Paola, C., Dietrich, W.E., and Voller, V.R., 2011, A new framework for modeling the migration of meandering rivers: Earth Surface Processes and Landforms, v. 36, p. 70-86.

Paull, C.K., Ussler, W., Caress, D.W., Lundsten, E., Covault, J.A., Maier, K.L., Xu, J.P., and Augenstein, S., 2010, Origins of large crescent-shaped bedforms within the axial channel of Monterey Canyon, offshore California: Geosphere, v. 6, p. 755-774.

Perron, J.T., Lamb, M.P., Koven, C.D., Fung, I.Y., Yager, E., and Adamkovics, M., 2006, Valley formation and methane precipitation rates on Titan: Journal of Geophysical Research-Planets, v. 111.

Pirmez, C., and Imran, J., 2003, Reconstruction of turbidity currents in Amazon Channel: Marine and Petroleum Geology, v. 20, p. 823-849.

Pizzuto, J.E., 1994, Channel adjustments to changing discharges, Powder River, Montana: Geological Society of America Bulletin, v. 106, p. 1494-1501.

Pyles, D.R., Jennette, D.C., Tomasso, M., Beaubouef, R.T., and Rossen, C., 2009, Concepts learned from a 3-D outcrop of a sinuous slope channel complex: Beacon Channel Complex, Brushy Canyon Formation, West Texas, U. S. A.: Journal of Sedimentary Research, v. 80, p. 67-96.

Rich, J.L., 1914, Certain types of stream valleys and their meaning: Journal of Geology, p. 469-497.

Rossen, C., 1985, Sedimentology of the Brushy Canyon Formation (Permian, Early Guadalupian) in the Onlap Area, Guadalupe Mountains, west Texas. : Masters Thesis.

Rubin, D.M., 1990, Origin, structure, and evolution of a reattachment bar, Colorado River, Grand Canyon, Arizona: Journal of Sedimentary Petrology, v. 60, p. 982-991.

Rubin, D.M., Nelson, J.M., and Topping, D.J., 1998, Relation of inversely graded deposits to suspended-sediment grain-size evolution during floods in Grand Canyon, Arizona: Spain, Univ. Alicante : Alicante, Spain, p. 678-678.

Sagan, C., and Bagnold, R.A., 1975, Fluid transport on Earth and aeolian transport on Mars: Icarus, v. 26, p. 209-218.

Seminara, G., Solari, L., and Parker, G., 2002, Bed load at low Shields stress on arbitarily sloping beds; failure of the Bagnold hypothesis: Water Resources Research, v. 38.

Shao, S., and Yan, Y., 2000, A quantitative study on paleo-river environment during Late Jurassic on Yaojie region, Minhe Basin: Chinese Journal of Geochemistry, v. 19, p. 366-372.

Shepard, F.P., 1966, Meander in valley crossing a deep ocean fan.: Science, v. 154, p. 385-&.

Shepard, F.P., and Buffington.E.C., 1968, La Jolla Submarine Fan Valley: Marine Geology, v. 6, p. 107-&.

Shepard, F.P., and Emery, K.O., 1973, Congo Submarine Canyon and Fan Valley: American Association of Petroleum Geologists Bulletin, v. 57, p. 1679-1691.

Shepherd, R.G., and Schumm, S.A., 1974, Experimental Study of River Incision: Geological Society of America Bulletin, v. 85, p. 257-268.

Shyu, J.B.H., 2006, A neotectonic model of Taiwan, with a focus on the Longitudinal Valley Suture: United States.

Sklar, L., and Dietrich, W.E., 1998, River longitudinal profiles and bedrock incision models; stream power and the influence of sediment supply: Geophysical Monograph, v. 107, p. 237-260.

Sklar, L.S., and Dietrich, W.E., 2004, A mechanistic model for river incision into bedrock by saltating bed load: Water Resources Research, v. 40.

—, 2006, The role of sediment in controlling steady-state bedrock channel slope; implications of the saltation-abrasion incision model: Geomorphology, v. 82, p. 58-83.

Smith, D.G., Hubbard, S.M., Leckie, D.A., and Fustic, M., 2009, Counter point bar deposits; lithofacies and reservoir significance in the meandering modern Peace River and ancient McMurray Formation, Alberta, Canada: Sedimentology, v. 56, p. 1655-1669.

Smith, D.P., Kvitek, R., Iampietro, P.J., and Wong, K., 2007, Twenty-nine months of geomorphic change in upper Monterey Canyon (2002-2005): Marine Geology, v. 236, p. 79-94.

Smith, D.P., Ruiz, G., Kvitek, R., and Iampietro, P.J., 2005, Semiannual patterns of erosion and deposition in upper Monterey Canyon from serial multibeam bathymetry: Geological Society of America Bulletin, v. 117, p. 1123-1133.

Smith, J.D., and Hopkins, T.S., 1972, Sediment Transport on the Continental Shelf Off of Washington and Oregon in Light of Recent Current Measurements: United States, Dowden, Hutchinson & Ross, Stroudsburg, Pennsylvania, p. 143-180.

Stark, C.P., Barbour, J.R., Hayakawa, Y.S., Hattanji, T., Hovius, N., Chen, H., Lin, C.-W., Horng, M.-J., Xu, K.-Q., and Fukahata, Y., 2010, The climatic signature of incised river meanders: Science, v. 327, p. 1497-1501.

Straub, K.M., and Mohrig, D., 2008, Quantifying the morphology and growth of levees in aggrading submarine channels: Journal of Geophysical Research-Earth Surface, v. 113.

Straub, K.M., Mohrig, D., Buttles, J., McElroy, B., and Pirmez, C., 2011, Quantifying the influence of channel sinuosity on the depositional mechanics of channelized turbidity currents: A laboratory study: Marine and Petroleum Geology, v. 28, p. 744-760.

Straub, K.M., Mohrig, D., McElroy, B., Buttles, J., and Pirmez, C., 2008, Interactions between turbidity currents and topography in aggrading sinuous submarine channels: A laboratory study: Geological Society of America Bulletin, v. 120, p. 368-385.

Taylor, G., and Woodyer, K.D., 1978, Bank deposition in suspended-load streams: Memoir - Canadian Society of Petroleum Geologists, p. 257-275.

van Rijn, L.C., 1984a, Sediment transport; Part I, Bed load transport: Journal of Hydraulic Engineering, v. 110, p. 1431-1456.

—, 1984b, Sediment transport; Part II, Suspended load transport: Journal of Hydraulic Engineering, v. 110, p. 1613-1641.

Whipple, K.X., 2004, Bedrock rivers and the geomorphology of active orogens: Annual Review of Earth and Planetary Sciences, v. 32, p. 151-185.

Whipple, K.X., Hancock, G.S., and Anderson, R.S., 2000, River incision into bedrock: Mechanics and relative efficacy of plucking, abrasion, and cavitation: Geological Society of America Bulletin, v. 112, p. 490-503.

Whiting, P.J., and Dietrich, W.E., 1993c, Experimental constraints on bar migration through bends- Implication for meander wavelength selection: Water Resources Research, v. 29, p. 1091-1102.

Wiberg, P.L., and Smith, J.D., 1987, Calculations of the critical shear-stress for motion of uniform and heterogenous sediments: Water Resources Research, v. 23, p. 1471-1480.

Williams-Jones, G., Williams-Jones, A.E., and Stix, J., 1998, The nature and origin of Venusian canali: Journal of Geophysical Research-Planets, v. 103, p. 8545-8555.

Wohl, E.E., 1998, Bedrock channel morphology in relation to erosional processes: Geophysical Monograph, v. 107, p. 133-151.

Wohl, E.E., and Ikeda, H., 1997, Experimental simulation of channel incision into a cohesive substrate at varying gradients: Geology [Boulder], v. 25, p. 295-298.

Wohl, E.E., Thompson, D.M., and Miller, A.J., 1999, Canyons with undulating walls: Geological Society of America Bulletin, v. 111, p. 949-959.

Woodyer, K.D., 1975, Concave-bank benches on Barwon River, N.S.W: Australian Geographer, v. 13, p. 36-40.

Wynn, R.B., Cronin, B.T., and Peakall, J., 2007, Sinuous deep-water channels: Genesis, geometry and architecture: Marine and Petroleum Geology, v. 24, p. 341-387.

Xu, J.P., and Noble, M.A., 2009, Currents in Monterey Submarine Canyon: Journal of Geophysical Research-Oceans, v. 114, p. 20.

Xu, J.P., Swarzenski, P.W., Noble, M., and Li, A.C., 2009, Event-driven sediment flux in Hueneme and Mugu submarine canyons, southern California: Marine Geology, v. 269, p. 74-88.

Xu, J.P., Wong, F.L., Kvitek, R., Smith, D.P., and Paull, C.K., 2008, Sandwave migration in Monterey Submarine Canyon, Central California: Marine Geology, v. 248, p. 193-212.